Growth dynamics and size determination in *Hydra*

Dissertation
zur Erlangung des Doktorgrades
der Mathematisch-Naturwissenschaftlichen Fakultät
der Christian-Albrechts-Universität
zu Kiel

vorgelegt von
Jan Taubenheim

Kiel, im Juni 2018

Erstgutachter: Prof. Dr. Dr. h.c. Thomas C. G. Bosch
Zweitgutachter: Prof. Dr. Thomas Roeder
Tag der mündlichen Prüfung: 23.07.2018

Contents

Abstract

Body size is one of the most important features for all life forms, affecting every aspect of the life style of an organism and is a major determinant for fitness. There has been a long history of developmental and evolutionary research, which tried to answer the questions of how animals determine their body size and which regulative mechanisms are involved. Although enormous progress has been made, these question are only insufficiently answered to date. Especially environmental factors, which have tremendous influence on the final body size of an organism, their effect on molecular and cellular programs and the translation into body size have been explored only unsatisfactory.

In this thesis I shed light on cellular and molecular mechanisms which determine size in the model organism *Hydra*. I developed a computational model, which simulates the cellular dynamics of *Hydra* and models developmental processes, cell homeostasis and fitness. The model uses a critical size threshold to control body size, which means the induction of asexual reproduction (budding) if the threshold is passed. I provided evidence, that budding and its regulative processes are crucial factors for cell homeostasis and stable body size in *Hydra*. Furthermore, I could deduce from the model, that proliferation and apoptosis rates define developmental timing and contribute to fitness of *Hydra*, but are not integrated into the body size regulation.

To gain insights in the molecular mechanisms of size regulation and their responsiveness to environmental factors, I analyzed transgenic polyps with a defective insulin/insulin like growth factor signaling and animals reared at different temperatures, which both affected the body size of otherwise genetically identical individuals. Assessment of the expression profile of these polyps revealed that both cues resulted in the deregulation of the transforming growth factor β pathway. I could furthermore show that pharmacological interference with this pathway resulted in premature induction of bud initiation, which led to smaller body sizes in *Hydra*, confirming the predictions of the model.

Body size in *Hydra* is hence regulated by budding. Budding itself is initiated after reaching a critical size, which in turn is defined by the signaling changes of the transforming growth factor β pathway. This study contributes to the understanding of how evolutionary conserved pathways integrate environmental and intrinsic genetic signals to control developmental staging and eventually regulate body size.

Zusammenfassung

Körpergröße ist eine der wichtigsten Eigenschaften aller Lebewesen, weil es jeden Aspekt des Lebenstils eines Organismus beeinflusst und somit dessen Fitness bestimmt. Seit den Anfängen der Evolutions- und Entwicklungsbiologie spielen die Fragen, wie Tiere ihre Körpergröße erlangen und welche regulativen Mechanismen in diesem Zusammenhang relevant sind, eine zentrale Rolle in der Forschung. Obwohl es große Fortschritte zu diesem Thema gegeben hat, sind sie weiterhin nur unzureichend beantwortet. Im Speziellen gibt es immer noch große Wissenslücken, z. B. wie Umweltfaktoren, die die Größe beeinflussen, auf molekularer und zellulärer Ebene wirken und ihre Wirkung auf die Körpergröße eines Organismus vermitteln.

In dieser Arbeit gebe ich Aufschluss über die zellulären und molekularen Mechanismen der Größenregulation im Modellsystem *Hydra*. Ich habe ein theoretisches Modell entwickelt, welches die zellulären Dynamiken simuliert und die Entwicklungsprozesse, die Zellhomöostase sowie die Fitness von *Hydra* abbildet. Das Modell nutzt eine kritischen Größe zur Regulation der Körpergröße, welche bei Überschreitung die asexuelle Reproduktion (Knospung) einleitet. Weiterhin konnte ich zeigen, wie die Knospung und deren Regulationsmechanismen entscheidend zur Zellhomöostase und einer stabilen Körpergröße in *Hydra* beitragen. Außerdem konnte ich aus dem Modell ableiten, dass die Proliferation bzw. Apoptose der Zellen keinen direkten Einfluss auf die Größenregulation haben, sondern eher den zeitlichen Ablauf der Entwicklungsprozesse und die Fitness eines Polypen beeinflussen.

Um die molekularen Mechanismen der Größenregulation und deren Abhängigkeit von der Umwelt zu verstehen, habe ich transgene Polypen mit dysfunktionalem Insulin-Signalweg und Tiere, die in unterschiedlichen Temperaturen gehalten wurden, analysiert. Beides verändert die Größe in ansonsten genetisch identischen Individuen. Die Auswertung von Genexpressions-Daten zu diesen Polypen zeigte, dass beide Faktoren den transforming growth factor β Signalweg regulieren. Anschließend konnte ich demonstrieren, dass Tiere, die mit transforming growth factor β-Rezeptor-Inhibitoren behandelt wurden, frühzeitig die Knospung initiierten und dadurch insgesamt kleiner waren, als die unbehandelten Kontrollen. Genau dieser Mechanismus wurde vom Model vorausgesagt.

Körpergröße wird in *Hydra* durch die Knospung reguliert. Die asexuelle Vermehrung wird im Polypen initiiert, nachdem dieser die kritische Größe überschreitet, was wiederum durch den transforming growth factor β-Signalweg vermittelt wird. Diese Arbeit trägt zum Verständnis bei, wie evolutionär konservierte Signalwege Reize aus der Umwelt sowie intrinsisch-genetische Signale integrieren, die Entwicklungsphasen eine Organismus kontrollieren und schließlich die Körpergröße regulieren.

1 Introduction

1.1 Size and its implications on the biology of animals

Body size is a major determinant of all biological lifeforms. It is an integrative part of the biology itself and influences all features of an organism and its way of life [1, 2]. Body size is also one of the most variable features in biology. Sizes in the animal kingdom comprises almost seven orders of magnitude, starting from extremely small *Myxozoa* at around 8.5 μm [3] to the largest living animal ever known the Blue Wale *Balaenoptera musculus*, reaching sizes of $\approx$ 25 m [4].

1.1.1 Allometries

Many features like mass, volume, and area scale directly with size in power law dependencies in so called allometries [5–7] (Figure 1). From these scalings, fitness parameters for a species can be estimated. With volume, there comes usually an increase in weight which has further implications on the anatomy. A higher mass requires body structures that are able to withstand the resulting forces. Consequently, the diameters of body characteristics scale with a $\frac{3}{8}$ power to the lengths of the body part and thus with size [8, 9]. This puts restrictions on anatomical adaptations to changing environments and simultaneously limits the maximum size for the given anatomy. Furthermore it has significant impact on the speed, the amount of energy needed for traveling and the home range of an animal [5, 6, 10–15].

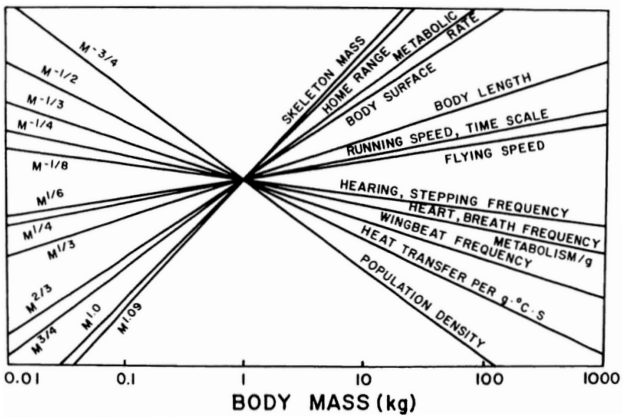

Figure 1: *Different generalized allometries which can be found in nature (mostly in mammals). Size is given as mass (Size^3). Both, mass and dependent variable is plotted on a log-scale. Original plot from [6].*

Another remarkable allometry seems to be the metabolic rate (the basal amount of energy per time an organism needs to retain its body mass) which scales with the power 3/4 the mass [7, 16–18]. This has implications for the energy homeostasis of an animal, where large individuals need less energy to maintain a certain amount of tissue but need overall more energy, compared to smaller animals. This has consequences for the whole life history of animals: if the metabolic rate is temperature corrected, body size can predict growth rates, developmental times, reproduction rates [19], aging, and senescence [20–22]. Furthermore this translates also to ecological parameters like population density [23],

interspecies interactions, and eventually to species diversity. All these factors dependent on metabolic rates and hence on size (see review [24]).

The allometries presented here are the most general ones and by far not encompassing all which have been discovered during the last 200 years of research on this topic. Nevertheless they demonstrate the significance of body size in physiology, metabolism, ecology and biology in general. However, allometries are only correlations between two or more traits of an animal and do not necessarily explain the causes underlying these correlations. The framework of allometries is useful to be aware of when dealing with size regulation and point to correlated phenomena which might be overlooked if not known. Their main compelling strength is the connection of biological traits via metabolism to physical and chemical foundations, which have impact on life histories and ecology.

1.1.2 Eco-Evo-Devo, environment and body size

Generally, being larger as animal is considered advantageous [7, 25–27] and is observed in evolutionary processes where most organisms tend to become larger with time [26, 28–31]. Although doubts on the universality of this so called "Cope's"-rule have been stated [32,33], there are good arguments for a fitness increase of larger individuals within a population. Sexual selection favors large body sizes if environmental conditions do not select for smaller individuals. Large males are more competitive against rivals, they are able to maintain larger harem sizes, are more likely chosen by females for mating and have thus higher rates in reproduction success [26,34,35]. This applies especially for polygamy mammals [36]. In all other animals a sexual size dimorphism can be seen, were females have increased in size, which seems to be correlated with higher fecundity [37–43]. However, natural selection favors shorter developmental times which is correlated with smaller body size [31, 44]. Development is usually a vulnerable time during the life histories of many animals due to predation and less resistance to environmental alterations, compared to adult individuals. It is also thought to be one of the major factors for fixing a certain size in species for the given environment [27]. Whether natural or sexual selection is predominant, depends on the environmental conditions. If these are very restrictive, survival until adulthood and sexual maturation is favored over reaching large body sizes.

Interestingly, body size is also directly coupled to environmental factors, with feeding and temperature as the two best described cues which have tremendous effect. On the one hand, malnutrition during the sensitive developmental time can reduce adult body size, though developmental time is prolonged [45–47] while on the other hand large size helps coping with periods of starvation [48, 49]. The adaptation of size to food availability is thought to be primarily due to metabolic restriction during the development, but there have been observations of epigenetic alteration in size regulating genes for a starving dutch population during the second world war as well, which implies additional evolutionary consequences [50].

Temperature has been long recognized to be associated with the size of an organism and in fact there have been two rules proposed describing the effect of lower temperatures resulting in an increased body size, Bergmann's rule [51] and the temperature size rule (TSR) [52, 53]. The former describes the effect for endotherms, while the latter explains observations in ectotherms. These correlations are intriguing, since the Bergmann's rule reflects an evolutionary adaptation, which is achieved over several generations, while the temperature size rule describes a form of phenotypic plasticity [54]. Ectotherms increase their body size at lower temperatures during their own ontogeny, which is accompanied with slower growth, but prolonged developmental time [52, 53]. However, these plastic changes in body size have also been observed to manifest on an evolutionary level and

may be genetically fixed in ectotherms, as reported in studies of *Drosophila melanogaster* [55–57]. Furthermore, this has an impact on body size in the face of climate change and global warming as it has been reported that body size in various species is affected [58]. Whether the temperature cues change the body size of animals by physical restriction (by metabolic and/or diffusion rates) or whether a gain in fitness is achieved, or both, is not clear to date. Neither is known, whether there are molecular mechanisms which relay the temperature cue to developmental or growth promoting pathways, as it is the case with many other environmental signals. The nutritional state of the organism is usually sensed by several pathways, with the insulin signaling in its center.

1.2 Size regulation

How body size is regulated has been one of the most fundamental questions in developmental biology and basic concepts have been understood quite well to day, though the resolution of our knowledge lack details on molecular level. The regulation of body size on a cellular level eventually depends only on the number, the size and the spatial organization of the cells an organism consists. The parameters acknowledged here can be regulated rather independently though the features itself depend on each other. Spatial organization depends on the amount of cells and their size, as does cell size depend on the proliferation rate, and so on. I will shortly give an overview of how cell size and proliferation are interdependent, afterwards I will introduce some concepts of total body size and organ size regulation of developmental biology. Finally, I will introduce basic pathways for regulation of cell proliferation and cell growth.

1.2.1 Proliferation and cell size

Proliferation describes the rate at which cells divide in the tissue and this rate can vary, depending on the environmental conditions and the developmental state of an organism. The cell division rate determines not only the cell number of an organism but is also tightly linked to the cell size, because higher proliferation rates tend to generate smaller cells (Figure 2). This is due to the fact that the cells have less time to grow before another mitosis takes place. However, proliferation and cell size are not independently regulated, although different modes of regulation seem to exist.

Cell size can be measured in some organisms/tissues and mitosis is (only) initiated if a certain threshold was exceeded [59, 60]. In other instances the growth rate of the cell is adjusted to the pace of the proliferation rate [61, 62]. Additionally there are suggestions that cell size is regulated in a 'sloppy' way, as the probability of division increases with cell size, which has proven to be in accordance with experimental data [63]. Furthermore there are examples of a total decoupling of cell size and cell proliferation regulation, where the two processes individually receive external signals, which cause either proliferation, or cell growth or both in these cells [64] (see [65] for review). How cell size sensing or the external control is functioning is still part of vivid research and mechanisms like DNA-titration (see [66] for review), mitochondrial activity [67], or the influence of separate growth promoting and mitotic growth factors have been found [68,69] (see [70] for review). It is noteworthy, that cell size is correlated with mitochondrial activity, which links the allometry of metabolic rate and body size back to a cellular level [67].

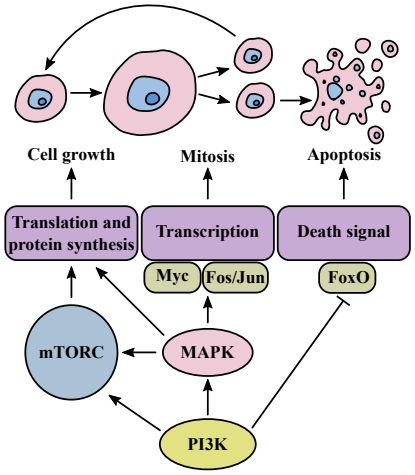

Figure 2: *Total body size is the product of cell size and cell number of an organism. Mitosis and cell growth (and thus cell size) are closely interrelated, while apoptosis is contributing to reduce and stabilize the total amount of cells in the adult animal. mTOR signaling regulates protein biosynthesis, which is primarily associated with cell growth, while the MAPK pathway promotes both, protein synthesis and gene transcription driving cell cycle progression and mitosis. The PI3K-cascade acts as a master regulator and activates both pathways, while additionally interfering with apoptosis mechanisms.*

1.2.2 Growth duration and termination of growth periods

Growth duration describes the time frame in which cell proliferation can happen. This time frame is usually restricted by some kind of regulation and depends on both environment and genetics. Interestingly, there are species with determinate (growth ceases at a certain age) and indeterminate growth (the organism growth until death), with several variants of both [71, 72]. While size regulation in indeterminate growing species is mainly dependent on proliferation rates and their regulation by extrinsic factors, like nutrient availability or temperature, determinate growth seems to be regulated by genetic factors to a larger extant [71, 72]. Few is known on the regulative mechanisms which determine the growth duration in animals and human but it seems closely related with sexual maturation.

In humans, height growth is arrested with bone maturation (closure of the epiphyseal plate), which in turn is induced by the onset of puberty and elevated levels of sex hormones, especially estrogen [73]. The induction of puberty seems to be regulated again by the size, since growth hormone (GH) deficient children are older at onset of puberty [74]. How size is actually measured and puberty induction is controlled, is still unknown, though suggestions on the regulation have been made. Leptin seems to be involved in the onset of puberty, as Leptin deficiency prevents puberty [75]. Leptin links long term nutrient availability to the hormonal system and thus might be permissive, but not necessary for puberty induction [75]. Other findings suggest a role of the tachykinin neurotransmitter family in the induction of puberty [76]. The most promising candidate for induction of puberty, however, is the RNA-binding protein LIN28, which was identified in genome wide association studies (GWAS) correlating polymorphisms with age at menarche [77]. In mouse it could be shown that LIN28 enhances insulin like growth factor (IGF) 2 translation and that overexpression of LIN28 prevents onset of puberty while increasing body size [78, 79].

A similar mechanism was described in insects, where pupation is initiated (and thus final size determined) after an increase of the hormone ecdysone [80]. Ecdysone is released after a 'critical size' has been reached in the larva, which afterwards initiates a final growth period and eventually pupation [81]. The regulation of ecdysone release is comparably well understood, but the precise mechanism on how animals measure their size is still elusive. However, oxygen distribution capacity of the organism has been described to regulate the ecdysone production in insects, which might be a regulating mechanism to sense total body size [82]. This provides arguments pointing in a similar direction as the metabolic rate and/or mitochondrial activity, both associated with body size and cell size, respectively. Indeed, oxygen levels have been suggested as a regulative factor for body size in ectotherms [83, 84] but a final proof and a corresponding mechanism is still missing. Furthermore it is not clear, whether this idea is transferable to homeotherms either.

On a more local level, growth duration in organs or tissue is regulated by pattern formation. Pattern formation is mediated either by morphogenetic fields (pathways like hedgehog (Hh), wingless and Int-1 protein (Wnt), transforming growth factor β (TGF-β)) or by direct cell-cell-contacts (e. g. Notch, or Hippo). Most of these pattern formation processes are associated with specific cell proliferation and differentiation, which define final sizes of organs and organ structures. The regulation is coupled to the expression of growth factors, which mediate the growth, either by proliferation or cell growth. A good example is the limb development in mammals which is regulated by a signaling network of bone morphogenetic protein (BMP), sonic hedgehog (Shh), fibroblast growth factor (FGF) and Gremlin [85]. BMP and Shh control the duration of growth of the limb and regulate the expression of FGF, which mediates the cell proliferation for limb growth.

Cell-cell contacts on the other hand, are usually associated with induction of growth arrest. This process has been termed contact inhibition and occurs in regenerating tissues, which reach the boundaries of their compartment. It stops tissue growth upon tight contact between cells [86]. Loss of contact inhibition is often associated with overgrowth of organ structures and tumorigenesis. Contact inhibition is mediated by the Hippo-pathway and interference with this pathway leads to overgrowth of tissues [87] or even changes in total body size [88].

How specific organ size is maintained and why some organs (e. g. muscle, or liver) can adjust their size to given environmental cues is still unknown. The integration of environmental cues in organ size and body size determination has major implications for the survival and mating success of an organism, thus is crucial to understand evolutionary mechanisms [89–91].

1.2.3 Cell cycle regulation

Cell proliferation implies that cells divide and thus have to go through a full cell cycle. A prototypic eukaryotic cell cycle can be split into four separate phases, G1-, S-, G2- and M-phase. In the G1 phase, the cell grows, drives protein synthesis, and recovers its volume after a preceding devision (Figure 2). Afterwards, the cell goes into the S phase, where DNA replication takes place. Subsequently, the cell grows again and prepares for mitosis in the G2 phase before it enters M-phase for the actual mitosis (and usually cytokinesis). There are G1-S, G2-M, and spindle checkpoints which ensure secure cell cycle progression. The cell cycle is controlled by the timed expression of usually phase specific cyclins which specifically bind to their respective cyclin dependent kinase (CDK). Upon binding, the CDK is activated and mediates cell cycle progression by phosphorylation of target proteins, thereby passing the respective checkpoint. Cell cycle progression through the different checkpoints is regulated by nutrient availability, external growth signals and

DNA-damage [92]. If the cell has a low energy status, cell cycle progression is inhibited by downregulation of the mTOR pathway (see subsection 1.2.5) while DNA-damage is sensed by several serin-threonin kinases which activate p53 [93].

However, most important seems to be the activity of Myc, which promotes transcription of many (mainly already active) genes in the genome [94] and drives protein synthesis by ribosome biogenesis [95] (Figure 3). For the cell cycle regulation, Myc has been described for activating/inducing expression of CDKs, cyclins, and other cell cycle promoting proteins on the one hand, while it antagonizes cell cycle inhibiting factors like p15, p21, and p27 on the other hand [96]. Myc itself is stabilized by various mitogenic signals and is one possible way for signal transduction of the Ras-Raf-MAPK pathway (see subsection 1.2.6) [97]. Interestingly Myc plays additional roles in cell size regulation and can also induce apoptosis in unfavorable conditions [98–100].

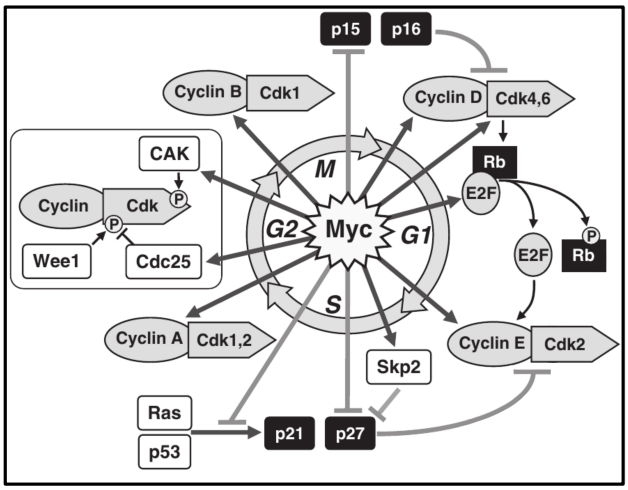

Figure 3: *Myc controls almost all aspects of cell cycle progression, by inducing phase specific cyclins, CDK-promoting factors like CAK or cdc25, and antagonizing cell cycle inhibition factors p15, p21, p27. Adapted from [96].*

G0 describes the cell state were no further mitosis takes place due to lack of nutrients/cell proliferation signals (quiescence), by repression of cell cycle after DNA-damages (senescence) [101], or due to exhausted mitosis capacity in specialized cell types (differentiation). The last of the listed forms of cell cycle arrest is actually caused by the nature of cell differentiation and comprises either quiescence or senescence in a physiological context. Differentiated cells usually loose their proliferation potential due to epigenetic changes, loss of the expression of cell cycle promoting factors, unresponsiveness to mitogenic signals, or shortage of telomere ends or a combination of these factors [102–106].

It is not surprising that cell cycle regulating components are crucial for body and organ size regulation. For example deregulation of p27 has been shown to change body size in mice, by alteration of cell number, but not cell size [107–110]. In *Drosophila* and in mice it has been described, that cyclin D and CDK4 can influence cell size and thus body size, illustrating the general implications of cell cycle regulation in body size [111–114]. Reduction of Myc in *Drosophila* and mice have also been associated with a small body size in the animals, though once with reduced cell size, once with reduced cell number [115, 116]. The mechanism of how cell number in the organism/organ is measured and how environmental factors affect these mechanisms is still unknown.

1.2.4 Apoptosis

There is not only the proliferation of cells and increase of tissue, which determine body size in an organism. Opposing cell proliferation, regulated cell death or apoptosis is an important factor for organism size (Figure 2). On the molecular level apoptosis is mediated by caspases. These are proteinases which need to be proteolytically activated and are organized in a cascade of initiator and effector caspases. After activation, the caspases proteolyse many cell contents, including structural cell proteins leading to the apoptosis phenotype [117](see [118] for review of caspase action). The initiator caspases are activated by two main pathways, the intrinsic or the extrinsic apoptosis pathway.

For the regulation of the intrinsic apoptosis pathway an interaction of the apoptosis initiating BH3-only proteins, the anti-apoptotic (cell guardian) B-cell lymphoma (BCL)-2 homologs and the two proapoptotic BCL-2 antagonist/killer (BAK) and BCL-2 associated X protein (BAX) on the mitochondrial membrane is necessary (see [119] for review). Apoptosis is initiated by the inactivation of the BCL-2 homologs, which are antagonists of the BH3-only proteins and/or BAK and BAX. These become activated and permeabilize the mitochondrial membrane, which leads to the release of cytochrome-c. Cytochrome-c is recognized by apoptotic protease activating factor 1 (APAF1), which bind and proteolytically activates one of the initiator caspases (caspase-9 in mammals), activating the caspase cascade and leading to inevitable cell death [119].

The extrinsic pathway is mediated by the tumor necrosis factor receptor (TNFR) and their ligands. Upon receptor binding an initiator caspase (caspase-10 in humans) is activated and initiates the proteolytic caspase cascade.

The signals which induce apoptosis are diverse and range from environmental stressors, like reactive oxygen species, hypoxia, nutrient deprivation, or UV-irradiation, to developmental and inflammatory signals. How the signals are integrated depends on the pathway which facilitates the transduction. A very common target is the p53 transcription factor, which upon activation drives the transcription of BAX as well as the BH3-only proteins Puma and Noxa. Furthermore it can induce expression of ligands for the extrinsic apoptosis pathway while reducing the survival signals in the cell (see [120] for details of p53 action in apoptosis). Apoptosis by reactive oxygen species is mediated on several levels by inducing p53 activity, activating the c-Jun N-terminal kinase (JNK) pathway (see subsection 1.2.6) or by directly damaging the mitochondrial membrane [121]. Hypoxia is another example, which induces apoptosis via the hypoxia induced factor 1α (HIF) transcription factors. On the one hand, this is mediated by direct interaction of HIF with the BCL-proteins, by the interaction with p53 [122] or forkhead box protein O (FoxO) [123]. Many more could be mentioned but usually induction of apoptosis almost certainly is mediated by one of the two apoptosis pathways and very often p53 is also involved in mediating the death signal.

However signals are mediated, apoptosis proofed to be a crucial building brick in organismal size determination, especially during developmental processes. There it can prevent compartment overgrowth and actively removes excess cells [124].

1.2.5 mTOR signaling

Cell proliferation is regulated on several levels. The most basic one is a check for the availability of resources like energy and oxygen which is regulated through the mTOR pathway. Nutrient and oxygen sensing is mediated by the two separate mTOR protein complexes, mTORC1 and mTORC2 (Figure 4). mTOR signaling responds to the resource status of the cell and functions as a gate keeper, inhibiting cell proliferation and growth, if

nutrient or oxygen levels are low. mTORC1 regulates primarily the translation of the cell via phosphorylation of eukaryotic translation initiation factor 4E binding protein (4EBP) and p70S6 kinase (S6K). 4EBP inhibits the translation by binding at the 5'UTR of the transcribed mRNA and prohibits the initiation of the translation activation protein complex. Phosphorylation of 4EBP results in the dissociation from the mRNA and thus releases the inhibitory effect of 4EBP. S6K in turn, induces protein synthesis of the cell by phosphorylation and activation of several targets which promote mRNA-processing, protein translation initiation and elongation, as well as folding. Mutations in S6K causes a slow growth phenotype in mice as well as in *Drosophila*, reduces cell, and body size [125, 126].

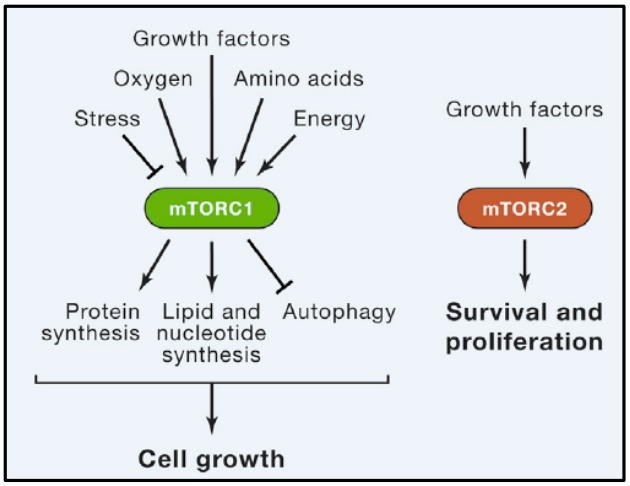

Figure 4: *The mTOR signaling pathway acts as a gate keeper for cell proliferation and growth. It relays various cell status information as well as the developmental signals which are eventually transduced in cell growth and proliferation. Adapted from [127].*

mTORC1 itself is directly inhibited by the AMP-activated protein kinase (AMPK) via tuberous sclerosis 2 (TSC2), which is activated upon high AMP to ATP levels, a signal for a low energy status in the cell. Furthermore high amino acid levels, especially leucine and isoleucine, induce mTORC1 activity by a TSC2 independent process. Thereby, the amino acid and a mitogen signal (e. g. MAPK signaling) have to operate at the same time to fulfill mTORC1 activation. Low oxygen levels are transduced via the stabilization of the transcription factor HIF-1α which induces the transcription of regulated in development and DNA-damage response 1 (REDD). REDD functions again through TSC2 and inhibits the mTORC1. The regulation of mTORC1 is even more complex, as different mitogenic, e. g. tumor necrosis factor α (TNF-α) or insulin, and developmental signals, as Wnt, are known to act as regulator for its functions (see reviews [127–130]).

Unlike mTORC1, mTORC2 is mainly regulated by the insulin signaling pathway (another global nutrient sensing system, see section 1.3) and mediates its functions by phosphorylation of protein kinase C (PKC), protein kinase B (PKB) (AKT), and serine/threonin protein kinase 1 (SGK1). PKC regulates the actin-cytoskeleton and cell migration. PKB is part of the insulin-PI3K signaling pathway, phosphorylating FoxO members, which have important roles in cell senescence and apoptosis (see section 1.3). Similarly, SGK1 is thought to affect FoxO regulation and additionally regulates various ion channels, which in turn are important for cell volume regulation (see reviews [127–130]).

Taken together the mTOR pathway is a major integrator for environmental and developmental signals to promote cell growth and coordinate cell proliferation, but is essentially not sufficient for promoting cell proliferation (Figure 2). Rather the mTOR-signals are necessary to allow cells to enter cell cycle upon mitogenic signals and play a permissive role in body size regulation [125, 126, 131–133].

1.2.6 MAPK signaling

The MAPK signaling pathway is an intracellular cascade of at least three different kinases, which are activated by various intra- and extracellular cues. The initial step contains the activation of a G-protein, which activates the first kinase in the cascade (mitogen activated protein kinase kinase kinase (MAPKKK)). This kinase activates another kinase (mitogen activated protein kinase kinase (MAPKK)) by phosphorylation, which in turn activates the effector kinase, the MAPK. The outcome of the signal depends on the cellular and environmental context of the cell and can range from activation of cell proliferation, differentiation to apoptosis. The variety of sensed signals and promoted functions is reflected in the vast number of proteins, that can act at different positions of the pathway and renders the pathway highly modular and adaptable with many possibilities for fine tuning of the signal. The prototype of the MAPK pathway is the Ras-Raf-MAPK signaling cascade.

The pathway itself may be differentiated into three main signaling cascades: extracellular receptor kinase (ERK), JNK, and p38 mediated signal transduction. They have their general mechanism of action in common, being activated by phosphorylation through a three staged kinase cascade after some sort of stimulus (see review [134] for details of signal transduction). However, their signaling outcome as well as their activation substantially differ.

The ERK pathway promotes primarily cell proliferation after activation by a variety of growth factors, like insulin, platelet derived growth factor (PDGF), epithelial growth factor (EGF) or FGF [135–138] (see review [139] for details on the molecular level) and a number of G-protein coupled receptors (GPCRs) [140] (Figure 2). Noteworthy is a close interaction with the cell proliferation promoting PI3K pathway on several levels. These interactions contain feedback-loops, cross-inhibition, cross-activation and pathway convergence, displaying a high level of signal integration of the two pathways [141]. ERK targets include the mTOR, S6K, which activate ribosomal translation (see subsection 1.2.5), and ternary complex factors (TCFs), which induce expression of immediate early genes, like Myc and Fos. The first promotes cell growth (see subsection 1.2.3), and the latter induces cell cycle progression from G1 to S phase [97,142,143]. Another transcription factor which is activated by ERK is the cAMP responsive element binding protein (CREB). CREB is best known for its role in learning, but has also been linked to regulate body size [134,144]. The ERK pathway is thus a main signal mediator for cell cycle progression, cell growth and proliferation. It is the generic answer of a cell to growth factors and indispensable in almost all developmental processes.

The JNK pathway differs from the ERK pathway, as the main input is a stress signal (like oxidative radicals, UV-radiation or pathogens) and the response is often apoptosis, but varies from senescence and cell differentiation, to even cell proliferation. How the very different signaling outcomes are regulated within the cells have not been well understood [145–147], not the least due to the diverse signals recognized [148], the many modes of regulation within each single step of the signaling cascade [148], the excessive crosstalk with other pathways [149–151], and the miscellaneous affected proteins, which eventually translate the signal into function [152, 153]. Activated JNK phosphorylates and promotes the function of Jun, activating transcription factor (ATF), FoxO, and p53 transcription

factors [152, 154], which induce apoptosis in the cell [145, 146, 149, 150].

The p38 pathway is alike to the JNK mediated signaling cascade in terms of signal reception and cell fate determination [134, 155]. The stress signals which are sensed are various and molecular mechanisms have been found for the integration of endoplasmatic reticulum (ER), oxidative, inflammatory, metabolic, and genomic stress [156]. Accordingly, the cell response to p38 activation is associated with apoptosis, inflammation, autophagy and senescence [156]. The main effector genes of p38 signaling are members of the activator protein 1 (AP-1) complex (ATF activation), p53, and p14ARF (a cell cycle progression antagonist which activates p53 [157]) [155, 156]. Thus, the p38 pathway is an important regulation for apoptosis in response to many environmental and intrinsic stresses, contributing to the control of total cell number in an organism.

1.2.7 PI3K signaling

Another central cellular signaling cascade regulating proliferation and growth, with many inputs and similar galore signaling modulating steps is the PI3K signaling pathway (Figure 2). All PI3Ks phosphorylate inositol-phosphate, which generates phosphatidyl-inositol-2-phosphate (PIP2) or phosphatidyl-inositol-3-phosphate (PIP3) or both, though differences in substrate specificity and reaction capability of the PI3Ks have been reported [158]. The PI3Ks are categorized in three different classes (I-III), with class I PI3K being well understood, while class II and III PI3Ks are still rather enigmatic in terms of function. The generated membrane lipids PIP2 and PIP3 can serve as second messengers for various targets [158, 159]. PI3K of the class I and II are activated via receptor tyrosine kinases (RTKs), GPCRs or small G-proteins like rat sarcoma (Ras) [160], while the PI3K class III protein is induced by AMPK and is rather known for its role in autophagy [161]

Generation of PIP3 leads to the activation of PKB (AKT). PKB has various targets which can mediate proliferation, cell growth, and serve as survival signal (see [162] for review). The most important targets for cell survival would be an inhibitory phosphorylation of FoxO transcription factors, which, unphosphorylated, promotes apoptosis and cell cycle arrest [163], or the phosphorylation and inhibition of BCL-2 antagonist of cell death (BAD), a BCL-only protein (see subsection 1.2.4). Additionally, PKB indirectly triggers the p53 degradation by the activation of mouse double minute homolog 2 (MDM2). For promotion of cell growth, PKB inhibits TSC2 and proline rich AKT substrate of 40 kD (PRAS40), which in turn triggers mTOR signaling. This is especially interesting, since mTOR activity is necessary to fully activate PKB, and thus a feedforward loop is established. The proliferative effect of PKB is mediated by the phosphorylation and inhibition of cell cycle inhibitors p27 and p21 [162].

Besides activating of PKB, PIP3 can be shed by phospho-lipase C (PLC) homologs. This results in the shedding of soluble inositol-3-phosphate (IP3), which is a second messengers for the inositol-3-phosphate receptor (InsP3R) in the ER. Binding to the InsP3R releases Ca^{2+} from the ER, which can now promote various cellular responses, which include proliferation in some cells [164]. More important for proliferation and cell growth is the remaining diacylglycerol (DAG), after shedding of the phospho-inositol. DAG is a potent activator of PKC which in turn is an activator for the MAPK pathway. There are several PKC isoforms, which are mainly regulated by different compartmentalization, which stresses the importance of local PIP3 generation [165].

For regulation of the PIP3 signal, phosphatase and Tensin homolog (PTEN) and SH2 domain containing and inositol-5-phosphatase (SHIP) are needed which dephosphorylate PIP3 and thereby interrupt the signaling cascade. While the two SHIP homologs are mainly expressed and function in immune cells [166], PTEN has been reported to be

the more ubiquitous regulatory phosphatase. Only a short version of SHIP (sSHIP), has been suggested to have functional relevance in embryonic stem cells and can influence differentiation and proliferative processes, though the regulation and the mode of action remained elusive [167]. PTEN is strictly regulated by various inputs, on the level of phosphorylation, protein-protein interaction and compartmentalization. Phosphorylation is thereby mostly of inhibiting nature and is performed by several kinases, like the glycogen signaling kinase 3 β (GSK3-β) (which creates a feedback loop as GSK3-β is activated by PKB [162]). Protein-protein interactions can be performed by many proteins in generally three manners: stabilization, competitive inhibition, or changing the localization of PTEN. For instance, the PDGF-Receptor binds and inactivates PTEN upon stimulation of growth factors [168]. This renders PTEN another possible PIP3 regulatory factor which modulates signal intensity and duration.

The PI3K pathway mediates a general proliferation and growth signal for the cell, which can be activated by many factors and conditions and can result in various cell reaction. It is tightly regulated on several steps with many side roads, and show intensive crosstalk with other major growth mediating signaling pathways, like the mTOR and MAPK pathways. Its central role in body size regulation was found in the reduction of PTEN levels in *Drosophila*, which increased total body size in larva and adults [169] or the control of PKB as deregulation causes size phenotypes in mammals and insects [170–173].

1.3 Insulin signaling as master control for cell proliferation and size determination

The insulin/IGF signaling (IIS) pathways is highly conserved among all metazoa from porifera [174, 175] to human [176]. It is the global sensor for nutrient availability in the organism and regulates cell growth as well as proliferation on the cellular level, but also shows implications in aging on organismal level [177]. Furthermore, the signal mediates several anabolic functions, like lipid and glucose storage, glucose uptake into cells or decreased lipolysis. How the signal in the cell is received and relayed depends on the ligand which is recognized, the cellular state (e. g. senescent vs. mitotic), and the expressed repertoire of signal cascade members and effectors. Besides its metabolic function, IIS acts on all pathways portrayed above (see section 1.2) via different mechanisms (Figure 5). The signal can be interpreted by the cell as anabolic, mitogenic, or both (or even not at all), dependent on the cell type, its expression profile, and its microenvironment.

The IIS is conveyed by the expression and secretion of insulins, IGFs, or insulin like peptides (ILPs) by usually a specialized tissue or cell type. Common is the expression of the ligand in the metabolic organ, like the liver in mammals [178], or the fat body [179] and the midgut [133] of *Drosophila*. Another reoccurring site of expression in invertebrates are neurons like in *Drosophila* [133] and *C. elegans* [180]. These two cells/tissues express ILPs not by chance, they fulfill important sensory function, mainly for nutrient availability and secrete ILP upon the nutrient stimulus. However, neurons expressing ILP can receive inputs from contacting neurons, which dramatically expands the number of potential signals which cause or modulate ILP secretion [181]. Given the expansion of the ILP homolog family in invertebrates (up to 40 in *C. elegans*), while there is usually only one receptor, it appears very likely that the distinct ILPs are differently regulated, respond to varying environmental signals, and induce different signaling outcomes. For instance, *C. elegans* uses its 40 ILPs to generate a network of ILP crosstalk, which fine tunes the response to certain nutrients and, depending on this, modulates the entry and exit of dauer states or the expansion of lifespan [182]. In mammals IGF production is regulated by the release of GH from the pituitary gland in the brain, which resembles another layer of regulation

and links neural sensory machinery to IGF release [183]. However, the integration of the nutritional signals (and others) appear to be species specific and a general concept of how ILPs are generated and secreted is missing.

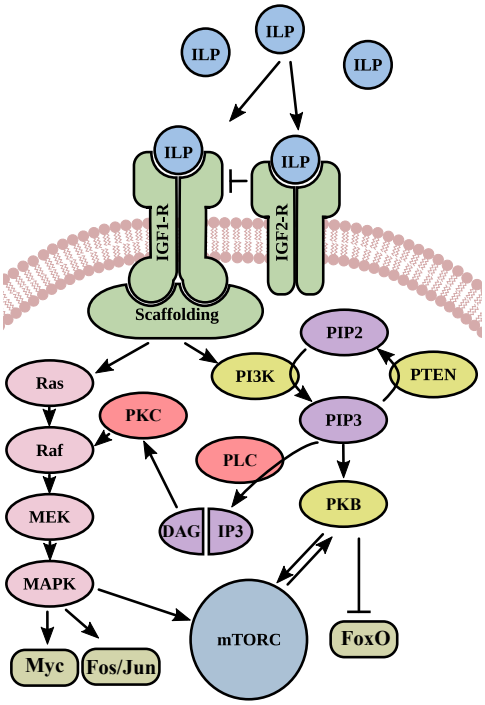

Figure 5: *The IIS pathway and its key downstream components regulate all important cell cycle/cell growth mechanisms. The displayed pathway shows the molecular interactions conserved among various species (see 1.2).* Hydra *possesses all the components displayed, which suggests a conserved mechanism of action even in prebilaterian organisms.*

On the receptor site, the pathway is clearly defined and there is usually only one insulin/insulin like peptide receptor (INSR) in invertebrates and two INSR (the insulin receptor and the IGF receptor) in vertebrates. The receptor is a classic growth factor receptor, which consists of a homo- or heterodimer containing an intracellular tyrosine kinase. Upon ligand binding, the tyrosine kinase becomes active, undergoes autophosphorylation, and generates SH-domain binding sites, which become occupied by scaffold proteins. These are again phosphorylated by the RTK and bind now specific proteins which mediate the function in the cell. Much of the signaling outcome for the cell is determined by the type of adapter protein and possible binding partner, which are present or absent in the cell. In mammals, the major factors for IIS relay are insulin receptor substrates (IRSs), which almost always activate the PI3K and the MAPK pathways [184–187] though specific functions for the different isoforms have been described [188–193]. IRS can also directly function as transcription factor to induce Myc and cyclin D expression [194] and is additionally a point in the cascade where much modulation takes place [195–198].

Further classical scaffold proteins which also activate at least one of the MAPK or PI3K pathways include IRS/downstream of kinase (DOK)-proteins, SHC, and growth factor receptor bound protein (GRB) associated binding protein (Gab) 1 [199–201]. There exist also inhibitory and enhancing scaffolding proteins like GRB10/GRB14 [202–204] and

SH2B [205], respectively.

Noteworthy is the reduced amount of docking proteins in *Drosophila*, which contains only three scaffolding proteins: Chico (the fly IRS1 homolog), Lnk (the SH2B homolog) and dreadlocks. Similarly, *C. elegans* utilizes only one known IRS, which is not even necessary for vital signal transduction but for potentiation of the response [206]. However, both invertebrate receptors contain a C-terminal extension, which resembles structurally and functionally the vertebrate IRS and is sufficient for transduction of the IIS [207–209]. This evolutionary diversification reflects the hub position of the IIS, which integrates environmental cues to regulate crucial developmental and metabolic responses in a variety of vertebrate tissues. Tissue specific expression mediates the diverse functions of IIS in higher organisms, while in invertebrate a single receptor, with a few modulating docking proteins are sufficient to convey a cell specific, though more general signal.

The most important signal of the IIS is the repression of FoxO, which is associated with survival, growth and proliferation. FoxO is phosphorylated by PKB after PI3K pathway activation, which leads to exclusion of FoxO from the nucleus and represses its transcription factor function [163]. Activation of FoxO also occurs by phosphorylation, for example by AMPK (see 1.2.5). FoxO itself induces an array of proapoptotic and cell cycle arrest genes including: p27, p21, p15, BCL-2 interacting mediator of cell death (Bim), first apoptosis signal ligand (FASL), and 4EBP [210,211]. Another key function of FoxO is the antagonism with Myc. Active FoxO promotes the expression of Myc associated factor X interacting protein (MXD) which bind to Myc promotors and prevent Myc transcription activity [212]. Additionally, FoxO increases the expression of micro RNAs (miRs) which target the Myc mRNA [212]. IIS reduces the nuclear availability of FoxO and thus promotes growth factor functions by interfering with FoxO as cell growth repressor.

SNP's in the human FoxO gene are associated with a reduced height and longevity [213]. Deregulation of FoxO was associated with a change in total body size in several model organisms [211, 214–216]. This stresses the important function of FoxO in body size regulation *in vivo*. Furthermore, FoxO has been linked to the induction of ecdysone in the fly [217], which promotes sexual maturation. Thus developmental staging of *Drosophila* dependents on the nutrient levels of the animal. This renders FoxO to a possible environmental sensor which influences development. FoxO has also been described to integrate signals other than IIS, to promote cell cycle and growth inhibition, e. g. by direct binding of HIF or JNK signaling, which both induce its transcriptional activity [123, 218].

Since IIS regulates all major pathways for cell growth and proliferation (PI3K, MAPK, and mTOR) it is not surprising that IIS has been identified as the most important and consistent regulator of body size throughout the animal kingdom. From *C. elegans* to *Drosophila* and mammals it was associated with body size regulation [169, 188, 219–222]. It thereby integrates the energy levels and available nutrients and determines growth phases during development. It might be interesting to see what effect IIS has on growth characteristics of temperature challenged animals, and whether environmentally plasticity of an organism is mediated by IIS. The IIS regulates many metabolic processes, which are as well temperature dependent, and the expression of ILPs or its regulatory molecules takes place in sensory organs, the IIS pathway a good candidate for environment dependent body size regulation.

1.4 *Hydra* as a model system

Hydra is a model system for regeneration and developmental biology since its discovery by Abraham Trembley in 1744, who described regeneration after cutting and the possibility to transplant small pieces of tissue within one species [223]. *Hydra* was used to generate the

developmental organizer concept by Ethel Brown Harvey, which was later recapitulated and Nobel price awarded by Spemann and Mangold in amphibians [224, 225]. This long history as a model system fashions *Hydra* a well investigated organism, with a good understanding in its cell and developmental biology and since recently its genetics. With the advent of a fully sequenced genome [226] and the possibility of genetic manipulation [227], *Hydra* can be used for functional studies on a molecular level. Combined with its simplicity on the cellular level and its easy cultivation, *Hydra* renders an ideal model to study body size under changing environmental conditions.

1.4.1 Taxonomy and life history of *Hydra*

Hydra is a genus within the phylum of Cnidaria. The latest phylogenetic study delineated 28 species, which can be divided into four groups: the viridissima (green algal bearing *Hydra*), the braueri, the vulgaris and the oligactis group [228]. Most of the lab strains used, belong to the vulgaris group. While naming was very inconsistent in the past, it is difficult to clearly assign the right names to the different species, but it should be noted, that the *Hydra vulgaris* AEP strain used in this study, is identical to *Hydra carnea*, *Hydra littoralis*, and certain *Hydra vulgaris* strains [228]. The valid name for this strain is most likely *Hydra carnea*, but for conformity with previous studies I will use *Hydra vulgaris* AEP throughout the text.

Within the Cnideria *Hydra* belongs to the class of Hydrozoa, the order of Anthomedusae and the family of Hydridae. Cnideria diverged from Porifera and Placozoa by the possession of real tissue with adherens junction and a nervous system [229, 230]. They are radial symmetric, so they miss a secondary body axis and they contain only two blastodermic layers, which separates them from the Bilateria [231–233]. All Cnidaria possess a specialized cell type, the cnidocyte (or nematocyte), which are stinging cells for defense or predation [234, 235].

Hydra is one of the few Cnideria which live in freshwater ponds and lakes, and can be found around the world. It can tolerate a wide range of temperatures and, though sessile, is able to actively move, through sommersaulting, crawling, or undirected drifting [223]. Drifting is mediated by a bubble of air which is generated at the foot of the polyp, which usually produces a mucin for adhesion to various substrata.

For reproduction, *Hydra* can produce gametes, which forms egg shelled embryos [236–238]. These develop within two to four weeks to a complete small *Hydra* [239]. More common, however, is asexual reproduction through budding [240]. With enough food, the polyp growths and eventually develops a small protrusion in the body column at around two third of the distance from head to foot. This protrusion generates a secondary axis and growths within 2-5 days, develops a foot and a new small polyp detaches [240, 241]. The majority of the cells comprising the bud, originate from the mother polyp, which migrate into the new polyp, while only a small portion of the cells in the offspring are generated by proliferation within the bud [242, 243].

1.4.2 *Hydra*'s body plan and cellular composition

Hydra has a fairly simple body plan which consists of a head, containing a hypostome surrounded by a ring of tentacles, a body column, and foot structure consisting of a stalk and basal disk for attachment to different surfaces (Figure 6a) [223, 244]. The single oral-aboral axis is patterned by the Wnt machinery and its signaling center is located in the hypostome [245–247]. Transplantation of this signaling center is capable of inducing a secondary axis in the body column of the recipient polyp and was the first evidence

of the organizer concept [224]. Interestingly, the position in the recipient, as well as the transplant localization in the donor, influences the chance, whether a head can be induced or not [248, 249]. Even more astonishingly, exactly this behavior was predicted by the diffusion rates in a self-organizing morphogenetic field by Turing, which was later specified for *Hydra* by Gierer and Meinhardt [250, 251]. This places the Wnt signaling pathway in the center of head, and thus axis formation, in *Hydra* and is important for head regeneration as well [245, 247, 252]. As bud formation resembles head formation in most parts, it requires Wnt signaling on the one hand, but has also been linked to TGF-β and FGF signaling [245,253,254]. However, transplantation of head tissue into the budding region of a donor polyp resulted in the formation of a new head, but did not lead to detachment of the resulting secondary axis [240]. This indicates, that head and bud formation are similar on the molecular and cellular level, but are still distinct processes, which are differentially regulated.

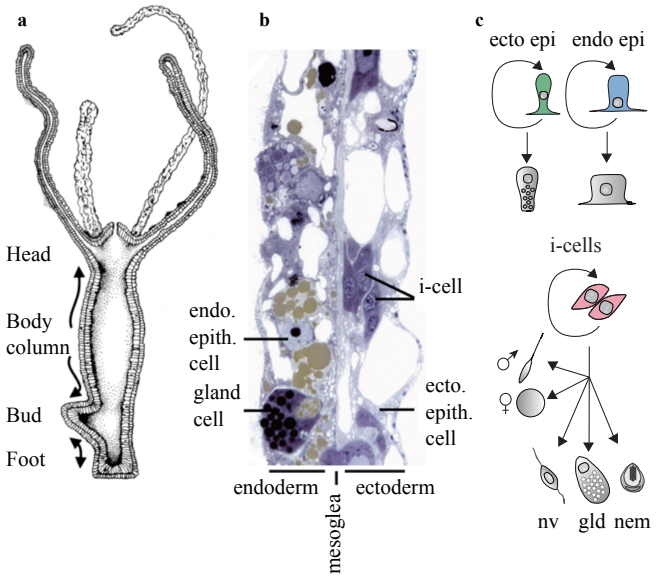

Figure 6: *The morphology and cellular composition of* Hydra. *(a) A tube like body column, with a head and a foot structure describes the body plan of* Hydra. *The head consists of a hypostome and a tentacle bearing ring. The foot contains a basal disk, which produces a sticky secrete for adhesion to substrate. (b) The histological image illustrates the two different epithelial layers separated by the mesoglea. Within the tissue distinction between ectodermal and endodermal epithelial cells, interstitial cells, and gland cells is possible. Adapted from [255]. (c) The unipotent epithelial stem cell lineage are able to self reproduce, while i-cells additionally give rise to nerve cells (nv), gland cells (gld), nematocytes (nem) and gametes. Adapted from [256].*

Histologically, *Hydra* consists of two cell layers, the endoderm and the ectoderm, which are separated by a basal lamina, the mesoglea (Figure 6b). On the the cellular level, *Hydra* has only few cell types which derive from three stem cell lineages [257]. The structurally important cells are the two (endodermal and ectodermal) epithelial cell lines, which both constitute separate unipotent stem cell lineages. All other cell types (including gametes, nerve cells, nematocytes, and gland cells) derive from the third stem cell lineage, the i-cells. As the name already suggests, the i-cells are embedded in the ectodermal epithelial

cell layer (Figure 6c). All stem cells undergo constant and rapid cell cycle [258, 259]. Interestingly, the different cell lineages divide at a different pace. While i-cells go through mitosis every ≈24 h, cell cycle length for epithelial cells is around ≈3.5 - 4 d [258,259]. This difference in proliferation rate is also reflected in the total cellular composition, as around 80 % of all cells are i-cells and its derivatives. The remaining 20 % are provided by the epithelial cells in closely equal parts [260]. However, for size determination, the relevant cell lineages are the epithelial cells. They determine the morphology of the polyp [261,262] and have been a good proxy for body size before [242, 263].

Proliferation of the cells is restricted to the body column, from where the cells are displaced to head and foot [243, 264, 265]. The cell cycle progression is astonishingly robust against environmental cues. It has been shown, that neither starvation, nor lower temperature had a significant effect on the proliferation rate or cell cycle length of epithelial cells [263, 266]. This contrasts the expectation in several ways: starving animals become smaller, as do overfed animals increase in size which is reflected in adjustment of epithelial cell numbers [242, 266]. Further, *Hydra* responds to cold temperatures as expected from the TSR and increases in size, again mirrored in an increase of epithelial cell number [263]. This implicates different mechanisms for size regulation than adjusting proliferation rates to nutrient availability or temperature (and thus possibly to oxygen levels). As polyps do shrink with low nutrient levels, the question arose, how the necessary energy was provided to the dividing cells. Bosch and colleagues already suggested cell death and autophagy as a possible mechanism to cope with malnutrition [266], although the apoptosis concept was still unknown at the time. Later, it became clear that the mechanisms and molecular machinery of apoptosis exist in *Hydra*, though the exact physiological trigger for its activation remained unclear [267, 268]. However, preliminary data suggest that the same trigger as in higher organisms lead to apoptosis in *Hydra* and that reduced IIS and activated FoxO may mediate an apoptosis signal [269, 270]. The importance and to what extant apoptosis contributes to tissue homeostasis and integration of environmental signals, has not been addressed to date.

1.4.3 Insulin/insulin like growth factor signaling in *Hydra*

The IIS pathway is present in *Hydra* as an INSR and three putative ILPs have been identified [271,272]. Furthermore, downstream effectors like PLC, PKB or FoxO have been identified and functional analysis showed that FoxO mediate important stem cell functions in *Hydra* [273–276]. Since the sequencing of the *Hydra* genome [226] and the availability of transcriptomic data [256] it became clear, that all essential parts of the IIS pathway are present in *Hydra* (Figure 5) and are conserved before the evolution of a circulatory system and the onset of Bilateria. The functions of the downstream targets of the IIS seem to be conserved as well in *Hydra* as treatment with inhibitors for PI3K causes apoptosis and cell cycle regression [277, 278], the interference with ERK reduced proliferation [277], and the inhibition of mTOR induces autophagy [278]. Intriguingly, starvation does not or only mildly induces expression changes of ILP, which raises the question of what function the IIS fulfills, if it does not respond to nutrient levels of the tissue [279]. MAPK and PI3K signaling have been shown to be necessary for head regeneration, implying a role in organizer function [280, 281]. Whether the pathways are actively regulated during regeneration or whether they have a permissive role in the process, remained elusive.

FoxO as a major signal transducer for IIS seems to have diverse and tissue specific function in *Hydra*. Initially it has been described as an integrator for stress signals which promotes apoptosis [270, 275], but later it has been established as stem cell factor in *Hydra* [276]. Reduction of FoxO by coexpression of a hairpin (HP)-construct in epithelial

cells resulted in a reduction of the stem cell compartment, and a slow growth phenotype, while overexpression of FoxO induced stem cell genes in terminally differentiated cells of the i-cell lineage [276].

The unresponsiveness of IIS and cell cycle to nutritional signals, as well as the inverse function of FoxO in *Hydra* suggests a different ancestral function of IIS than in Bilateria. However, nutrients are sensed and integrated in the molecular pathways, as different feeding regimes show an influence on the budding rate, and starvation leads to a shrinkage of the polyps, while staying structurally integer [242, 266]. If IIS regulates body size in *Hydra* and by what means is unknown to date.

1.5 Aims of the study

The asexual reproduction mode of *Hydra*, its constantly proliferating stem cell pool, and its regenerative capacity necessitates constant pattern formation in the polyp, which controls the dynamics and spatial organization of cellular processes to generate a functional and morphological integer polyp. This attributes *Hydra* with many embryonic features and high adaptive capacity which has great advantages for experimental developmental biology. Genetically identical clones can easily be generated and developmental processes can be observed in different environmental and experimental set ups. However, it brings certain issues with classifications with it. Is the *Hydra* of determinate or indeterminate growth? It reaches stable sizes in terms of cell number but never reaches a state of 'adulthood', where proliferation of most cells ceases and tissue growth terminates. Environmental triggers, like temperature, dynamically alters the set point for size determination and a single animal can obtain different sizes during its life time. There has been an IIS pathway described in *Hydra*, but no function could be attributed till now. This led to following questions, which I aimed to answer in this thesis:

1. Can one derive a conceptional model for tissue homeostasis of *Hydra*?
    - Does an application of the 'critical size' concept provide reasonable results to predict developmental processes and population trajectories in *Hydra*?
    - What are the boundary values for stable tissue homeostasis and what impact do they have on the biology of *Hydra*?
    - Is apoptosis important in such a model and what implications does it have for the size determination of *Hydra*?
2. How is body size regulated in *Hydra*?
    - How does *Hydra*'s body size change upon different temperatures?
    - What is the role of the IIS pathway in size regulation of *Hydra*?
    - How are both signals integrated into known developmental pathways in *Hydra*?

2 Chapter I - The 'virtual *Hydra*': *in silico* predictions match experimental size, cell growth, and population growth in *Hydra*

2.1 Introduction

Homeostasis of a multicellular organism is marked by an intricate balance between stem cell proliferation, differentiation and death. Depending on this balance, the organism is either growing, fading, or in equilibrium for its cell dynamics. Developmental biology is currently focused on the isolated effects in the developmental phase (usually the growing phase) of oganisms, like the differentiation routes of stem cells, the transmission of position information or the tracking of single cell lineages. However, developmental programs take place in a growing organism, which comprises all organs/tissues and its developmental regimes. A model is needed that combines the mechanistic effects of growth with the developmental programs on a cellular level, to get a holistic understanding of the development of a complete organism. This model is than able to identify underestimated aspects of the biology of the organism and can provide insights which go beyond solitary molecular, cellular and mechanistic predictions.

Hydra is one of the oldest model system for developmental biology [223] and has since been established in research for cell biology, evolution and host-microbe interaction [269, 282–287]. Its simple body plan and its assessable cell composition, renders *Hydra* an ideal organism to derive general concepts and transfer the knowledge to more complicated systems. Research of recent decades yielded detailed understanding of cell type complexity, cell proliferation kinetics, cell number dynamics and developmental time frames in *Hydra*, providing enough information to derive such a holistic model.

It has a simple body plan which resembles a tube-like structure with one main body axis, which is only broken by a developing bud [253], appearing $\approx \frac{2}{3}$ from head to foot on the body column [241]. *Hydra*'s main reproduction route is asexual through budding and has important functions for cell homeostasis by removal of excess cells [242].

On cellular level, *Hydra* consists of three constant proliferating stem cell lineages: interstitial, endodermal and ectodermal cells. The two latter are epithelial and determine morphology and size of the polyp [261, 262]. The third i-cell lineage contributes only little, if any to the morphology or size. Epithelial cells undergo constant mitosis every 3.5-4.5 days and their proliferation rate is remarkably robust [258]. Even drastic changes in environmental conditions, like temperature decrease [263] or starvation [266], do not significantly change the mitotic rate of these cells. The amount of generated epithelial cells thereby exceeds the number of cells which are lost by cell death [242]. In order to maintain cell homeostasis, excess cells are displaced into buds for asexual reproduction. Additionally, the components of the apoptosis machinery have been identified [267]. Furthermore, regulated cell death has been described as driver for regenerative processes [281] and is considered to have important functions for cell homeostasis [270].

This framework describes *Hydra*'s whole structural cell system and forms the basis for population growth as an asexual reproducing organism. The simplicity of these processes and their dependencies allows the development of a 'virtual *Hydra*', a compact description of an organism with a few mathematical tools. Here, I develop and validate a simple, yet informative holistic model that simulates cell homeostasis, growth and development for *Hydra*. It can be used to assess fitness (population growth), derive yet unknown parameters (for instance apoptosis/cell death rates) and interpret the results of genetic manipulations.

2.2 Results

2.2.1 Modeling the growth of *Hydra*

The simple metazoan *Hydra* comprises only two epithelial cell layers which define the size and morphology of the polyp. It is feasible to model the growth assuming a constant proliferation rate of these cells, opposed by a constant rate of cell death (Equation 1). These two factors should be sufficient to model the growth of a small polyp, which just hatched from an egg or detached from a parent polyp. The current cell number x_t at a certain time point t is then given by the initial cell number x_0 at time point $t = 0$ added by the cells which where generated due to proliferation and reduced by the number of cell death which occurred. These can be expressed as fractions of cells which divide (p) or die (d) within a certain time frame (τ_p and τ_d, respectively). Hereafter the combination of both parameters, cell fraction and time frame, will be referred to as proliferation and cell death rates, respectively.

$$x_t = x_0 + x_0\left(p^{(\frac{t}{\tau_p})} - x_0 d^{(\frac{t}{\tau_d})}\right) \tag{1}$$

If the polyp eventually reaches the critical size (adulthood in other words) for the given conditions, a bud is initiated at time t_i. Excess cells are then deposited into the bud and an equilibrium between proliferation, cell death and cell loss by budding (x_{dep}) is established. This adds a boundary condition to the equation 1 (Equation 2).

$$x_t = \begin{cases} x_0 + x_0\left(p^{(\frac{t}{\tau_p})} - d^{(\frac{t}{\tau_d})}\right), & \text{if } x < x_{crit} \\ x_0 + x_0\left(p^{(\frac{t}{\tau_p})} - d^{(\frac{t}{\tau_d})}\right) - (t - t_i)x_{dep}, & \text{if } x \geq x_{crit} \end{cases} \tag{2}$$

The cells deposited into the bud within a certain time frame can be derived from the number of epithelial cells in a bud right after detachment and the fraction of the cells, which the bud gained without proliferation. According to the literature, the amount of cells, which are deposited from the parent polyp to the bud was assessed to $\approx 80\,\%$ over the course of the development of the bud [265]. x_{dep} is thus calculated by equation 3, where x_{bud} is the epithelial cell number of a freshly detached bud, N is the number of initiated buds, and ΔT_2 is the developmental time of the bud. ΔT_2 in turn is defined as the time, between initiation of the bud by the parent polyp, until the bud finally detaches and lives on as an individual (Figure 7a).

$$x_{dep} = \sum_{i=1}^{N} \frac{0.8 x_{bud,i}}{\Delta T_{2,i}} \tag{3}$$

Knowing the amount of cells deposited from the parent polyp and assuming the same proliferation and cell death rates, one can estimate the bud size at a given time (Equation 4).

$$x_{bud,t} = x_{bud,0} + x_{bud,0}\left(p^{(\frac{t}{\tau_p})} - d^{(\frac{t}{\tau_d})}\right) + t x_{dep} \tag{4}$$

A bud will detach if a given bud size is reached, which establishes a new polyp where the mechanisms of equation 2 can be applied. Repeating this procedure would simulate a whole population of polyps and predicts values for important developmental times like ΔT_1, ΔT_3, and the population growth rate (PGR). These parameter are defined as follows: the time a freshly detached bud needs to reach critical size and initiate a new bud itself (ΔT_1), the time which passes between two subsequent bud initiation events on the same

parent polyp (ΔT_3), and the fraction of polyps in one population generated anew within one day (PGR)(Figure 7). Note that the reciprocal of PGR equals the doubling time of the population.

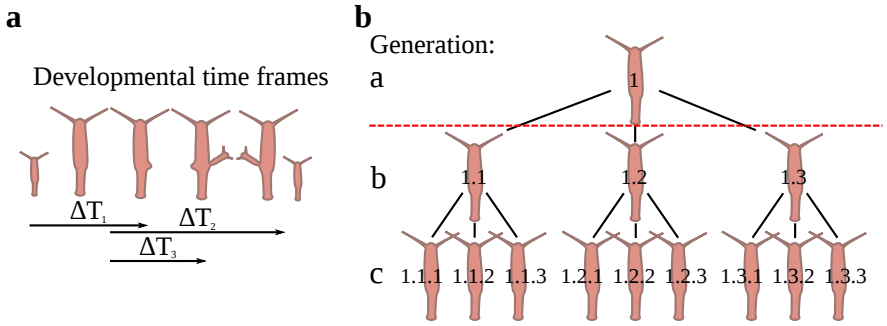

Figure 7: *Experimental setup for the growth rate experiment. (a) The important developmental time frames include the time from a freshly detached bud to an adult polyp, itself initiating a new bud, ΔT_1, the time a bud develops on the parent polyp until it detaches, ΔT_2, and the time between two bud initiation events, ΔT_3. (b) A growth rate experiment was started with only one polyp, following up its offspring and recording crucial developmental time frames for each polyp in the experiment. For growth rate calculation animals of the "b"-generation were treated as founder of a new growth rate experiment and served as biological replicates (dashed red line).*

2.2.2 Validation of the 'virtual *Hydra*'

Critical values of three genotypically different *Hydra vulgaris AEP* lines (F2A4, D11a[1], and C1-1) were measured to validate the described model. All polyps tested were reared at stable and equal environmental conditions and with a standardized feeding regime. Epithelial cell proliferation was estimated using Bromodeoxyuridine (BrdU) labeling rates after incubation for 72 h in BrdU. The fraction of epithelial cells which divided within the 3 d varied between 56 % and 72 % for the three lines (Table 1).

Table 1: *The table displays mean values and standard deviations for growth rate and cell proliferation rates (after a 72 h BrdU-labeling).*

Line	PGR	BrdU 72 h
F2A4	0.21 ± 0.02	0.68 ± 0.02
D11a	0.28 ± 0.06	0.72 ± 0.03
C1-1	0.19 ± 0.05	0.56 ± 0.05

Epithelial cell numbers of adult polyps and freshly detached buds were assessed by flow cytometry. Adult size was defined as a polyp, which has just initiated a bud protrusion, which is also considered as maximum size. In contrast to maximum size, I will refer to a second size value, the critical size, which is the size, where budding is initiated. Both values almost coincide *in vivo*, while the first describes the potential maximum size a polyp can reach, the critical size is a threshold, where the polyp decides to cease growth and

[1]The D11a line is the control line to a FoxO-knockdown (KD) line, which was analyzed by Benedikt Mortzfeld [288]. All values concerning this line given here is result of his research.

starts reproduction. As the simulation will instantly induce a bud after the critical size was passed, I will assume that critical size approximately equals maximum size. However, only maximum size is experimentally assessable to date and served as reference point. All three lines significantly differ in maximum size, with polyps of the F2A4 line gaining most epithelial cells ($20,871 \pm 2,993$, mean $\pm$ SD), C1-1 being the smallest line ($9,903 \pm 2,447$) and D11a ranging between the other two lines ($15,616 \pm 2,050$)(Figure 8a). The bud size scales with the adult polyp size, thus the F2A4 line produces buds with most epithelial cells ($11,320 \pm 1,868$), followed by the D11a line ($8,200 \pm 1,510$) and the buds of the C1-1 line being the smallest of the tested ($5,713 \pm 1,163$) (Figure 8b). While I observed significantly different maximum sizes in the three investigated lines, the tissue dynamics should follow the same basic principles. This allowed me to test the developed model for consistency and stability throughout the experimentally used lines.

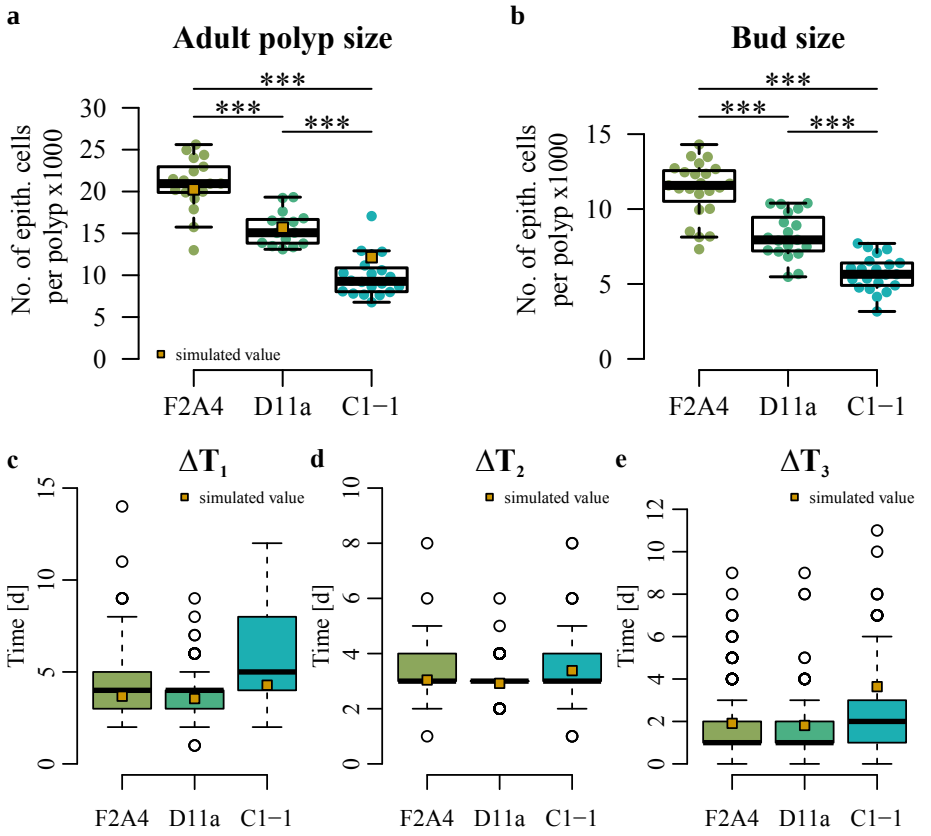

Figure 8: *Experimental data is needed to feed the model. After a simulation of the 'virtual* Hydra*' has been run the predictions fit experimental data, which where not used for feeding the model. Epithelial cell number per polyp was measured for (a) adult polyps, which just initiated a bud protrusion and for (b) buds which just detached from the parent polyp and used as input parameter to simulate cell dynamics in* Hydra*. Furthermore, developmental time frames (ΔT_1, ΔT_2, and ΔT_3) were assessed to use ΔT_2 as another input parameter. The other developmental time frames served for validation of the 'virtual* Hydra*'. Predicted values from the simulation (yellow squares) fall into the data range of the experimentally acquired data.*

Furthermore, I determined the developmental times (ΔT_1, ΔT_2, ΔT_3) and the PGR by a population growth rate experiment. The experiment was started with a single polyp, which was fed four times the week and followed up on its progeny until a number of at least 100 polyps were reached (Figure 7). For each single polyp the developmental times were recorded. Since the *Hydra* lines grow clonally, the experiment was split in the second generation (the direct offspring of the initial polyp) and analyzed independently, in order to calculate the PGR. The results of the analysis did not differ dramatically between the three lines and are given in figure 8c-e and in the tables 1, S1, S2.

With this analysis, all values except the cell death rates were evaluated to run a simulation. Cell death can be roughly distinguished into apoptosis and necrosis (though with many intermediate states). Necrosis is the form of cell death which is primarily induced by extreme environmental conditions and happens rarely under physiological conditions [289]. Thus, the major factor for cell loss in *Hydra* is caused by regulated apoptosis, which, for the sake of simplicity, I will consider as only cause for cell loss hereafter. Though multiple efforts have been undertaken to detect apoptotic cells [266–270, 290], determining apoptosis rates in *Hydra* is difficult for various reasons: (I) Dedicated assays usually measure apoptosis at the given point of analysis, but not apoptosis rates. (II) The assay needs to discriminate between cell lines, which requires preservation of cell morphology for quantification, which is not given for all apoptosis assays. (III) DNA-based apoptosis assays are masked by DNA-containing food vesicles in the epithelial cells of *Hydra*. There is only one rough approximation of apoptosis rates in *Hydra* by Bosch *et. al.* [266] which translates into 18 % loss of epithelial cells within 72 h.

With this, the formulas can be filled and a 'virtual *Hydra*' can be simulated. For the critical size I decided to use the upper boundary of the standard deviation to account for the largest reasonable value of maximum size ($\approx$ critical size) at the given conditions for the respective *Hydra* line while staying rather close to the mean of the experimental data. Utilizing the real data points I simulated the experiments, similar to the ones performed to determine the PGR, ΔT_1, and ΔT_3. The simulations, matched the real data, giving a similar range of values for the developmental times, growth rates and mean cell number per polyp (Figure 8, 9 and Table S2). The simulated values of the developmental times and the epithelial cell number are all within one standard deviation of the measured data. This gives good evidence, that the theoretical consideration for growth and cell homeostasis are correct, resulting in a valid model, which describes cell dynamics in *Hydra*.

Interestingly, simulated growth rates are constantly overestimated (Figure 9b,c,d). This might result from an optimized growth situation in the simulation. Fluctuation of budding rates of single polyps in the real data, depending on their position in the family tree, can have serious impact on the growth rate of the whole family. Polyps which appear early in the family tree and show some minor defect in first bud initiation or a little slower budding rate will decrease growth rate rather dramatically. Their offspring appears later, already decreasing the PGR, and the imposed delay on the offspring's progeny amplifies this effect further. Additionally, feeding of the animals was restricted to four times the week, which might cause further deviation from an ideal growth situation. However, the simulation gave reasonable results for all values evaluated, making it a valuable tool to understand the interplay between size, proliferation/apoptosis, developmental time frames and PGR. Furthermore it can be utilized to predict mechanisms underlying observed phenotypes in PGR or developmental time frames.

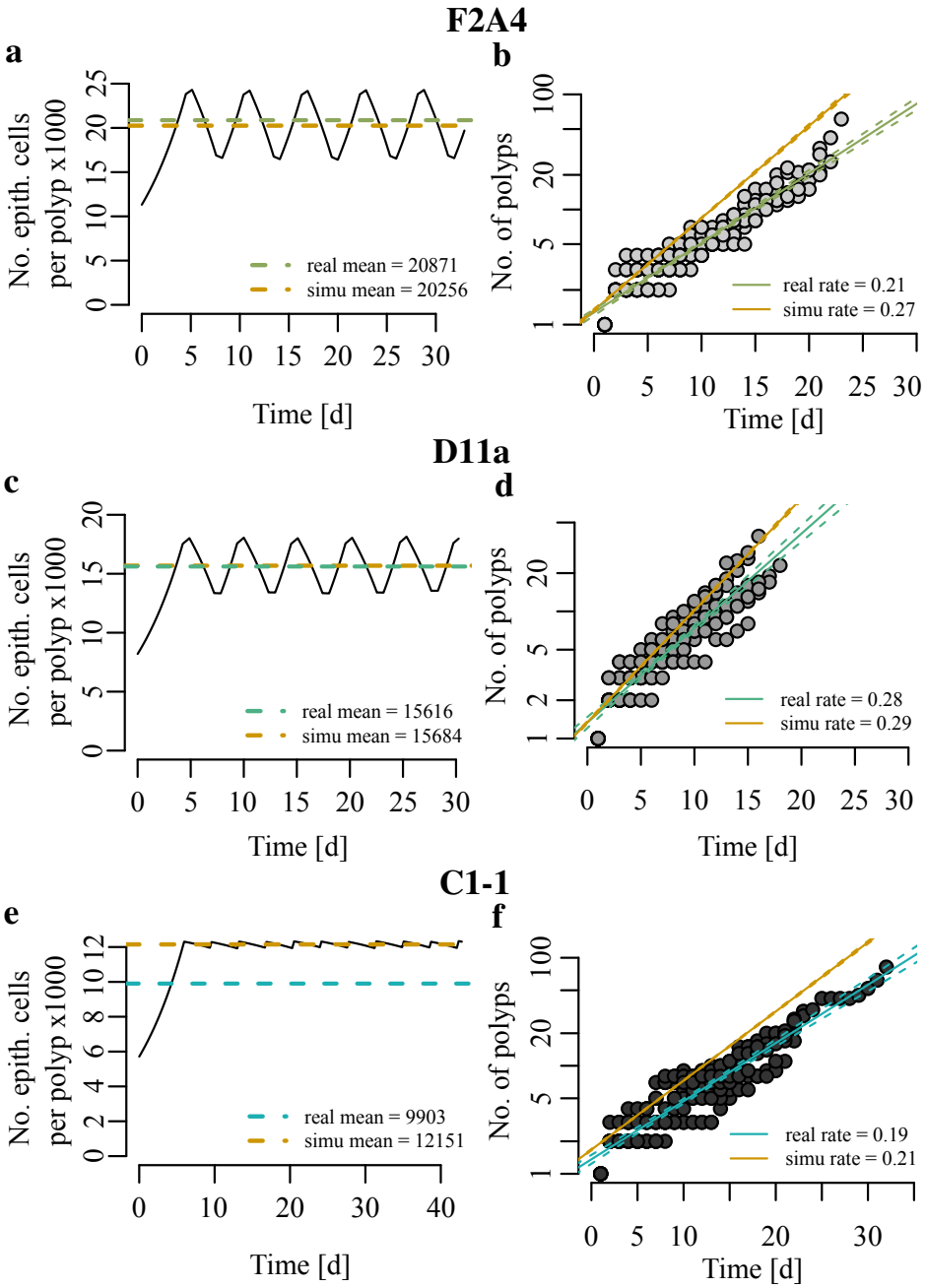

Figure 9: *The 'virtual* Hydra*' yields growth trajectories for a epithelial cell number per polyp (black line) and whole populations (yellow regression line). Comparison of mean cell number of the founder polyp in the simulation is in good concordance to the experimental data (a, c, e). Additionally PGRs were simulated and compared with the ones which were assessed experimentally (grey dots and green/blue regression lines) (b, d, f).*

2.2.3 Interplay of different simulation factors

To investigate the interplay of different simulation parameters, I simulated the change of a single input factor over a range of values, while all other input parameters were fixed, and analyzed important factors like size, developmental times (ΔT's) and PGR. To have a basis to simulate the different changes in the simulation, I generated a 'model polyp', by averaging the values for the three control polyps analyzed above (see Table 2 for values). Starting with this standard polyp I changed the values for the proliferation and apoptosis rates, the maximum size, the bud size, and the bud developmental time (ΔT_2) to assess their effect on the aforementioned factors.

$$x_t = x_0(p-d)^{\frac{t}{\tau}} \tag{5}$$

The proliferation and the cell death/apoptosis rates are directly coupled to each other. Assuming $\tau = \tau_p = \tau_d$ the equation 1 can be expressed as displayed in equation 5. Hence, the term $p - d$ can be considered as a proliferation index p_{ind} as long as $p > d$. For exploration of the variable space I used this proliferation index to describe the dependence of mean cell number of a polyp, the PGR, ΔT_1, and ΔT_3 on proliferation and apoptosis, respectively (Figure 10. I varied the proliferation index from 0.1 to 1, while $\tau = 72h$).

Table 2: *Values which were determined to represent a "standard polyp" as the basis to analyze variable space in the simulation.*

	ΔT_2	BrdU 72h	Adults	Buds	Bud/Adult
Value	3.24	0.65	15,464	8,411	0.55

The mean cell number varied between 13,083 and 18,705 with changing proliferation indices, which is within the variation of a singular line if measured experimentally (compare Figure 8 and Table S1). Through the simple mechanism of budding and cell loss to progeny the increase of the proliferation index could be equalized on the level of the individual size of a polyp (Figure 10a) within certain boundaries. Striking was the rather slow increase of mean number of epithelial cells per polyp with the increase of the proliferation index until a rapid drop of average cell number per polyp. This pattern reoccurred four times over the range of the simulated proliferation indices and was depended on the number of parallelly initiated buds on the polyp and the cell loss through these. If the polyps need to recover from a relatively low cell number after bud detachment, it will spend more time with fewer cells, which translates into a lower mean cell number per polyp (compare Figure 9a, two buds initiated in parallel and Figure 9e, only one bud initiated). The continuous increase of the mean cell numbers, reflected the increase in proliferation index and thus the faster recovery from the low cell number after bud detachment. The sudden drop of cell number per polyp was then induced by induction of a new parallel bud.

The PGR depended linearly on the proliferation index (Figure 10b). With an increase in the proliferation index, an increase in the PGR could be observed. This suggests that the gain in cell proliferation of a polyp was converted in the increase of population growth, rather than into polyp size.

Consistent with that, both, ΔT_1 and ΔT_3 depended logarithmically on the proliferation index. Both values decreased with increase of the proliferation index, which means a shorter time frame was needed for the freshly detached bud to reach adulthood, as well as the time shortened between the initiations of two consecutive buds. The exponential nature of this dependence can be explained by the exponential growth which is described by the proliferation index. The developmental times ΔT_1 and ΔT_3 describe the time

needed to overcome a size differences between two states of *Hydra*'s development and thus shorten in the same manner as cells are gained, in this case exponentially/logarithmically.

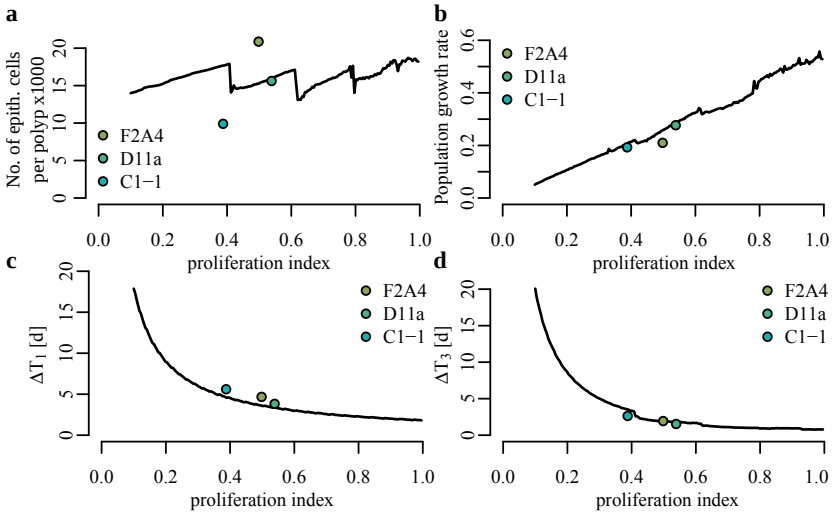

Figure 10: *Dependency of the mean number of epithelial cells per polyp (a), the PGR (b), ΔT_1 (c), and ΔT_3 (d) on the proliferation index. The green/blue dots represent the experimental data in the variant space and serve as orientation to reflect biological relevant variance.*

To explore the effect of alterations in the critical polyp size, I performed two sets of simulations. First, I increased the critical polyp size and defined the bud size as a fixed ratio of the adult size. Thus, buds became larger with the critical polyp size and consequently drew more cells from the polyp during development. This is the more natural situation, since all three measured lines, were quite different in total size but very similar in bud to adult size ratio (Figure 8, Table S1).

As expected, the mean epithelial cell number per polyp raised, as the critical cell number per polyp increased in a linear dependency (Figure 11a). Rather surprising was the fact, that neither PGR nor the developmental time frames (ΔT_1, ΔT_3) did change upon critical polyp size alterations (Figure 11b-d). This shows very impressively, that the PGR and the developmental times are independent of the critical polyp size, as long as the bud size adjusts with the polyp size.

In the second set of simulations, the bud size was fixed ($8,411$ cells, Table 2), while the critical size was changed. Fixing the bud size, while changing the critical size of the polyp had more drastic effects on all these values. Within the range of $\approx 10,000$ to $\approx 50,000$ epithelial cells of critical polyp size, the mean cell number was again linearly dependent on the critical polyp size (Figure 11e), having a slope of ≈ 1.1. However, at the point were critical epithelial cell numbers reached $\approx 51,000$ cells, the linear dependency changed drastically and the slope was ≈ 16.85. This reflects the effect, that a polyp with many cells also generates more cells per time unit. If this large polyp has only a small bud, which draws only a small fraction of cells, the polyp has to initiate more buds to counteract its own cell proliferation. If the cell proliferation exceeds the amount of cells deposited into the bud, and the maximum rate of bud initiation is reached, the growth control of the polyp is lost, the system becomes instable, and much higher epithelial cell numbers are reached.

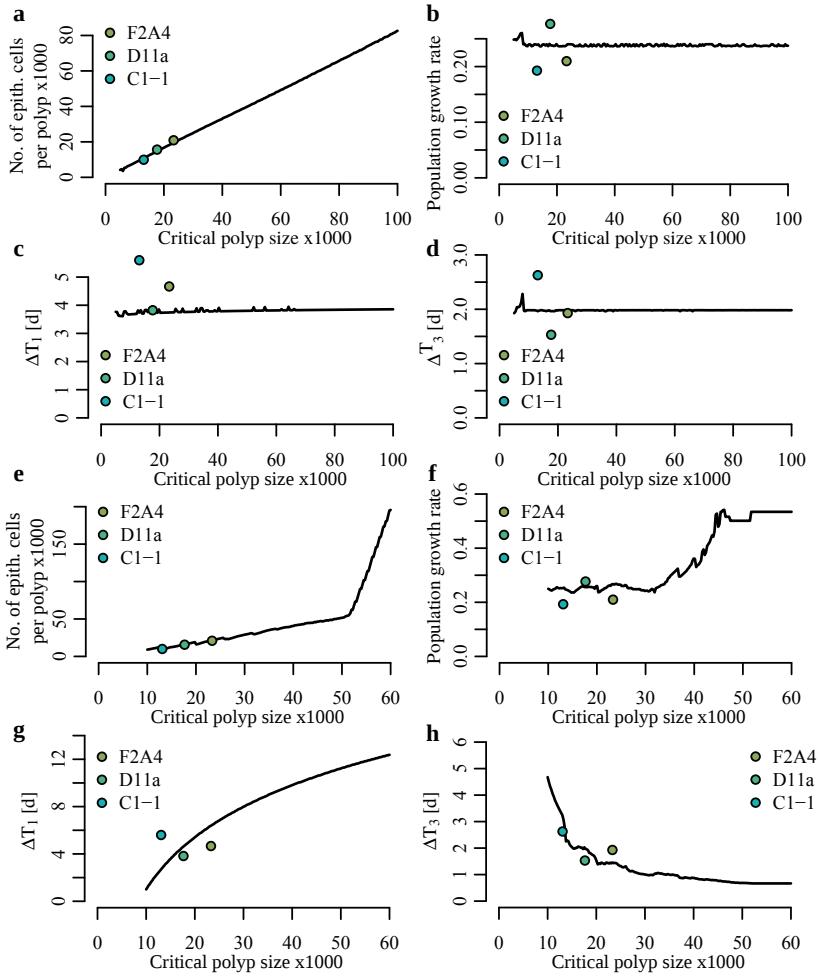

Figure 11: *Dependency of the mean number of epithelial cells per polyp (a,e), the PGR (b,f), ΔT_1 (c,g), and ΔT_3 (d,h) on the critical size of a polyp with (a-d), and without a size adjustment of the bud (e-f). The green/blue dots represent the experimental data in the variant space and serve as orientation to reflect biological relevant variance.*

Similar effects can be seen for the PGR, which is stable for a critical polyp size smaller than $\approx 35,000$ cells (Figure 11f). Beyond this, PGRs increase dramatically and reach a maximal value for critical polyp size of $\approx 51,000$ cells. The effect of generating more cells than that being lost through budding was visible much earlier here. For values larger than $\approx 35,000$ cells the polyp barely falls below its critical size by cell loss through budding and almost constant bud initiation at a high rate started to take place. This is also reflected in the dependence of ΔT_3 on the critical polyp size (Figure 11h). ΔT_3 decreases with the increase of the critical polyp size, in a logarithmic manner. Eventually the boundary of 0.6667 d (16 h) for ΔT_3 is reached at $\approx 51,000$ cells for the critical polyp size (the boundary is defined as fraction of ΔT_2).

ΔT_1 showed a root dependence on the critical epithelial cell number in the simulation and increased with it. This is expected, as the cell difference from a freshly detached bud to an adult polyp increases with larger values for critical epithelial cell values. This

difference is overcome by an exponential growth and thus takes a time frame which is logarithmically depend on it.

Next, I investigated how the epithelial cell number, population growth and developmental times do change with alteration of the bud size of the polyp (Figure 12a-d). Bud size was defined as fraction of the adult polyp size. Since, again, the cell difference between bud and adult polyp is changed, the dependencies of mean epithelial cell number, population growth and ΔT_1 are very similar to those seen with alterations of the maximum polyp size, while keeping the bud size fixed.

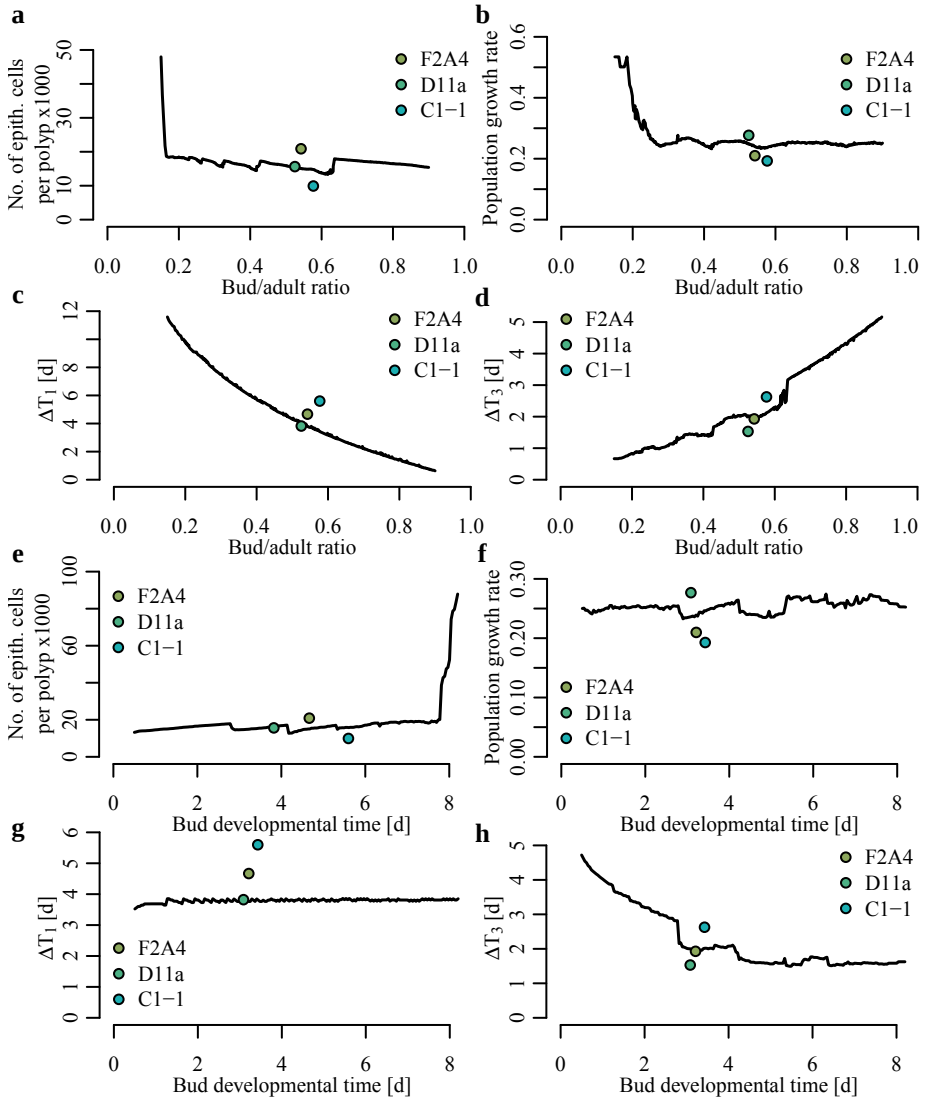

Figure 12: *Dependency of the mean number of epithelial cells per polyp (a,e), the PGR (b,f), ΔT_1 (c,g), and ΔT_3 (d,h) on the bud size (a-d) and developmental time (ΔT_2) of a bud (e-f). The green/blue dots represent the experimental data in the variant space and serve as orientation to reflect biological relevant variance.*

A low bud/adult ratio (< 0.1613) led to a massive increase in the mean epithelial cell number per polyp (Figure 12a), since the small buds would not draw enough cells from the polyp to counteract the constant proliferation and thus the system is destabilized. With increasing bud/adult ratios the system stabilized again and constant fluctuation around the maximum polyp size can be seen. Accordingly, the population growth massively increased with decreasing bud/adult ratios (Figure 12b), since the polyp constantly initiated buds in order to reduce the amount of cells in the polyp. For higher values of bud/adult ratios, the population growth stabilized. Budding in those polyps led to sufficient reduction in polyp size, so that the proliferative cell pool produces fewer cells than the amount which can be removed by budding in the same time. This prevents constant initiation of buds and thus reduces PGRs.

ΔT_1, decreased with increase of the bud/adult ratio, approaching 0 in an logarithmic dependency (Figure 12c). The explanation is the same as above: the difference in epithelial cell number between buds and adults decreases with higher bud/adult ratios and thus less time is needed to overcome this difference.

Interestingly, ΔT_3 increases with the bud/adult ratio in a rather linear manner (Figure 12d). For low bud/adult ratios (< 0.1613), the lower boundary of 0.6667 d (16 h) is reached, which results in a massive increase in epithelial cell number and consequently in PGR. Increasing the bud/adult ratio increased the amount of cells displaced from the adult polyp to the bud and thus the polyp was smaller after the bud(s) detached. Consequently, the difference between number of cells in the polyp after bud detachment and the maximum epithelial cell number is larger, which requires more time to overcome by proliferation.

The last factor I tested was the alteration for bud developmental times (ΔT_2) (Figure 12e-h). Number of mean epithelial cells is stable until ΔT_2 exceeds $\approx$ 7.75 d. With larger values, mean epithelial cell number per polyp increases rapidly, again indicating that the number of cells generated due to proliferation is much higher, than is lost due to budding. Interestingly, no increase in PGR could be seen in the simulation where cell number control in the polyp fails already (Figure 12f). This is due to the implementation of a boundary value for ΔT_3. The implementation for the simulation dynamically sets the boundary for lowest ΔT_3 ($\Delta T_{3min} = 0.2\Delta T_2$). This caused ΔT_3 to slightly increase with ΔT_2, when proliferation exceeded cell loss through budding on the one hand (Figure 12h) and prevented increase of PGR on the other hand (Figure 12f). ΔT_1 was not affected by the alteration of ΔT_2.

Taking these results together, several conclusions can be drawn by this simple model. (i) Cell proliferation cannot account for (large) size differences in *Hydra*, as long as the budding process is able to counteract the gain of cells by production of progeny. Hence, the rate of cell proliferation (or the proliferation index) is a good descriptor for PGR of the polyps (and *vice versa*). (ii) The critical size of a polyp has no influence on either PGRs, nor on developmental time frames. It is simply determined by genetics of the animal and its environment and has rather fitness implications for *Hydra*. (iii) A key point of a stable *Hydra* model is the epithelial number difference of bud and adult polyp. While larger bud/adult ratios are well handled by the model, smaller ratios will generate a state of constant bud initiation, increase population growth and generate polyps with a multiple of the cell number of which would be expected by the constraints given to the model. (iv) The PGR is tightly coupled to ΔT_3 in a negative correlation. Small ΔT_3 values result always in high PGRs.

This simple model sheds light on the relation of PGR, developmental times and stability of the *Hydra* system and their dependence on few input parameters. It gives a better understanding on how different parameters influence each other and gives hints where to look for phenotypes with knowledge of only some variables of the simulation. Furthermore,

complex situations, e. g. changing more than one parameter to explore variable space, could be applied to predict outcomes of population growth or developmental times under conditions of interest.

2.2.4 Predicting apoptosis using the 'virtual *Hydra*' model

As mentioned above, apoptosis rates are difficult to assess in *Hydra*. The model could give good approximations for apoptosis rates, since PGR, ΔT_1, and ΔT_3 are dependent on the proliferation index. These values are easy to obtain and the proliferation index can be predicted from them. The proliferation index itself is easily calculated by subtraction of the cell death rate ($\approx$ apoptosis rate) from the proliferation rate ($p_{ind} = p - d$). Thus, apoptosis rates can be obtained, if proliferation rate and one or more values of PGR, ΔT_1, or ΔT_3 are known.

To utilize the 'virtual *Hydra*' to predict apoptosis rates, it is necessary to generate regression models for the parameters (PGR, ΔT_1 and ΔT_3) and its predictive value for the proliferation index. In order to achieve this, I utilized the experimental data of the three *Hydra vulgaris AEP* lines for the simulation and varied the proliferation index for several simulation runs (comparable to Figure 10). I calculated linear regression models from the simulated data (seven in total, each predictive parameter and their combinations) to predict the proliferation index for the specific line. With the experimental data for PGR, ΔT_1, and ΔT_3, I predicted proliferation index values and calculated an apoptosis rate for each line-specific regression model. In the last step I evaluated the single apoptosis rates by how well a simulation did fit the real data, after applying the experimentally determined proliferation rate and the predicted apoptosis rate.

First step for linear regressions were the transformation of predicted ΔT_1 and ΔT_3 values from the simulation with different proliferation indices to achieve linear representation of the data. I found transformation of $\ln(\ln(\ln(\ln(\Delta T_1))))$ and $\ln(\ln(\ln(\Delta T_3)))$ as best fitting to achieve linearity to the proliferation index. For simplicity I will refer the transformed values as $\Delta T_1'$ and $\Delta T_3'$ in the descriptions for the regression models. The PGR was already in linear dependency to the proliferation index and was not transformed (Figure 10b). From there, different linear models were generated to predict apoptosis value from either a single value of PGR, ΔT_1, ΔT_3, or a combination of these values. Intercepts and correlation coefficients, as well as statistics for each model are summarized in table S3. As expected, the regression models showed a high statistical support ($p < 1e\text{-}16$) and an almost perfect explanation of data variability ($R^2 > 0.97$). Lastly, I predicted a single apoptosis rate for each regression model with the corresponding experimental values as predictors (Table 3).

Since apoptosis rates are not measurable in *Hydra* to date, I assessed the predicted apoptosis rate by utilizing the value in the simulation and compared the predicted simulation values for PGR, ΔT_1, ΔT_3 with the values which were experimentally obtained. The smaller the differences of the simulated values to the experimental data, the more accurate is the simulation on the one hand. On the other hand it is more likely that the predicted apoptosis rate is close to the actual apoptosis rate in the animal. I used the predicted apoptosis rates to perform a simulation to obtain simulated PGR, ΔT_1, and ΔT_3. These simulated values were now used to calculate relative distances (as fraction of the experimental data) (Table S4). The sum of all distances for one regression model in one *Hydra* line was then determined as distance score and served as a measure for total deviation of the predicted and simulated data from the experimental data (Equation 6 and Table 3). This value was further used to evaluate the best regression model for each line and the best performing regression model over all three lines.

Table 3: *The apoptosis rates and distance scores for the three lines investigated and the seven models which were tested. The apoptosis rates are given in fractions of total epithelial cells number which go into apoptosis within 72 h. The table is sorted by the lowest overall (Q-Sum) distance score.*

	Apoptosis rates			Distance scores			
Model design	F2A4	D11a	C1-1	F2A4	D11a	C1-1	Q-Sum
PGR+$\Delta T_1'$+$\Delta T_3'$	0.247	0.174	0.204	0.234	0.27	0.702	1.298
PGR+$\Delta T_3'$	0.230	0.167	0.168	0.318	0.293	0.686	1.554
$\Delta T_1'$	0.264	0.192	0.260	0.448	0.268	1.133	1.633
PGR	0.278	0.197	0.197	0.785	0.266	0.703	1.679
$\Delta T_1'$+$\Delta T_3'$	0.269	0.193	0.273	0.482	0.277	1.226	1.801
$\Delta T_3'$	0.143	0.107	0.109	0.69	0.418	0.728	1.926
PGR+$\Delta T_1'$	0.270	0.194	0.234	0.763	0.278	0.894	1.971

$$S = \sum_{i=0}^{N} \frac{|X_{sim,i} - X_{real,i}|}{X_{real,i}} \tag{6}$$

For the F2A4 line the regression model with the design PGR+$\Delta T_1'$+$\Delta T_3'$ had the best distance score of 0.234. It predicted an apoptosis value of 0.247 (24.7 % of epithelial cells in 72 h) and using this rate in the simulation resulted in the lowest deviation of simulated and experimental data for PGR, ΔT_1, and ΔT_3 (Table 3). Overall, the predicted apoptosis values from all regression models ranged from 0.143 to 0.278, while distance scores lay between 0.234 and 0.785. Notably, the predicted apoptosis rates are close to 0.18, which was observed by Bosch et al. [266]. Interestingly, already very small changes in the apoptosis rate can have huge impact on the distance score. The predicted apoptosis rates for the regression models with the design PGR+$\Delta T_1'$ and $\Delta T_1'$+$\Delta T_3'$ had a difference of only 0.01 and resulted in an increase of 1.5 times (from 0.482 to 0.763) the distance score. This reflects how subtle changes of the apoptosis rate can lead to very different distance scores and demonstrates the importance of a reliable regression model to predict reasonable apoptosis values.

The D11a line showed slightly lower apoptosis rates for the different regression models, ranging from 0.107 to 0.197 (Table 3). Again, the values are close to the 0.18 apoptosis rate described earlier [266]. Also distance scores were smaller than for F2A4, lying in the range of 0.266 to 0.418. The regression model with the lowest score predicted the proliferation index only by the PGR with a value of 0.197 for the apoptosis rate. However, the distance score for the model with the design PGR+$\Delta T_1'$+$\Delta T_3'$ was only slightly larger with 0.27 and seemed still a very good model to predict apoptosis rates in the line.

The experimental data of the C1-1 line predicted the largest range of apoptosis rates (between 0.109 to 0.273) and had the general highest distance scores (ranging between 0.686 to 1.133) (Table 3). The best predictive regression models (PGR+$\Delta T_3'$) predicted an apoptosis rate of 0.168 and had a distance score of 0.686. The high distance scores (compared to the ones of the other lines), suggests a less confident prediction in the apoptosis rates. However, the range of the apoptosis rates were around the value 0.18 and were still very reasonable.

For further usage I tried to identify the most general regression model, which gave constant low distance scores and thus most reliable results among a range of input parameter. I used quantile normalization on the distance scores for all lines and regression models,

since their distribution were significantly different between the three lines and not comparable. Afterwards, I summed the normalized distance score for each regression model (Q-Sum), to obtain a measure for the least divergence of all simulations from the experimental data (Table 3). A low Q-Sum indicates overall low distance scores and suggests a good regression model on varying the simulation conditions. The regression model with the design PGR+$\Delta T_1'$+$\Delta T_3'$ showed the lowest distance score and was chosen for further predictions of apoptosis rates.

Table 4: *Experimental data for adult and bud size, epithelial cell proliferation rate after 72 h BrdU-labeling, PGR and developmental times of the FoxO-KD line and its control (D11a).*

FoxO-KD	Adults	Buds	Bud/adult	BrdU 72h
ctrl (D11a)	$15,616 \pm 2,050$	$8,200 \pm 1,519$	0.525	0.72 ± 0.03
endo	$14,608 \pm 2,401$	$6,595 \pm 1,045$	0.451	0.73 ± 0.05
ecto	$8,507 \pm 1,401$	$3,980 \pm 1,057$	0.468	0.69 ± 0.07
ecto/endo	$8,108 \pm 1,435$	$3,123 \pm 658$	0.385	0.8 ± 0.03

FoxO-KD	PGR	ΔT_1	ΔT_2	ΔT_3
ctrl (D11a)	0.28 ± 0.06	3.82 ± 1.47	3.09 ± 0.55	1.53 ± 1.32
endo	0.2 ± 0.03	5.46 ± 2.57	3.13 ± 0.5	2.52 ± 1.95
ecto	0.27 ± 0.05	4.41 ± 1.6	2.59 ± 0.66	1.81 ± 1.17
ecto/endo	0.25 ± 0.04	5.3 ± 3.82	2.54 ± 0.64	1.97 ± 1.26

The establishment of an apoptosis prediction model enabled me to predict discrete values for apoptosis rates in *Hydra* lines which showed population growth phenotypes which could not be explained other than with altered apoptosis rates. One of these examples was the endodermal FoxO-KD line, previously reported [288]. FoxO is a key regulator of stem cell maintenance [291], translates stress signals to cellular responses, and controls apoptosis [275, 292] in *Hydra*. The FoxO knockdown lines were generated in a previous study [291], though just recently split into an endodermal, ectodermal, endo-ectodermal epithelial FoxO-KD lines, and an control line [288]. The knockdown of FoxO showed several cell line specific phenotypes, one of them was a retarded PGR for the endodermal FoxO-KD line (Figure S1). There was no obvious cause for reduction of growth rates, since neither bud/adult ratio nor proliferation rates significantly changed (Table 4). I hypothesized that apoptosis rates may have changed, but to what extant cannot be assessed directly from the data. I used the present simulation to generate a specific regression model which estimated the apoptosis rate for all FoxO-KD lines (Table S5). Afterwards, I predicted apoptosis rates with this model, using data from the growth rate experiments performed earlier [288]. The growth rate experiments were again split at generation "b" (Figure 7) to obtain biological replicates for values for PGR, ΔT_1, and ΔT_3. The predicted apoptosis rates increased to a mean of $\approx 33.7\,\%$ of epithelial loss within 72 h in the endodermal FoxO-KD line, which is a 2-fold increase compared to the control line (Figure 13). As expected the predicted apoptosis rates for the ectodermal FoxO-KD line did not change, since no change in the PGR was obtained. Intriguingly, the model predicted apoptosis rates of $\approx 40.9\,\%$ within 72 h for the full epithelial KD of FoxO. This is a 2.5-fold increase in apoptosis rate compared to the control line (Figure 13), though no drastic decrease of PGR could be observed (Figure S1). Nevertheless, the predicted values fit, if one considers the increased proliferation rate of the epithelial FoxO-KD (Table 4), which is not reflected in the PGR (Figure S1).

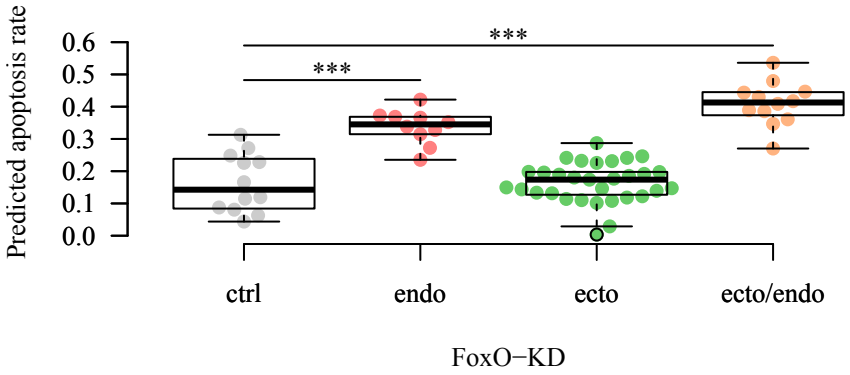

Figure 13: *Predicted apoptosis rates for several growth rate experiments of FoxO control and endodermal FoxO-KD lines are significantly different (Mann-Whitney-U test* $p \leq 0.001$*).*

The aforementioned reasons prevented me from assessing the apoptosis rates experimentally to confirm the prediction of the simulation. However, the simulation fits experimental data in most other aspects and it is most probable that the predicted apoptosis rates are close to the ones in living *Hydra*. The change in apoptosis rates account for fitness decrease in terms of reduced PGR in FoxO-KD mutants. Interestingly, my results suggest an endodermal specific control for apoptosis in a FoxO dependent manner in *Hydra*. 01749984523

2.3 Discussion

The 'virtual *Hydra*' showed how mathematical simple and yet biological complex the growth and size regulation of *Hydra* is and how stability of this system is maintained. It provides insights into the interactions of size, proliferation rates, growth rates and developmental times. It can be used to explore observed variations in these values and predict dependent variables, as well as causes for these variations.

A similar model was introduced by Dańko et. al. [293], which even integrated a damage system for the cells, to model (non-)senescence in *Hydra*. However, Dańko's model did not consider developmental processes in its predictions. It was focused on explanation of non-senescence of *Hydra* and relied on many approximations and assumptions, which had no or insufficiently experimentally support, while being still valuable for conceptual thinking. I now used experimental data to generate the 'virtual *Hydra*' and extended its predictive capabilities to population growth and development. I could demonstrate the influence of single input parameters on developmental processes and the predictive characteristics of those parameters, using 'virtual *Hydra*'.

Many predicted features of the 'virtual *Hydra*' were observed previously, like the reduction of ΔT_1 and ΔT_3 with the increase of the PGR, though the underlying mechanisms were not understood [294]. I showed how these features can be explained by an altered proliferation index and shed light on the interactions of these parameters. Counterintuitively, it was observed that polyp size is not determined by proliferation rates nor did it affect the PGR [263], which I also nicely modeled here.

Even a case of an instable system of *Hydra* has been described earlier [242], though the cellular or developmental mechanisms remained elusive. Excessively fed *Hydra* failed to stabilize their number of epithelial cells, while budding rate in those polyps approached

a maximum (compared to less fed polyps in this study), with about one bud per polyp and day. This would reflect the modeling case, where the polyp cannot dissipate enough cells into a bud and generates more cells in one time unit, than can be equalized by the number of buds initiated. Again the 'virtual *Hydra*' can give hints, where to look for the reasons of the systems instability, which lay most likely in the small bud/adult ratio.

The 'virtual *Hydra*' integrates the idea of critical size as point of bud initiation and thus follows the known developmental processes in other model organisms. Critical size or mass/weight is usually the point where an organism switches its developmental program and initiates a new developmental process. In insect development, the initiation of pupation is controlled by the mass of the larvae [81, 295, 296] and in *C. elegans* development, the nematode only moult after achieving a threshold size [297]. *Hydra* seems to employ a similar mechanism, to control its size and this model has been suggested already very early in developmental research of *Hydra* [242, 263, 294]. The embryonic like state of *Hydra* with constant stem cell proliferation necessitates a tight control of cell number, which is achieved by cell loss through bud initiation. How this critical size is determined or measured and how it is translated in cellular and molecular responses, remains elusive. However, earlier considerations about budding suggested a disbalance of a head activating and head inhibiting agent in the budding zone, as initiator for bud development [298]. The disbalance is determined by the traveling distance and time of the two agents and thus can be interpreted as the number of cells (size) in these animals. The head activator was found in the Wnt signaling molecule [245] and the role of Wnt and TGF-β signaling in bud formation has been described as well [253]. This gives good reasons that a critical size model reflects reality in *Hydra* and proves validity of the 'virtual *Hydra*' concepts. The 'virtual *Hydra*' now contributes to understand the consequences of such a regulatory mechanism. I emphasized the need of bud size control to maintain cell homeostasis and showed independence of the PGR and adult size.

Apoptosis is recognized as a phenomenon in *Hydra* [267–270], but its important role in the mechanics of developmental processes and cell homeostasis was less investigated in recent years. There have been several attempts to estimate apoptosis rates in *Hydra*, but none were able to reliably quantify them [242, 266, 267] or to distinguish apoptosis in the different cell types [290]. This is the first time, discrete numbers for apoptosis rates could be estimated in *Hydra* performing a rather simple experiment. Furthermore the simulation can be extended to more extreme cases to determine apoptosis rates. Bosch *et. al.* described discontinuation of budding in polyps under starvation, without reduction in mitosis rates, indicating an increased apoptosis rate [266]. The 'virtual *Hydra*' could be used to determine apoptosis rates in such a case as well, though the approach would have to change, since neither developmental times nor population growth rate can be determined.

With this, the 'virtual *Hydra*' provides a framework for conceptual *Hydra* biology, evaluating fitness parameter like population growth rates in dependence of developmental and cell biological properties. It is meant to guide future work on *Hydra* developmental and ecological research and can be used to deduce cell biological properties from simples macroscopic experiments. It falls in line with similar theoretical models of other model systems [299, 300] and eventually might be generalized to fit the empirical data of other metazoans or even proportion regulation in human organ development.

2.4 Material and methods

2.4.1 'Virtual *Hydra*'

The simulations were written in Python 2.7.12 [301] and are available at `https://github.com/porthmeus/Hypy`.

2.4.2 Animal culture

Hydra vulgaris (AEP) [239] were cultured at 18 °C in *Hydra* medium (HM, 0.28 mM $CaCl_2$, 0.33 mM $MgSO_4$, 0.5 mM $NaHCO_3$ and 0.08 mM KCO_3) according to standard procedure [302]. Animals were fed four times the week. Transgenic FoxO-KD animals were generated as described earlier [227, 291].

2.4.3 Growth rate experiment

For population growth rate and developmental time estimation, a single polyp were placed in a 12-well plate in at least 2 ml *Hydra* medium (HM). The polyp served as founder polyp for the experiment. Progeny of this polyp and all other following offspring were set individually in single 12-well plate cavities until at least 100 polyps were generated in one experiment. Developmental stages of all polyps were assessed every 24 h during the course of the experiment. For population growth rate calculation the experiment was split in sub-experiments at the second generation. Since *Hydra* grows clonally and the genotype is the same for one line, the resulting sub-experiments were treated as independent replicates. For growth rate calculation a regression of the log_2-transformed polyp number per time unit was performed and the slope of the curve as descriptor for growth rate was used. For data analysis a MySQL-database as well as custom written python and R functions were utilized.

2.4.4 Cell cycle analysis

In general, cell cycle analysis was performed as previously described using BrdU labeling [243]. For 72 h BrdU labeling, animals were incubated in HM containing 1 mM BrdU. For analysis of BrdU labeled cells using a cytometer, cells were dissociated as described below (see subsection 2.4.5) and fixed for 10 min in 4 % PFA. The cell's DNA was denatured using 1.5 M HCl for 45 min at room temperature, primary antibody (mouse-α-BrdU, *Roche*) was applied 1:100 in PBS + 1 % BSA over night at 4 °C. Secondary antibody (goat-α-mouse 488 alexa flour coupled, *Invitrogen*) was incubated 1:500 in PBS + 1 % BSA for 1 h at room temperature. Samples were analyzed immediately after staining.

2.4.5 Tissue digestion and size determination

For maximum size determination, animals in the early budding state were selected from the mass culture. Per replicate, individual polyps were digested in 100 μl of 50 U/ml Pronase E (Serva) in an isotonic culture medium [303] and inverted every 10 minutes for four hours at 18 °C. The living cells were then measured on a BD FACSCalibur with CellQuestPro v5.2 (*Becton–Dickinson*) using forward scatter and side scatter with a blue 488 nm laser to gate the epithelial cells. Epithelial cells were previously localized by measuring transgenic GFP expressing epithelial *Hydra vulgaris* (AEP) lines [227] using the FL-1 filter (530/30 nm). Gating and further analyses were performed with FCSalyzer 0.9.13-alpha (`https://sourceforge.net/projects/fcsalyzer/`). Cells of the interstitial cell lineage

were not evaluated to exclude effects of germ line producing cells under varying environmental conditions. However, because of their role in determination of morphological features of *Hydra* [261,262] and since they are much larger than cells from the interstitial cell lineage, epithelial cells are a very good proxy for the maximum polyp size [303,304].

2.4.6 Statistics

Statistical analysis were performed using two-tailed Student's-t-test or Mann-Whitney-U-test where applicable. If multiple testing was performed, p-values were adjusted using the Benjamini-Hochberg correction [305].

2.5 Supplementary information

Table S1: *Epithelial cell number per polyp/bud and the standard deviation are input parameters for the 'virtual* Hydra*'. See also figure 8.*

Line	Adults	Buds	Bud/Adult
F2A4	$20,871 \pm 2,993$	$11,320 \pm 1,868$	0.54
D11a	$15,616 \pm 2,050$	$8,200 \pm 1,519$	0.53
C1-1	$9,903 \pm 2,447$	$5,713 \pm 1,163$	0.58

Table S2: *Comparing developmental times of* Hydra *(see Figure 7) with the simulated values reveals good fit of the simulation to experimental data. The Experimental data is given as mean with standard deviation, while simulated data is expressed as mean values.*

	Measured			Simulated		
Line	ΔT_1	ΔT_2	ΔT_3	ΔT_1	ΔT_2	ΔT_3
F2A4	4.67 ± 2.01	3.21 ± 0.81	1.92 ± 1.59	3.68	3.04	1.91
D11a	3.82 ± 1.47	3.08 ± 0.54	1.53 ± 1.32	3.55	2.92	1.81
C1-1	5.60 ± 2.52	3.43 ± 0.96	2.63 ± 1.98	4.28	3.38	3.64

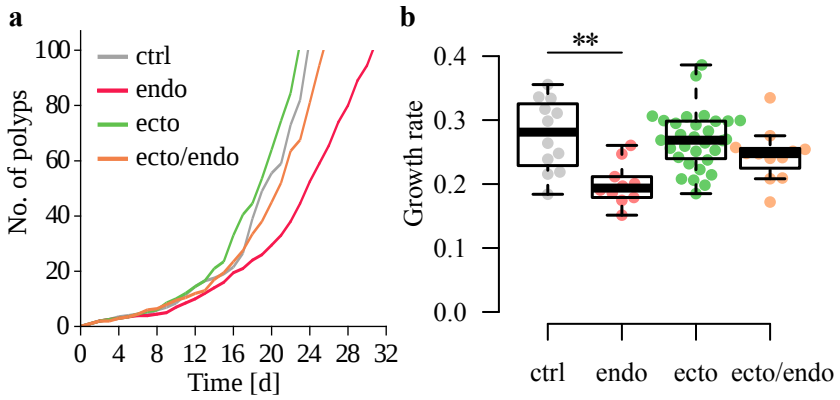

Figure S1: *Growth curves and growth rates of the different FoxO-KD lines. The endodermal KD line shows significantly reduced growth rates. Adapted from the PhD thesis of Benedikt Mortzfeld [288].*

Table S3: *The coefficients and intercepts for the different models are displayed with corresponding p-values from the F-Statistics and adjusted R^2 values for the regression. All models display a high statistic support as well as they explain almost 100 % of the variability.*

	Model design	Inter.	PGR	$\Delta T_1'$	$\Delta T_3'$	p-value	adj R^2
F2A4	PGR	0.021	1.810	NA	NA	$< 1e$-16	0.990
	$\Delta T_1'$	-0.657	NA	-1.302	NA	$< 1e$-16	0.993
	$\Delta T_3'$	1.007	NA	NA	-1.596	$< 1e$-16	0.975
	PGR+$\Delta T_1'$	-0.369	0.785	-0.744	NA	$< 1e$-16	0.997
	PGR+$\Delta T_3'$	0.376	1.170	NA	-0.585	$< 1e$-16	0.997
	$\Delta T_1'$+$\Delta T_3'$	-0.727	NA	-1.357	0.068	$< 1e$-16	0.993
	PGR+$\Delta T_1'$+$\Delta T_3'$	0.024	0.928	-0.377	-0.332	$< 1e$-16	0.997
D11a	PGR	0.016	1.829	NA	NA	$< 1e$-16	0.992
	$\Delta T_1'$	-0.678	NA	-1.355	NA	$< 1e$-16	0.992
	$\Delta T_3'$	1.012	NA	NA	-1.611	$< 1e$-16	0.975
	PGR+$\Delta T_1'$	-0.341	0.904	-0.692	NA	$< 1e$-16	0.997
	PGR+$\Delta T_3'$	0.351	1.223	NA	-0.552	$< 1e$-16	0.998
	$\Delta T_1'$+$\Delta T_3'$	-0.711	NA	-1.381	0.032	$< 1e$-16	0.992
	PGR+$\Delta T_1'$+$\Delta T_3'$	0.128	1.068	-0.246	-0.394	$< 1e$-16	0.998
C1-1	PGR	0.024	1.796	NA	NA	$< 1e$-16	0.992
	$\Delta T_1'$	-0.618	NA	-1.204	NA	$< 1e$-16	0.994
	$\Delta T_3'$	1.026	NA	NA	-1.613	$< 1e$-16	0.976
	PGR+$\Delta T_1'$	-0.344	0.783	-0.685	NA	$< 1e$-16	0.998
	PGR+$\Delta T_3'$	0.371	1.184	NA	-0.569	$< 1e$-16	0.998
	$\Delta T_1'$+$\Delta T_3'$	-0.765	NA	-1.310	0.145	$< 1e$-16	0.994
	PGR+$\Delta T_1'$+$\Delta T_3'$	-0.017	0.910	-0.395	-0.280	$< 1e$-16	0.998

Table S4: *The table shows evaluation of the different regression models for apoptosis prediction. I predicted values for apoptosis rate, ΔT_1, ΔT_3, and PGR with regressions using different model designs. For evaluation, relative distances to the experimental data were calculated and a distance score was computed.*

	Model design	Apo. rate	ΔT_1	ΔT_3	PGR	ΔT_1 dist.	ΔT_3 dist.	PGR dist.	Dist. Score
F2A4	PGR	0.278	4.520	3.330	0.215	0.031	0.727	0.027	0.785
	$\Delta T_1'$	0.264	4.433	2.615	0.219	0.050	0.356	0.042	0.448
	$\Delta T_3'$	0.143	3.428	1.790	0.284	0.265	0.072	0.353	0.690
	PGR+$\Delta T_1'$	0.270	4.518	3.241	0.220	0.032	0.681	0.050	0.763
	PGR+$\Delta T_3'$	0.230	4.054	2.101	0.230	0.131	0.090	0.097	0.318
	$\Delta T_1'$+$\Delta T_3'$	0.269	4.520	2.744	0.216	0.031	0.423	0.028	0.482
	PGR+$\Delta T_1'$+$\Delta T_3'$	0.247	4.303	2.192	0.214	0.078	0.137	0.019	0.234
D11a	PGR	0.197	3.720	1.888	0.278	0.027	0.234	0.005	0.266
	$\Delta T_1'$	0.192	3.679	1.859	0.281	0.037	0.215	0.016	0.268
	$\Delta T_3'$	0.107	3.137	1.607	0.329	0.179	0.050	0.189	0.418
	PGR+$\Delta T_1'$	0.194	3.679	1.884	0.279	0.037	0.231	0.010	0.278
	PGR+$\Delta T_3'$	0.167	3.511	1.727	0.300	0.081	0.128	0.084	0.293
	$\Delta T_1'$+$\Delta T_3'$	0.193	3.679	1.874	0.281	0.037	0.225	0.014	0.277
	PGR+$\Delta T_1'$+$\Delta T_3'$	0.174	3.594	1.755	0.294	0.060	0.147	0.064	0.270
C1-1	PGR	0.197	4.451	3.898	0.195	0.205	0.484	0.014	0.703
	$\Delta T_1'$	0.260	5.332	5.074	0.163	0.048	0.932	0.153	1.133
	$\Delta T_3'$	0.109	3.643	2.130	0.229	0.349	0.189	0.190	0.728
	PGR$\Delta T_1'$	0.234	4.994	4.492	0.178	0.108	0.710	0.076	0.894
	PGR$\Delta T_3'$	0.168	4.115	3.497	0.210	0.265	0.331	0.090	0.686
	ΔT_1+$\Delta T_3'$	0.273	5.624	5.373	0.159	0.005	1.046	0.176	1.226
	PGR+$\Delta T_1'$+$\Delta T_3'$	0.204	4.576	3.982	0.193	0.183	0.516	0.004	0.702

Table S5: *The table shows the regression model statistics for the different FoxO-KD lines. All regression models have the design: PGR+ΔT_1+ΔT_3. Coefficients for all design factors, the intercepts, p-values from the F-statistics, and adjusted R^2 are given.*

FoxO-KD	Inter.	PGR	$\Delta T_1'$	$\Delta T_3'$	p-value	adj R^2
ctrl (D11a)	-0.017	0.910	-0.395	-0.280	$< 1e$-16	0.998
endo	0.192	1.318	-0.084	-0.387	$< 1e$-16	0.997
ecto	0.240	1.013	-0.187	-0.531	$< 1e$-16	0.998
ecto/endo	0.653	1.432	0.439	-0.780	$< 1e$-16	0.997

3 Chapter II - Environment dependent body size in *Hydra* is controlled by TGF-β signaling

3.1 Introduction

Body size is assumed to be a species-specific feature with physical/physiological restrictions and major implications for the fitness of an organism [1, 2, 5]. Yet, tremendous variations in size are reported for individuals of the same species [306, 307]. Assuming a common genetic background for a species poses the question, which factors determine the size of an individual organism. Even after decades of molecular research, the mechanisms underlying body size determination are still unsolved. How body size is sensed therefore remains one of the fundamental unsolved problems in developmental biology [308, 309].

On a cellular level, only three basic factors contribute to size control: the period of time until growth termination (developmental time) and the amount of cells gained during this period (growth rate) as well as the individual cell size [310, 311]. Genetic factors are considered to be a major determinant of these factors and studies on vertebrates and invertebrates revealed that some genetically conserved genes and pathways are able to contribute to size phenotypes. These are either homeobox genes [312], or components of the Insulin [219, 222, 313, 314], Wnt [315, 316], or TGF-β [317–319] signaling pathways.

A recent GWAS on human height control suggests that only 27 % of adult height can be explained by heritability [320]. Consequently, environmental factors including diet, exercise or geographic variation account for more than 70 % of size determination in humans. Malnutrition during development causes stunted growth in mammals [321, 322] and invertebrates [323, 324]. The surrounding temperature as another environmental factor is well known to have great impact on size determination in homeotherms and poikilotherms [51, 325, 326]. This change in developmental processes and the generation of different phenotypes of animals with the same genotype in response to changing environmental conditions is termed phenotypic plasticity [327]. Since such plasticity can increase organism survival under varying conditions, it is hypothesized to contribute to evolutionary processes and speciation [54, 89–91, 286, 328–331].

However, even though alterations of environmental factors or conserved pathways seem to affect body size, it is not well understood, (i) how environmental cues affect genetic programs, (ii) how size is measured by cells or tissue during growth or (iii) by what processes termination of growth is initiated. Indeed, understanding of these processes does not only contribute to the comprehension of ecological and developmental interactions on a molecular level, but has major implication for evolutionary concepts.

While developmental programs determine an irreversible phenotype (e.g. size) for most organisms [327], cnidarians such as *Hydra* are extremely flexible throughout their life history. Adult polyps possess many embryonic characteristics such as constant cell proliferation and continuous developmental patterning, while being non-senescent [332] and clonal in growth [223]. Its morphological appearance is determined by the two unipotent epithelial stem cell lines, which have a remarkably robust cell cycle [243, 258] and whose proliferation is unaffected even by harsh environmental conditions like starvation [266]. Together with the ongoing, Wnt-mediated patterning process of the single body axis, they build the foundation of *Hydra*'s vast regeneration capacity [245, 247, 251, 298, 333]. Applying different environmental cues to clonal animals which are still in a developmental life stage presents the rare opportunity to study phenotypic plasticity of size and intrinsic size determination within a single genotype. In this study I aimed to reveal conserved molecular mechanisms underlying individual size control by environmental and genetic triggers in *Hydra*.

3.2 Results

3.2.1 Temperature-induced phenotypic plasticity of body size

Hydra can be cultured at a wide temperature range [334]. Clonal polyps reared at different temperatures grow to a temperature-dependent size (Figure 14a, b): At low temperatures (8 °C, 12 °C) animals are visibly larger than at higher temperatures (18 °C, 22 °C). To quantify these size differences, we[2] established a sensitive flow cytometry protocol and determined the total epithelial cell number per individual polyp that just generated a small bud protrusion, further referred to as maximum size. Epithelial cells of dissociated polyps were gated using only forward and side scatter values from the cytometer (Figure S2, Table S6). In accordance to the maximum size, *Hydra*'s epithelial cell number was temperature dependent, which was reflected in the lowest number of epithelial cells ($12,963 \pm 3,555$; mean ± SD) at 22 °C. With decreasing temperature the number of epithelial cells increased by 83 % (12 °C; $23,698 \pm 3,537$) with no further gain in cell number at 8 °C ($21,441 \pm 8,565$) (Figure 14b). Moreover there was an 22 % increase in cell diameter for epithelial cells with the decrease of temperature from 22 °C ($25 \pm 0.6\ \mu m$) to 8 °C ($31 \pm 0.4\ \mu m$) (Figure S3a, b). I further asked whether the size difference can be explained by increased growth rate and measured cell proliferation using BrdU labeling at 12 °C and 18 °C rearing temperature. No difference in labeling efficiency could be detected after 3 h of incubation in BrdU (Figure S4a), suggesting that the length of cell cycle is not affected. Remarkably, after 72 h labeling with BrdU resulted in decreased BrdU incorporation at 12 °C, suggesting less cell proliferation in larger animals. Therefore, reduced proliferation rate cannot account for larger maximum size and other mechanisms should be involved. In order to resolve this discrepancy and to elucidate the molecular mechanisms which underlie the size determination in *Hydra* I compared transcriptomes of polyps reared at different temperatures.

I generated 20 total RNA sequencing libraries and together with another 5 RNA sequencing libraries from a related study in my working group [288] I performed a *de-novo* transcriptome assembly using Trinity [335] to uncover changes even in low expressed genes. 513,413 contigs were assembled and clustering reduced this number to 220,458. The mean contig length was 578 bp with an N50 of 746 bp. Further statistics are summarized in Table S7. Mapping rates for all 40 samples against the transcriptome reached 95-98 %. The transcriptome contains 31,325 contigs with a predicted open reading frame (ORF), longer than 100 amino acids and a translation start or stop or both within the sequence range. I used ORF containing contigs for further analysis, and therefore refer to the 31,325 members as genes. BUSCO [336] analysis revealed a transcriptome completeness of 86.4 % confirmed by manual evaluation of known genes in the data set: All 20 genes I checked could be found in full length and without frame shift. After annotation I concluded that 58 % of the ORFs contain conserved motifs, while 42 % show no homologous regions to various databases (including SMART, Pfam, PANTHER, KEGG) and therefore can be considered as orphan genes (Figure S5a) [337, 338].

I performed a differential expression (DE) analysis comparing the transcriptomes of clonal animals at different rearing temperatures in a pairwise manner (8 °C vs. 12 °C, 12 °C vs. 18 °C, and 18 °C vs. 22 °C). I found a total of 1,580 differential ORFs induced by temperature shifts in *Hydra* associated with size differences (Figure 14c, **bold**). Since a temperature shift from 12 °C to 8 °C did not result in a significant increase in cell number per polyp (Figure 14b), genes which were differentially expressed in this comparison (1,226, grey) were excluded from further analysis. Three different expression patterns were found

[2] The establishment of the cytometry protocol was done in collaboration with Benedikt Mortzfeld [288].

in the comparisons over the different temperatures (Figure 14d). While the expression of most gene clusters increased or decreased in a gradual manner (green), the expression of some genes responded solely to one condition (yellow). Moreover, especially genes specific for the 12 °C vs. 18 °C comparison acted biphasically as a direct switch between lower and higher temperatures (red). 205 DE genes were shared between temperature switches associated with altered epithelial cell numbers, making them the most promising candidates for size regulation.

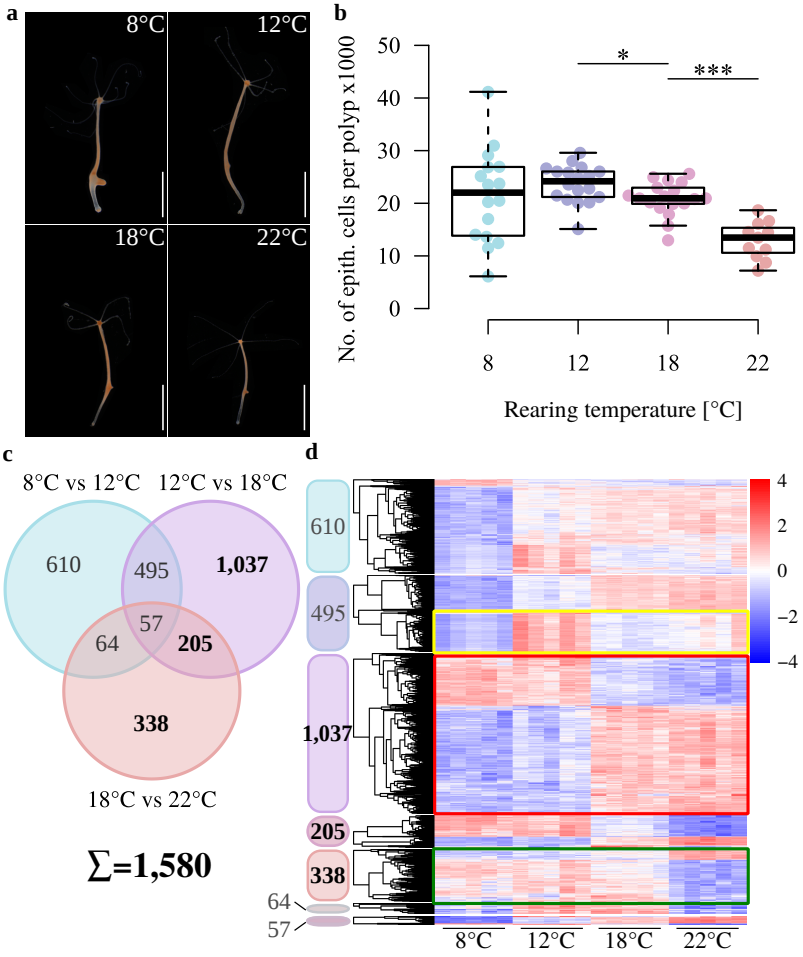

Figure 14: *Temperature-induced phenotypic plasticity. (a)* Hydra *polyps reared at 8 °C, 12 °C, 18 °C and 22 °C at maximum polyp size with first bud protrusion. Scale bar: 5 mm. (b) Clonal* Hydra *polyps reared at temperatures from 8 °C to 22 °C showed decreasing numbers of epithelial cells at maximum size. $n \geq 11$, *:$p \leq 0.05$, ***:$p \leq 0.001$. (c) Venn diagram showing number of differentially expressed genes comparing the different temperature treatments (8 °C vs. 12 °C, 12 °C vs. 18 °C, 18 °C vs. 22 °C). 1,580 genes (**bold**) are associated with a significant change in maximum size by temperature shift. (d) Heatmaps representing the relative expression level of the differentially expressed genes (rows) from the Venn diagram over the different temperatures. Genes were clustered hierarchically per heatmap. Expression values were* $\log_2$*-transformed and median-centered by transcript.*

Remarkably, size-associated genes which have a clear domain prediction were enriched among the 1,580 DE genes compared to the average distribution (Figure S5b). This is somewhat surprising, since orphan genes are believed to be the effector genes responding to environmental conditions and thus expected to be enriched among DE genes [338]. Interestingly, within the DE gene clusters I identified several conserved genes that could be involved in size regulation, according to their role in other model organisms: e. g. in apoptosis (Caspase 3) [339], proliferation (FGF receptor (FGFR), R-Ras) [138,340] and developmental processes (Notum, Notch, thrombospondin (THBS)1, calmodulin (CALM)) [341–344] (Figure S6, Table 5). The DE genes from the different temperature comparisons and putative candidates for size determination showed neither an enrichment for a particular pathway nor an obvious functional overlap. However, temperature is not only known to affect size but also metabolic pathways and physiology [345]. I suspected that size determination could be a general, comprehensive mechanism for phenotypic plasticity and intrinsic size regulation. Consequently, I chose conserved genes known to contribute to regulating adult size determination in more complex organisms for functional analyses in order to reduce the number of putative size candidates.

3.2.2 INSR-knockdown induces larger polyp size

IIS is known to be involved in size regulation in other organisms [219, 222, 313, 314] and in recognition of environmental signals [346]. I hypothesized the INSR to be a promising candidate for environmentally dependent size regulation in *Hydra*. I generated transgenic animals carrying an shRNA construct against the putative *insR* gene [271] to disrupt INSR-dependent signaling (Figure S7a,b) and functionally tested its involvement in environmental signaling, development and size determination. Indeed, the maximum polyp size increased visibly (Figure 15a) due to the knockdown of *insR*. Consistently, the epithelial cell number per polyp in INSR-KD animals at 18 °C and 22 °C increased significantly and had tendencies of larger sizes at lower temperatures compared to the control (Figure 15b), though no alteration in cell diameter could be observed (Figure S3c-e). The mean maximum size increased at 18 °C and 22 °C by 16 % ($9,903 \pm 2,447$ vs. $11,498 \pm 2,950$) and 21 % ($7,328 \pm 1,154$ to $8,876 \pm 1,237$). Since IIS is known to control cell proliferation [291, 347, 348], I compared BrdU labeling rates in INSR-KD and control animals. I found no difference in cell proliferation between transgenic and control polyps, neither after short BrdU pulse (3 h) nor after prolonged incubation (72 h) (Figure S4b). Therefore, differences in cell cycle could again not account for increased number of epithelial cells per polyp and consequently for larger size. Remarkably, INSR-KD animals were still responsive to temperature changes and a similar gradient of size as in wild type controls with significant differences in epithelial cell number and cell diameter between 12 °C to 18 °C and 18 °C to 22 °C could be observed (Figure 15, Figure S3). Therefore, I concluded that the phenotypic plasticity observed between temperature differences is not directly mediated via INSR-dependent signaling. Since no changes in cell diameter could be seen for INSR-KD animals, I focused the analysis in further experiments to explain the difference in epithelial cell number, since it is the common phenotype shared between the two conditions altering body size in *Hydra*.

Table 5: *The table shows the regulation of putative candidate genes and corresponding KEGG numbers for size regulation in polyps with INSR-KD and after temperature shift.*

	Gene	KEGG	Temperature		INSR-KD
			12 °C vs. 18 °C	**18 °C vs. 22 °C**	**ecto/endo 18 °C**
TGF-β	ACV (INHB)	K04667	↓	↓	↓
	ACVR2A	K04670	↑	o	o
	Cer-1	K01645	o	↓	o
	DAN (NBL1)	K19558	↑	↑	o
	TGF-β2	K13376	↑	↑	o
	THBS1	K16857	↑	↑	o
Wnt	Notum	K19882	↓	↓	o
Others	CALM	K02183	↑	↓	o
	Casp3	K02187	↑	↓	o
	Casp7	K04397	↑	o	o
	FGFR1	K04362	↑	↑	o
	Notch	K02599	↓	↓	o
	K-ras	K07827	o	↓	o
	R-ras	K07829	↓	↓	o

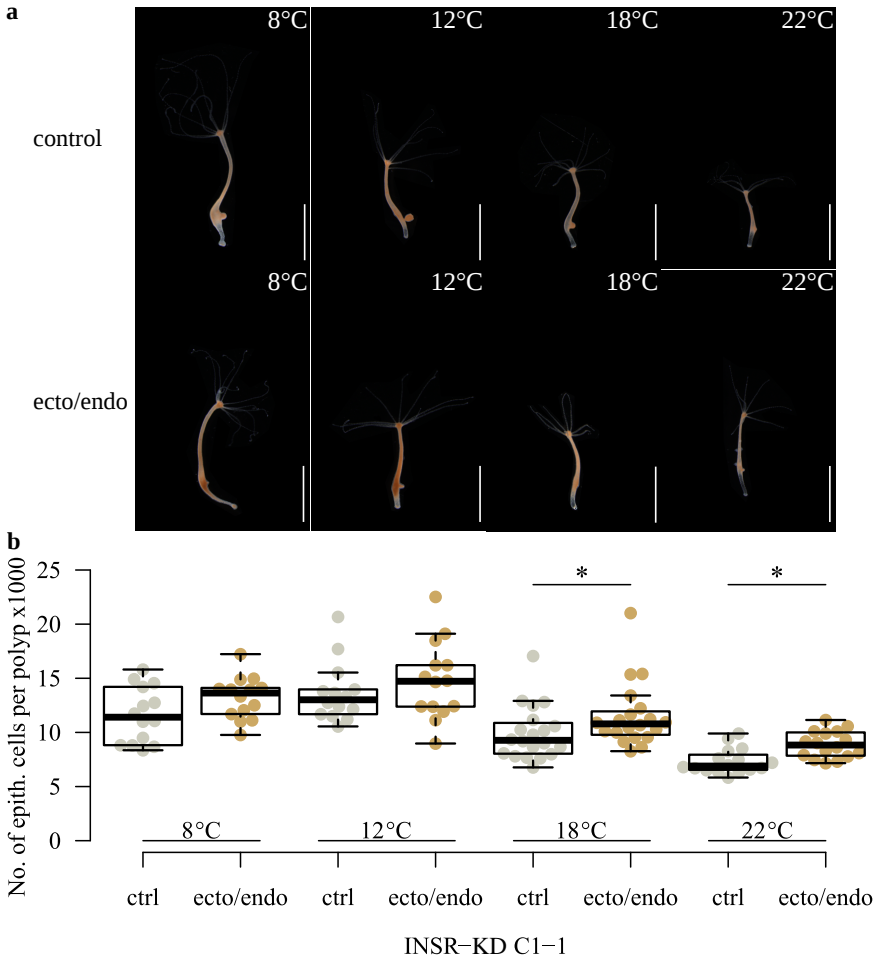

Figure 15: *INSR-KD induces larger polyp size. (a) Pictures of control and INSR-KD polyps from 8 °C to 22 °C with bud protrusion. Scale bar: 5 mm. (b) Control and INSR-KD polyps reared at temperatures from 8 °C to 22 °C. The INSR-KD results in larger maximum size with more epithelial cells per polyp at 18 °C and 22 °C. Note, that INSR-KD animals still increase in size at lower temperatures.* $n \geq 14$, *$:p \leq 0.05$.

However, I utilized the phenotype of the INSR-KD animals to get further insights into the size control in *Hydra*. I compared the transcriptomes of control and epithelial KD animals reared at 18 °C and 8 °C to identify genes that account for the size difference and which are independent of temperature but dependent on INSR signaling. Consequently, I compared INSR-KD and control polyps at both temperatures and utilized the animals reared at 8 °C as control, since the size difference is not significant at lower temperatures. Intriguingly, I found only five differentially expressed genes at both conditions (Figure 16a). Instead, distinct sets of genes were affected by INSR-KD at the two different temperatures, implying divergent roles of the insulin signaling at 8 °C and 18 °C. 36 genes were exclusively differentially expressed between INSR-KD and control animals at 8 °C (Figure 16a). Among these, only six genes could be annotated with a known conserved function, four involved in metabolic processes (protein phosphatase 1 regulatory subunit 3 (PPP1R3), electron transfer flavoprotein dehydrogenase (ETFDH), tetratricopeptide repeat domain

19 (TTC19), and polyamine oxidase (MPAO)) and two involved in stabilization of the membrane potential of cells (polycystic kidney disease protein 1 like 2 (PKD1L2) and sodium/potassium transporting ATPase subunit alpha (ATP1A)). The larger fraction (80, **bold**) of exclusively DE genes was found in the comparison of INSR-KD to control animals at 18 °C rearing temperature (Figure 16a), suggesting a much larger physiological role for the INSR at this temperature. Again, only few genes (36/80) could be clearly annotated with known gene function (Figure S5c). I saw an enrichment of orphan genes among DE genes which are considered species-specific effector genes, and thus could be expected to be regulated in the INSR-KD animals [338]. Among the annotated genes a fraction is involved in translation (large subunit ribosomal protein (RP)-L14, RP-L26e), indicating a role of the insulin pathway in regulation of metabolic events and protein synthesis at 18 °C. Additionally, I found one gene, otoferlin (OTOF), which is associated with cell membrane vesicle transport in an ion dependent manner. Most interestingly, an activin-like protein (ACV), also known as inhibin (INHB) was found among the DE genes, a secreted component of the TGF-β signaling pathway (Figure S6, Table 5). This was the only obvious link between temperature-dependent genes and size regulation via INSR.

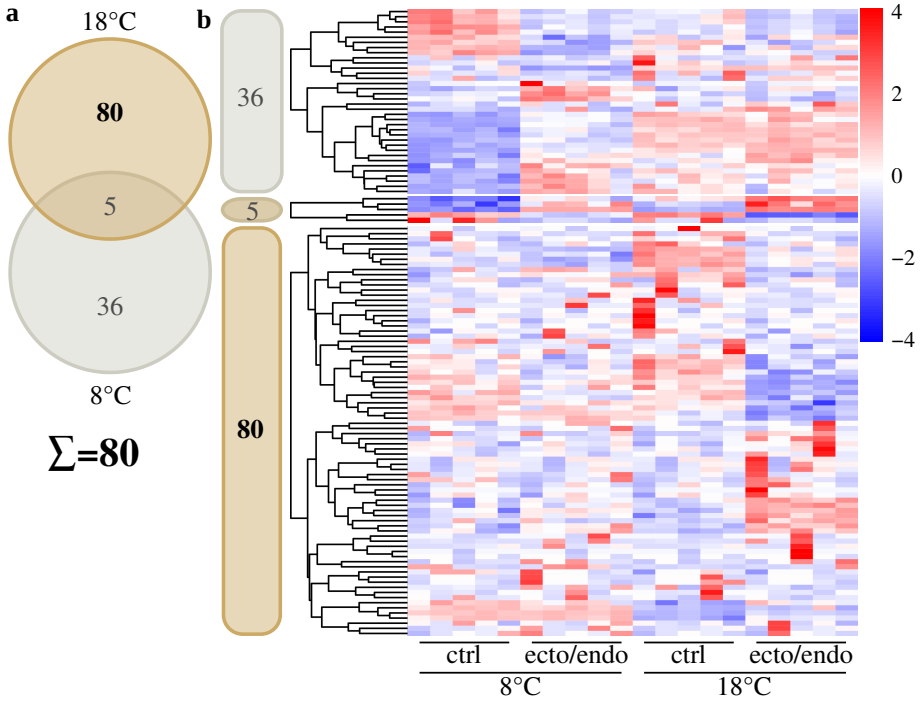

Figure 16: *Transcriptome analysis reveal INSR target genes. (a) Venn diagram showing the overlap of differentially expressed genes by INSR-KD at 8 °C and 18 °C. 80 genes (**bold**) are associated with increased size at 18 °C. (b) Heatmaps representing the relative expression level of the differentially expressed genes (rows) from the Venn diagram at 8 °C and 18 °C. Genes were clustered hierarchically per heatmap. Expression values were* $\log_2$*-transformed and median-centered by transcript.*

3.2.3 TGF-β signaling as effector of size determination

Among the candidate genes for size regulation in the TGF-β pathway were ACV, Activin-Receptor IIa (ACVR2a), THBS1, domain BMP antagonist (DAN), cerberus (Cer)-1 and TGF-β (Table 5). Remarkably, one of the two ACV homologs was regulated in INSR-KD animals and after temperature shift, making it the most promising candidate to be involved in size determination.

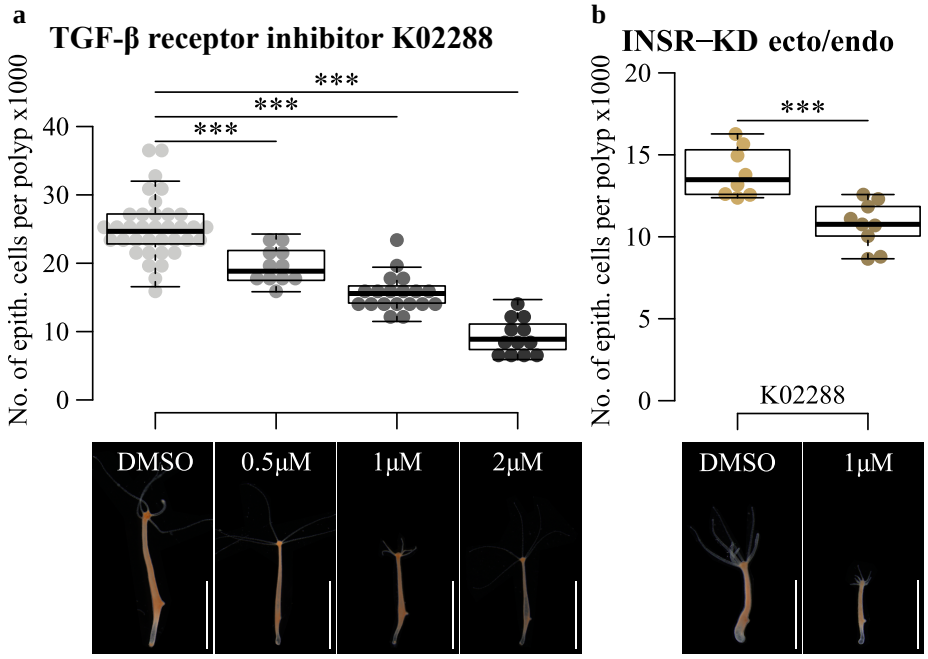

Figure 17: *TGF-β signaling affects maximum size. (a) Applying TGF-β receptor inhibitor K02288 reduced size in a concentration dependent manner. (b) Additionally, large-sized INSR-KD animals were reduced in maximum size. Scale bar: 5 mm. $n \geq 8$, *:$p \leq 0.05$, **:$p \leq 0.01$, ***:$p \leq 0.001$.*

The precise role of the TGF-β pathway in *Hydra* is not known, yet analysis of alsterpaullone (ALP) treated animals demonstrated its action to be downstream of Wnt signaling in a related study of my working group [288] and previous studies suggested a role of Nodal in bud initiation [253]. I used pharmacological interference to test the involvement of the TGF-β pathway in maximum size regulation. I continuously applied the specific TGF-β-receptor inhibitor K02288 [349] at subtoxic concentrations for at least one week under feeding to *Hydra* wild type polyps. The inhibitor resulted in a reduction of epithelial cell number in maximum polyp size in a concentration dependent manner (Figure 17). At a just non toxic concentration of 2 μM the maximum size was reduced by 63 % ($25,127 \pm 4,172$ to $9,330 \pm 2,667$). In order to confirm the position of the TGF-β pathway in the signaling hierarchy of molecular mechanisms controlling size, I treated the large-sized INSR-KD animals with K02288 and observed a reduction in size by 23 % (13,928 $\pm$ 1,518 to 10,755 $\pm$ 1,407) at 1μM in the polyps (Figure 17b). The potential to alter maximum size in insulin signaling-deficient animals with TGF-β inhibitors verifies the hierarchical action of the TGF-β pathway downstream of insulin signaling. Interestingly, K02288 did not affect cell size neither in wild type animals, nor in INSR-KD

animals (Figure S8a, b). Furthermore it seems likely, that Wnt signaling is controlled by the insulin signaling and the temperature input since K02288 treated animals altered their response to alsterpaullone (ALP) in other experiments [288]. Among the temperature dependent genes NOTUM was identified, a part of the Wnt signaling machinery, which further substantiates a Wnt signaling involvement in size regulation (Table 5).

Together with the candidate genes from the transcriptomic analyses these results demonstrate a signaling hierarchy of TGF-β signaling being downstream of the insulin signaling pathway. However, if bud initiation eventually determines the maximum size of a polyp, but cell proliferation does not (Figure S4), I assumed that the developmental time until first bud protrusion determines the maximum size of a polyp.

3.2.4 Maximum size is dependent on developmental time

In order to test whether maximum size and developmental time (ΔT_1) are directly affected by bud initiation, I measured the time of a detached bud to develop the first protrusion (Figure 18a). For a *Hydra* polyp, bud initiation determines the end of the developmental growth phase since cells gained from proliferation do not contribute to larger size but are displaced to bud development. K02288 indeed decreased ΔT_1 significantly by 23 % (8.1 d $\pm$ 0.8 d to 6.2 d $\pm$ 0.7 d), thus induced bud initiation earlier in development which eventually led to less epithelial cells per polyp (Figure 18b). Applying the described inhibitor, I demonstrate that maximum polyp size is dependent on the duration of developmental growth. While a shorter developmental time accounts for smaller maximum size, large animals can be induced via bud suppression and a longer ΔT_1 (Figure 18a). This process might be further controlled by Wnt signaling and a corresponding head inhibition potential, because of its role in the axis stabilization [245, 288, 298]. Thus smaller animals show a higher disposition to form a secondary axis earlier and induce budding.

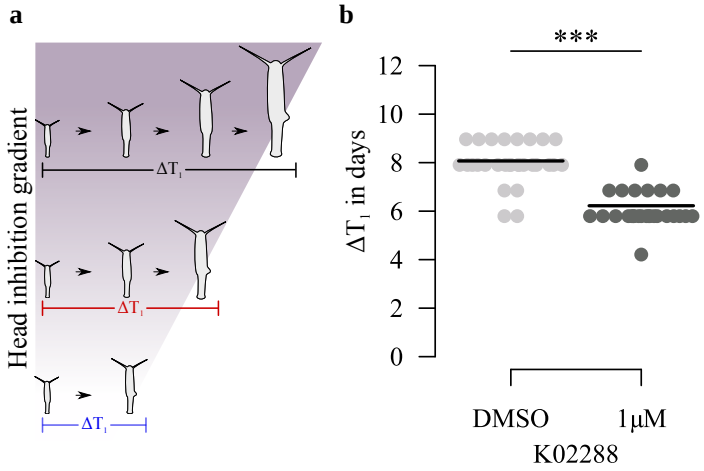

Figure 18: *Changing developmental time by application of the TGF-β receptor inhibitor K02288. (a) The schematic representation shows the correlation of maximum size and head inhibition gradient. Larger lines have a higher head inhibition potential and extend in developmental time (ΔT_1). (b) K02288 antedated the time point of bud initiation in developmental time (ΔT_1), eventually resulting in smaller maximum size. $n \geq 27$, ***:$p \leq 0.001$.*

Taken together, transcriptomic analyses as well as pharmacological interference revealed hierarchical action of environmental and genetic factors on size regulation. Here, I describe how temperature change and insulin signaling control bud initiation via TGF-β signaling and thereby maximum polyp size. Accordingly, without changes in proliferation rates, phenotypic plasticity as well as intrinsic maximum size determination are both mediated via developmental time and the point of bud initiation (Figure 19).

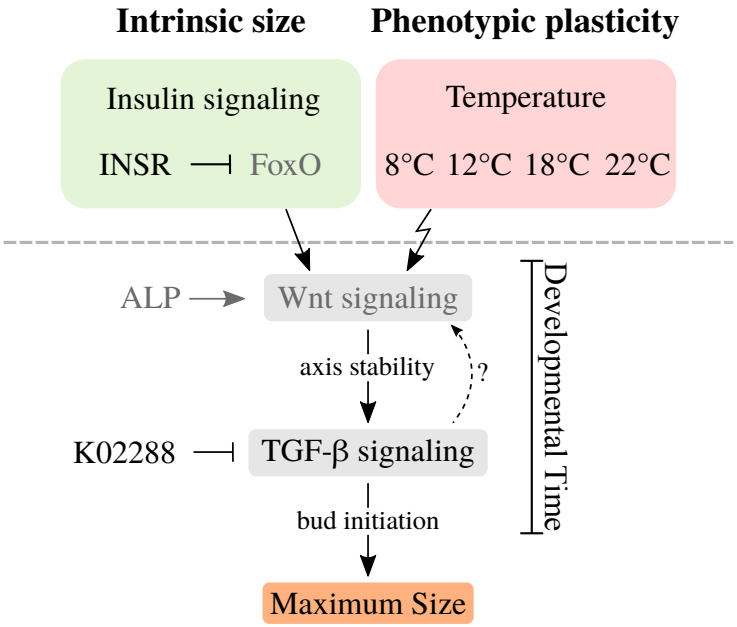

Figure 19: *Both intrinsic size and phenotypic plasticity of size are controlled via TGF-β signaling. The scheme shows the regulation of intrinsic size and phenotypic plasticity as independent inputs on Wnt signaling, which is most likely [288]. Wnt-dependent axial patterning induces bud initiation via TGF-β signaling, thereby stops the developmental growth phase and determines maximum polyp size. This process can be induced using K02288.*

3.3 Discussion

The mechanisms of species-specific and individual body size determination in animals are not well understood. Using an integrated approach combining comparative transcriptomics and functional studies in transgenic animals in an evolutionary context, I contributed to filling the knowledge gap. I could show that *Hydra*'s body size regulation in response to temperature cues and genetic factors such as INSR directly affect common developmental mechanisms including the TGF-β signaling pathway.

Hydra is an exceptional model allowing studies of phenotypic plasticity and functional genetic approaches in animals sharing the same genetic background. I were able to show that individual size regulation in *Hydra* is heavily dependent on both environmental cues and genetic factors. Polyps become larger with decreasing rearing temperatures, resulting in a doubling of epithelial cell number and a 22% increase in cell diameter within a 14 °C range (Figure 14a, b, Figure S3a, b).

I found IIS as a genetic factor to determine maximum body size in *Hydra*. INSR-KD

led to an increase in polyp size (Figure 15a, b). Insulin signaling has been described in many organisms to be a major determinant for size, as it controls cell proliferation and promotes growth on the cellular level [350]. Insulin signaling promotes long bone elongation in mammals [351], and drives larval growth in Drosophila [221]. Interference with the insulin signaling pathway lead to smaller animals in *C. elegans* [222], *Drosophila* [352], and mice [219].

I further found that TGF-β is the effector for regulation of cell number in *Hydra*. TGF-β signaling is likewise associated with size regulation. In *C. elegans*, TGF-β causes changes in cell size and controls cell mass directly [353]. In *Hydra*, cell size is temperature-dependent but seems to be independent of TGF-β signaling. How cell size is regulated in *Hydra* remains elusive for now, but TGF-β signaling seems to control only cell number, not cell size. In mammals, size is determined by long bone growth and TGF-β signals are needed for bone elongation as well as bone maturation, and thus size determination [351]. I thus suggest a highly conserved role of IIS and TGF-β signaling for size regulation in metazoans.

Interestingly, *Hydra*'s size regulation is independent of cell proliferation and mediated by bud initiation. Bud initiation can be considered as a developmental switch between growth and reproductive phase, as it is described for most determinate growing animals [354, 355]. Timing of this switch is determined by a cascade of IIS and TGF-β signaling in *Hydra*.

IIS and TGF-β signaling have been described in several model organism to promote progression through developmental stages. In *C. elegans*, both pathways control formation of the dauer form and are needed to correctly induce moulting at appropriate sizes [356]. In *Drosophila* exists a similar regulation, as IIS drives pupation at adequate sizes and TGF-β seems to be needed to prime the tissue to receive the insulin signal [350, 357]. Mammals show delayed sexual maturation with defects in the IIS [74], and TGF-β signaling is needed for the production of sexual hormones to induce puberty [358, 359].

All described model systems seem to measure size and switch developmental programs after passing a 'critical size' threshold [297,308]. Developmental timing depends on reaching this target sizes and can be delayed or shortened, depending on the size of the animal. The threshold sizes are genetically determined and IIS and TGF-β signaling are needed to promote growth to these developmental brinks and to induce the developmental switch. Once the developmental programs have changed, IIS and TGF-β signaling outcomes change as well and drive developmental programs to fix size [308,350]. It was shown that Wnt signaling is involved in regulation of developmental time [288] and might act as mediator between the insulin/temperature signaling and the TGF-β pathway described in this work here. This proposes a role of Wnt signaling in body size measurement, which in turn functions as a reference point to determine developmental timing, at least in *Hydra*. This finding poses the question, of whether this form of size measurement is specific to *Hydra* or whether a similar mechanism exists in other model organisms. Wnt signaling has been shown to be a genetic contributor to body and organ size in other species, rendering it a good candidate for size measurement among all animals.

My study shows, that *Hydra* integrates temperature signals into TGF-β signaling. While the mechanism of temperature sensing remains elusive to date, TGF-β signaling has been associated with mainly intrinsic developmental cascades. *C. elegans* releases TGF-β in response to the reception of population density, as an environmental factor [360]. My results add temperature to the list of environmental cues which are processed by the TGF-β signaling and which determine body size in *Hydra*. This suggests a role of TGF-β signaling as a more general environmental signal integrator and it might be worth to look for environment dependent TGF-β signaling in other model organisms. Finally, the

integration of environmental signals into conserved developmental processes highlights the potential of external factors shaping individual development and evolution in all metazoa.

With this study I generated a model, where intrinsic and environmental cues utilize the same developmental pathways to regulate body size in *Hydra*. I suggest, that Wnt signaling serves as a size measuring tool for the tissue and determines critical size by control over axis stability, based on the research of others on this topic [253,288]. Once the critical size is reached, TGF-β signaling is activated and induces a secondary axis through bud formation, determining maximum size in a cell number dependent manner. Both pathways determine the developmental time for *Hydra* to grow and reach its final body size (Fig. 7). Thus, intrinsic and environmental signals control a hierarchical signaling cascade of TGF-β signaling, which mediate developmental timing and finally body size.

3.4 Methods

3.4.1 Animal culture

Experiments were carried out with *Hydra vulgaris* (strain AEP) [239]. All lines were continuously cultured under the described temperature conditions (8 °C, 12 °C, 18 °C or 22 °C) in HM (0.28 mM $CaCl_2$, 0.33 mM $MgSO_4$, 0.5 mM $NaHCO_3$ and 0.08 mM KCO_3) according to the standard procedure [302]. The animals were fed two times a week at 8 °C and 12 °C and three times a week at 18 °C and 22 °C. During experimental setups the animals were fed four times a week.

3.4.2 Transgenic animals

The stable knockdown line for the INSR was achieved by generating transgenic polyps expressing an INSR hairpin construct fused to eGFP under control of an actin promoter (Figure S7). The vectors were injected into *Hydra vulgaris* (AEP) embryos as previously described [227]. By selecting for egreen fluorescent protein (GFP)-expression, mass cultures with epithelial expression of the construct were generated. Clonal animals without any eGFP expressing cells served as control for the KD line [361].

3.4.3 Tissue digestion and size determination using flow cytometry

For maximum size determination, animals in the early budding state were selected from the mass culture. Per replicate, individual polyps were digested in 100 μl of 50 U/ml Pronase E (*Serva*) in an isotonic culture medium [303] and inverted every 10 min for four hours at 18 °C. The living cells were then measured on a BD FACSCalibur with CellQuestPro v5.2 (*Becton–Dickinson*) using forward scatter and side scatter with a blue 488 nm laser to gate the epithelial cells. Epithelial cells were previously localized by measuring transgenic GFP expressing epithelial *H. vulgaris* (AEP) lines [227] using the FL-1 filter (530/30 nm) (Figure S2). Gating and further analyses were performed with FCSalyzer 0.9.13-alpha (https://sourceforge.net/projects/fcsalyzer/). Cells of the interstitial cell lineage were not evaluated to exclude effects of germ line producing cells under varying environmental conditions. However, epithelial cells are a very good proxy for the maximum polyp size [303,304], since they are much larger than cells from the interstitial cell lineage and because of their role in determination of morphological features of *Hydra* [261, 262].

3.4.4 Transcriptome assembly and annotation

To improve mapping of low expression genes, a new *Hydra vulgaris* (AEP) transcriptome was assembled from 25 libraries of the control samples (including 5 samples from another project of my working group [288]). The libraries were corrected for sequencing errors using Rcorrector 1.0.2 [362]. Afterwards possible adapter sequences tailing the reads were removed applying Cutadapt 1.13 [363] and residual rRNA reads were filtered by mapping the libraries against the SILVA rRNA database [364] using Bowtie 2 2.2.9 [365]. The Trinity assembler [335] was used to generate a *de-novo* transcriptome, performing *in silico* normalization to keep a maximum of 50 redundant reads and allowing a minimal coverage of five bases for generating confident contigs. To reduce the size of the resulting transcriptome I performed two clustering steps: First I clustered the sequences by similarity applying CD-HIT-EST, allowing 1 % divergence [366]. Second, I quasi-mapped all 60 libraries (20 samples came from a related project [288]) to the given transcriptome using sailfish 0.10.0 [367] and clustered the sequences for similarity of shared equivalence classes using RapClust 0.1.2 [368]. I isolated the longest sequence as the gene representative from the resulting clusters and used the obtained and reduced transcriptome to predict ORFs utilizing Transdecoder 5.01 (https://github.com/TransDecoder/TransDecoder). The predicted peptides were than submitted to a web based KEGG ontology (KO)-annotation tool BlastKOALA [369]. Furthermore a SMART, Pfam domain and PANTHER family prediction was performed using the InterProScan tool 64.0 [370]. Where possible, I obtained a reviewed UniProt member of all annotated PANTHER subfamilies and annotated the KO number of this UniProt member.

3.4.5 RNA-Seq analyses

For transcriptome sequencing transgenic lines were cocultured in shared HM with according controls for at least four weeks in five independent replicates. After sampling, animals were frozen in TRIzol (*Thermo Fisher Scientific*) at -20 °C until RNA-extraction with the PureLink RNA Mini Kit (*Ambion*) according to the manufacturer's protocol. Additionally, the optional on-column DNA digestion was performed. The RNA was eluted in 30 μl and checked for sufficient quality. If necessary, the RNA was purified using 1-butanol and diethyl ether [371] and frozen at -80 °C until further use. Total RNA sequencing with previous ribosomal depletion was performed for the 40 libraries on the *Illumina HiSeq2500 v4* platform, with 125 bp paired-end sequencing of 12 libraries per lane. This resulted in 30-40 million reads per sample after quality control. Quality and adapters were trimmed using PRINSEQ-lite 0.20.4 [372] and Cutadapt 1.13 [363]. Subsequently, mapping against the newly assembled transcriptome was performed using Bowtie2 2.2.9 [365]. All downstream analyses were conducted in 'R' [373]. Differentially expressed contigs were identified with the package DESeq2 1.16.1 [374] after batch correction with SVA 3.28.0 [375].

3.4.6 TGF-β receptor inhibitor experiments

To investigate the effect of TGF-β signaling on maximum polyp size, budless animals were continuously treated with different sublethal concentrations of the TGF-β-receptor inhibitor K02288 (*Sigma-Aldrich*). K02288 stock solutions of 10 mM in DMSO were stored at -20 °C and further diluted with HM to the according concentrations. After at least one week of incubation with daily feeding, animals with a bud protrusion were collected and digested for flow cytometry analysis and maximum size determination. To show the involvement of developmental time ΔT_1 (bud detachment to first bud protrusion) in the maximum polyp size, overnight detached buds were immediately incubated in 1 μM

K02288 and starved for five days. Under daily feeding the animals were further cultured in the inhibitors until first bud protrusion. In all experiments control medium contained an equal concentration of DMSO ($< 0.05\%$(v/v)).

3.4.7 Cell cycle analysis

In general, cell cycle analysis was performed as previously described using BrdU labeling [243]. For 72 h BrdU labeling animals where incubated in HM containing 1 mM BrdU. For analysis of BrdU labeled cells using a cytometer, cells were dissociated as described above and fixed for 10 min in 4 % PFA. The cell's DNA was denatured using 1.5 M HCl for 45 min at room temperature, primary antibody (mouse-α-BrdU, *Roche*) was applied 1:100 in PBS + 1 % BSA over night at 4 °C. Secondary antibody (goat-α-mouse 488 alexa fluor coupled, *Invitrogen*) was incubated 1:500 in PBS + 1 % BSA for 1 h at room temperature. Samples were analyzed immediately after staining.

3.4.8 Statistics

Statistical analyses were performed using two-tailed Student's-t-test or Mann-Whitney-U-test where applicable. If multiple testing was performed, p-values were adjusted using the Benjamini-Hochberg correction [305].

3.5 Supplementary information

Table S6: *The table shows statistics for the gating strategy in order to count epithelial cells of the polyps. Percentages are related to the total cell counts for GFP+ and eptithelial cells. Accuracy is given as the ratio of GFP+ epithelial cells to gated epithelial cells in the upper right quadrant (Compare to Figure S2).*

GFP ecto/endo (n=4)	Mean	SD
Total cells	70477	11367
GFP+	15458	2878
Epis gated (+/+)	15936	4070
GFP+ (%)	21.9	0.9
Epis gated (%)	22.4	2.9
Accuracy (%)	98.4	8.7

Table S7: *Statitistics for the assembly gives information about number of sequences, length and ORFs distribution, for clustered nucleotide and protein sequences.*

Nucleotides		Protein	
n seqs	220458	n seqs	38261
smallest	201	smallest	99
10th perc	220	10th perc	105
25th perc	257	25th perc	118
mean len	578.59	mean len	293.06
median len	361	median len	164
75th perc	611	75th perc	329
90th perc	1136	90th perc	602
largest	36341	largest	12022
n bases	127555099	n AA	11212618
> 200	220458	> 200	15703
> 500	72383	> 500	5198
> 1000	27014	> 1000	1399
> 5000	697	> 5000	15
> 10000	102	> 10000	1
N90	258	contigs w. ORF	31325
N70	434		
N50	746		
N30	1375		
N10	3052		
GC%	0.31		

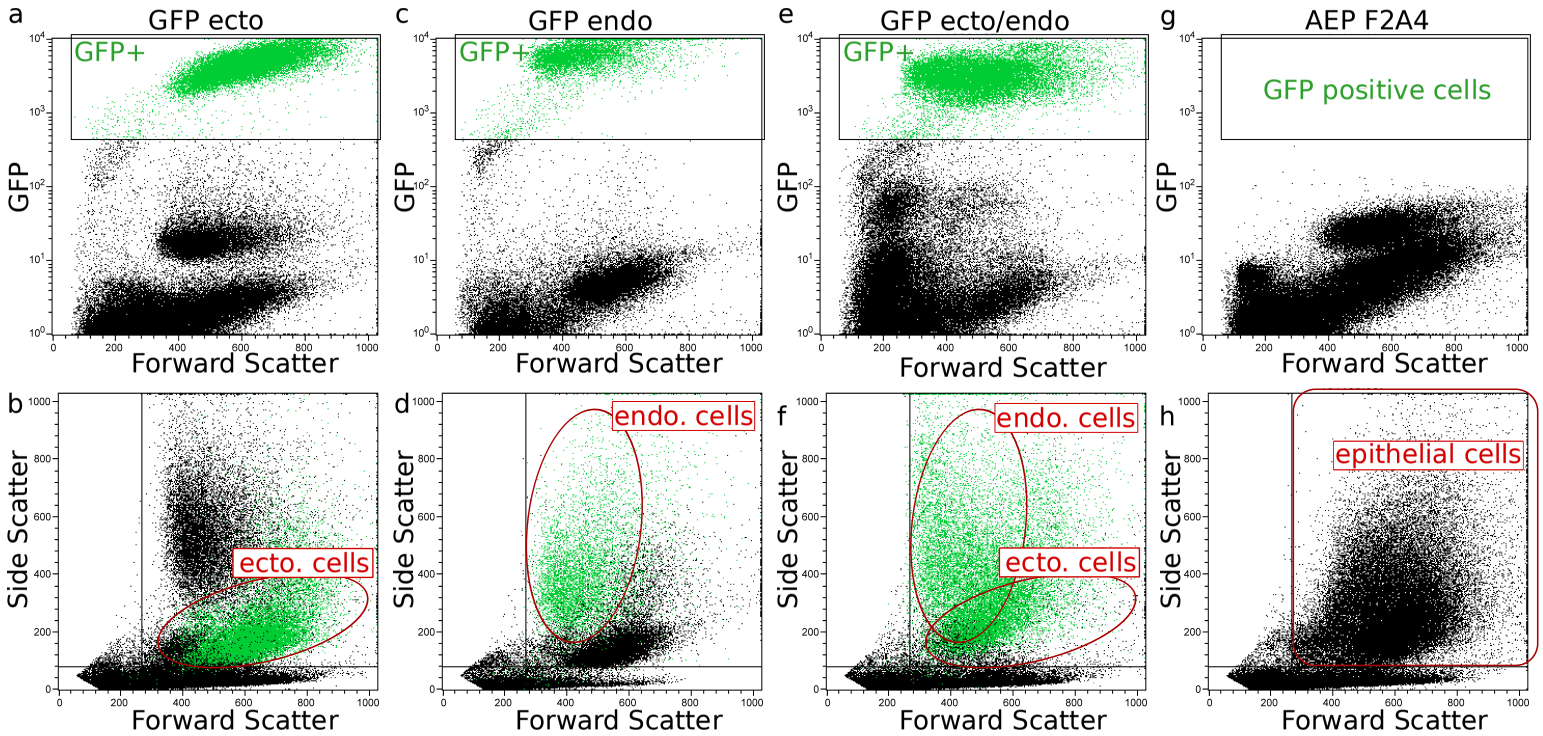

Figure S2: *Flow cytometry allows counting of epithelial cells. For calibration we (collaboration, see text [288]) used previously published transgenic Hydra lines expressing GFP in the epithelium [227]. Ectodermal and endodermal GFP expressing cells were gated for forward scatter and the GFP channel (a,c,e). Gated cells were localized in plots for forward and side scatter (b,d,e). Wildtype epithelial cells (AEP F2A4) were localized using the gates for GFP epithelial cells and counted utilizing the upper right quadrant for the forward and side scatter only (g+h).*

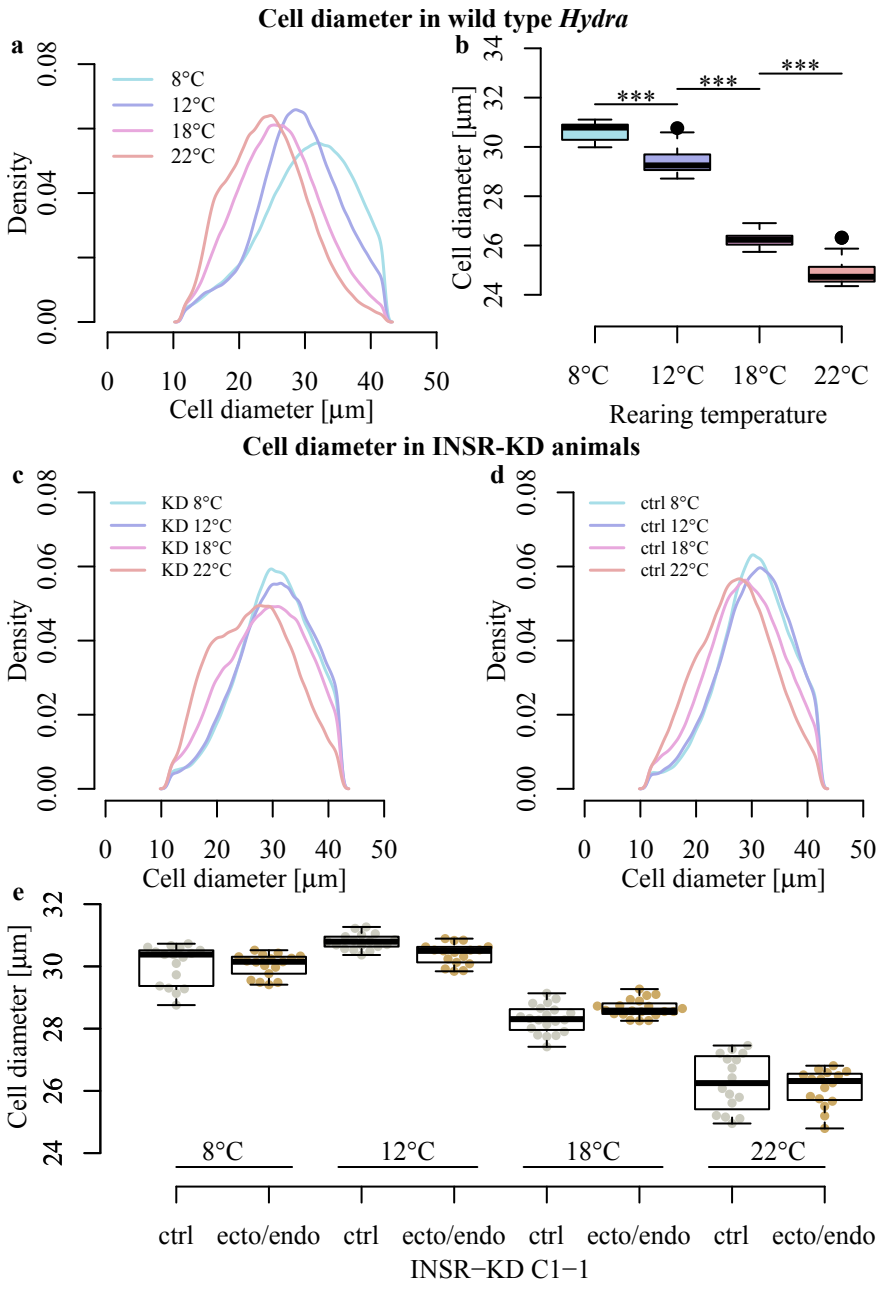

Figure S3: *Cell sizes increased in* Hydra *reared at lower temperatures. Cell diameters were measured using the forward scatter of the flow cytometer. Density plots show the distribution of epithelial cell sizes across all samples and cells of one conditions and illustrate clear shifts of cell diameters with alteration of temperature in wild type (a), INSR-hairpin control (b), and INSR-KD animals (c). (b,e) Comparing the mean epithelial cell diameter of replicates between different conditions revealed significant differences in cell sizes with temperature but not with INSR-KD. *:$p \leq 0.05$, **:$p \leq 0.01$, ***:$p \leq 0.001$*

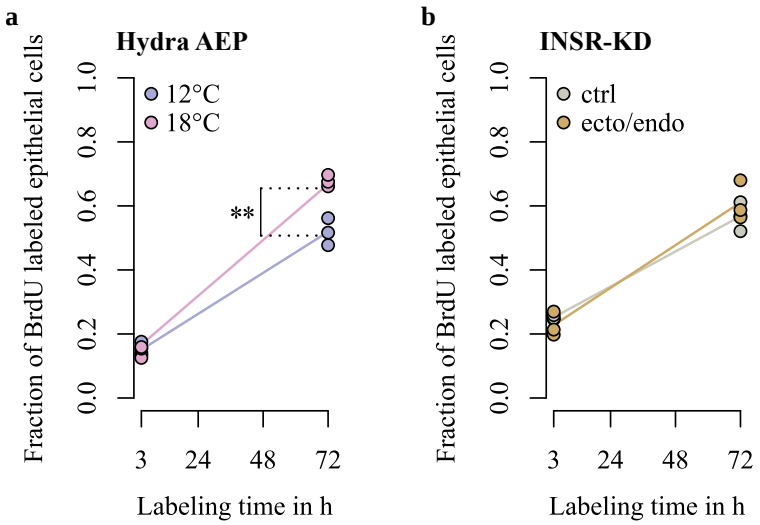

Figure S4: *Cell proliferation was determined using BrdU labeling for 3 h and 72 h. (a) Labeling for* Hydra *wildtype polyps (AEP F2A4) reared at 12 °C and 18 °C showed higher proliferation at 72 h for animals cultured at 18 °C. n = 3 (b) INSR-KD vs. control showed no difference in proliferation after 3 h or 72 h (n = 3).*:p ≤ 0.05, **:p ≤ 0.01*

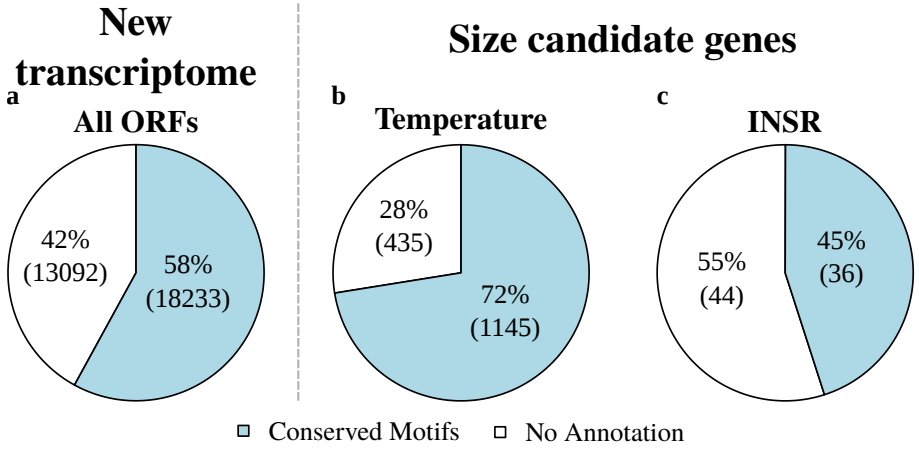

Figure S5: *Proportions of ORFs containing conserved motifs to orphan genes without any annotation. Ratio of annotation of all ORFs of the newly assembled transcriptome (a) and candidate genes for size determination from temperature (b), and INSR-KD (c).*

a
Normalized read counts for ACVR2A (cluster44841)
0 400 800
**
08°C 12°C 18°C 22°C
Rearing temperature
b
Normalized read counts for ACVR2A (cluster44841)
0 400 800
ctrl KD
8°C INSR−HP
c
Normalized read counts for ACVR2A (cluster44841)
0 400 800 1200
ctrl KD
18°C INSR−HP
d
Normalized read counts for CALM (cluster119842)
0 1000 2500
**
08°C 12°C 18°C 22°C
Rearing temperature
e
Normalized read counts for CALM (cluster119842)
0 1000 3000
ctrl KD
8°C INSR−HP
f
Normalized read counts for CALM (cluster119842)
0 1000 2000
ctrl KD
18°C INSR−HP
g
Normalized read counts for CALM (cluster17829)
0 50 100
***
08°C 12°C 18°C 22°C
Rearing temperature
h
Normalized read counts for CALM (cluster17829)
0 20 40 60
ctrl KD
8°C INSR−HP
i
Normalized read counts for CALM (cluster17829)
0 50 100 200
ctrl KD
18°C INSR−HP
j
Normalized read counts for CASP3 (cluster162063)
0 200 400 600
* ***
08°C 12°C 18°C 22°C
Rearing temperature
k
Normalized read counts for CASP3 (cluster162063)
0 200 400 600
ctrl KD
8°C INSR−HP
l
Normalized read counts for CASP3 (cluster162063)
0 200 500
ctrl KD
18°C INSR−HP
m
Normalized read counts for CASP3 (cluster128189)
0 200 400
***
08°C 12°C 18°C 22°C
Rearing temperature
n
Normalized read counts for CASP3 (cluster128189)
0 100 300
ctrl KD
8°C INSR−HP
o
Normalized read counts for CASP3 (cluster128189)
0 200 400
ctrl KD
18°C INSR−HP

p
Normalized read counts for CASP7 (cluster28982)
0 100 300
**
08°C 12°C 18°C 22°C
Rearing temperature
q
Normalized read counts for CASP7 (cluster28982)
0 50 150 250
ctrl KD
8°C INSR−HP
r
Normalized read counts for CASP7 (cluster28982)
0 100 300
ctrl KD
18°C INSR−HP
s
Normalized read counts for CASP7 (cluster61482)
0 100 300
* **
08°C 12°C 18°C 22°C
Rearing temperature
t
Normalized read counts for CASP7 (cluster61482)
0 50 100 200
ctrl KD
8°C INSR−HP
u
Normalized read counts for CASP7 (cluster61482)
0 100 300
ctrl KD
18°C INSR−HP
v
Normalized read counts for CER1 (cluster44629)
0 50 100 200
**
08°C 12°C 18°C 22°C
Rearing temperature
w
Normalized read counts for CER1 (cluster44629)
0 50 150
ctrl KD
8°C INSR−HP
x
Normalized read counts for CER1 (cluster44629)
0 50 100 150
ctrl KD
18°C INSR−HP
y
Normalized read counts for FGFR1 (cluster26848)
0 100 300
**
08°C 12°C 18°C 22°C
Rearing temperature
z
Normalized read counts for FGFR1 (cluster26848)
0 20 40 60 80
ctrl KD
8°C INSR−HP
a'
Normalized read counts for FGFR1 (cluster26848)
0 50 100 200
ctrl KD
18°C INSR−HP
b'
Normalized read counts for FGFR1 (cluster74599)
0 500 1500
**
08°C 12°C 18°C 22°C
Rearing temperature
c'
Normalized read counts for FGFR1 (cluster74599)
0 500 1500
ctrl KD
8°C INSR−HP
d'
Normalized read counts for FGFR1 (cluster74599)
0 500 1500
ctrl KD
18°C INSR−HP

e'
Normalized read counts for INHB (cluster160630)
0 200 500
***
*
08°C 12°C 18°C 22°C
Rearing temperature
f'
Normalized read counts for INHB (cluster160630)
0 200 500
ctrl KD
8°C INSR−HP
g'
Normalized read counts for INHB (cluster160630)
0 100 300
**
ctrl KD
18°C INSR−HP
h'
Normalized read counts for KRAS (cluster144503)
0 100 200 300
***
***
08°C 12°C 18°C 22°C
Rearing temperature
i'
Normalized read counts for KRAS (cluster144503)
0 50 100
ctrl KD
8°C INSR−HP
j'
Normalized read counts for KRAS (cluster144503)
0 50 100 200
ctrl KD
18°C INSR−HP
k'
Normalized read counts for NBL1 (cluster172682)
0 500 1000
***
**
08°C 12°C 18°C 22°C
Rearing temperature
l'
Normalized read counts for NBL1 (cluster172682)
0 200 600
*
ctrl KD
8°C INSR−HP
m'
Normalized read counts for NBL1 (cluster172682)
0 500 1000
ctrl KD
18°C INSR−HP
n'
Normalized read counts for NOTCH1 (cluster33833)
0 200 400
***
08°C 12°C 18°C 22°C
Rearing temperature
o'
Normalized read counts for NOTCH1 (cluster33833)
0 200 400
ctrl KD
8°C INSR−HP
p'
Normalized read counts for NOTCH1 (cluster33833)
0 100 300
ctrl KD
18°C INSR−HP
q'
Normalized read counts for NOTCH1 (cluster2180)
0 1000 3000
**
*
08°C 12°C 18°C 22°C
Rearing temperature
r'
Normalized read counts for NOTCH1 (cluster2180)
0 2000 4000
ctrl KD
8°C INSR−HP
s'
Normalized read counts for NOTCH1 (cluster2180)
0 1000 2500
ctrl KD
18°C INSR−HP

t'
Normalized read counts for NOTCH1 (cluster71467)
0 400 800
**
08°C 12°C 18°C 22°C
Rearing temperature
u'
Normalized read counts for NOTCH1 (cluster71467)
0 200 400 600
ctrl KD
8°C INSR−HP
v'
Normalized read counts for NOTCH1 (cluster71467)
0 200 600
ctrl KD
18°C INSR−HP
w'
Normalized read counts for NOTUM (cluster117759)
0 200 600
** ***
08°C 12°C 18°C 22°C
Rearing temperature
x'
Normalized read counts for NOTUM (cluster117759)
0 400 800
ctrl KD
8°C INSR−HP
y'
Normalized read counts for NOTUM (cluster117759)
0 200 400 600
ctrl KD
18°C INSR−HP
z'
Normalized read counts for RRAS (cluster184674)
0 200 600
*** ***
08°C 12°C 18°C 22°C
Rearing temperature
a''
Normalized read counts for RRAS (cluster184674)
0 200 600
ctrl KD
8°C INSR−HP
b''
Normalized read counts for RRAS (cluster184674)
0 100 300
ctrl KD
18°C INSR−HP
c''
Normalized read counts for TGFB2 (cluster152880)
0 50 150
** *** *
08°C 12°C 18°C 22°C
Rearing temperature
d''
Normalized read counts for TGFB2 (cluster152880)
0 5 10 20
ctrl KD
8°C INSR−HP
e''
Normalized read counts for TGFB2 (cluster152880)
0 50 100 150
ctrl KD
18°C INSR−HP
f''
Normalized read counts for THBS1 (cluster86269)
0 5000 15000
*** *** **
08°C 12°C 18°C 22°C
Rearing temperature
g''
Normalized read counts for THBS1 (cluster86269)
0 100 200 300
ctrl KD
8°C INSR−HP
h''
Normalized read counts for THBS1 (cluster86269)
0 2000 4000
ctrl KD
18°C INSR−HP

Figure S6: *Normalized read counts of the transcriptome analysis for the candidate genes from Table 5 under the different conditions tested (INSR-KD vs. control at 8 °C and 18 °C, and temperature shift; n = 5). Note that some candidate genes from Table 5 have several isoforms, which are plotted individually. *:p ≤ 0.05, **:p ≤ 0.01, ***:p ≤ 0.001*

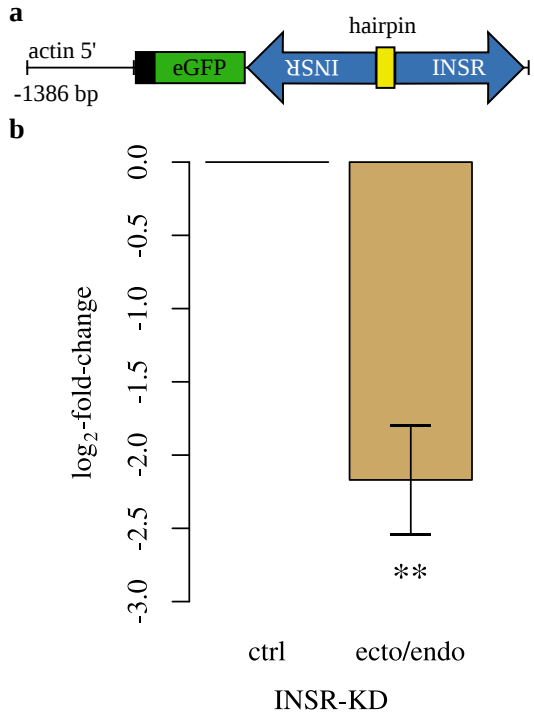

Figure S7: *Schematic representation of the shRNA constructs for* insR *(a) leading to transcript downregulation (b). n ≥ 5*

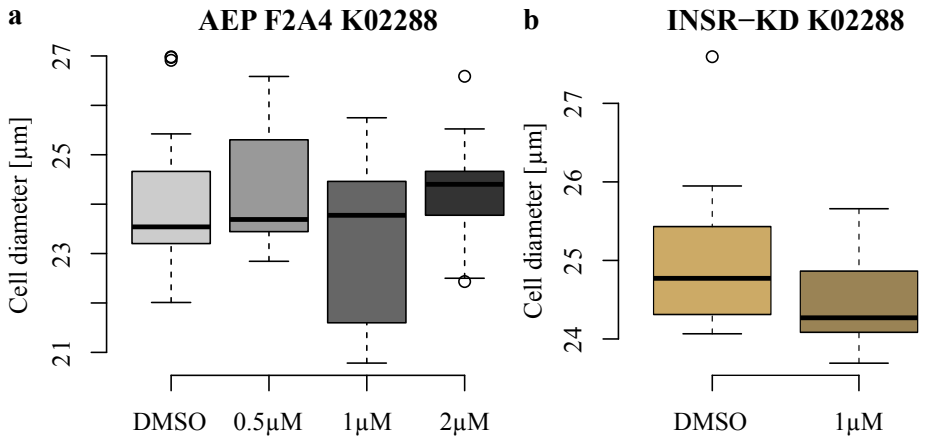

Figure S8: *Treatment with the specific TGF-β-recptor inhibitor K02288 did not alter cell size, neither (a) in the control* Hydra*-line F2A4 nor (b) in the INSR-KD polyps.*

4 General discussion

4.1 Growth patterns in evolution

The presented semi-discrete model in this thesis resembles typical growth dynamics observed in most metazoan species, characterized by an initial growth phase followed by a cessation of growth [354,355]. The growth of *Hydra* can thus be described as determinate, because polyps reach a final size and allocate energy surplus to reproduction (asexual or sexual), rather than further growth, given a constant environment. However, *Hydra* is able to dynamically adapt its maximum size to changes in the environment, which gives it features of both, determinate and indeterminate growth.

Most growth models use experimental data to derive/predict certain time points or sizes in development of an organism [376], which is different to the approach presented here. I used theoretical considerations of cell dynamics in *Hydra* and filled variables with experimental data, to predict developmental time points and population dynamics for individual strains of one species. A similar model has been generated in a more general approach for metabolic rates and is most probably applicable to *Hydra* as well, though metabolic rate data is missing for *Hydra* [377]. The predictions made here, can be fitted to the experimental data afterwards, demonstrating validity of the model. I used the model to explore variable space and to generate regression models for prediction of unknown values.

Interestingly, the model predicts no influence of body size on asexual population growth in *Hydra*, raising the question, why size adjustments occur to environmental conditions. The two major size adjustment parameters are nutritional state and temperature in *Hydra* [242,263]. Both are associated with contrary PGR. In the first case, more feeding resulted in larger polyp size and more offspring per polyp and time, while in the latter case, lower temperature results in larger body size with smaller PGR [242,263]. More feeding provides more resources which can be allocated to cell proliferation, which results in more cells being available for displacement into a new bud. My model predicts a certain degree of size variation with changes in proliferation rates which may explain the observed size differences in a study by Otto and Campbell, though this remains only speculative, since numbers for epithelial cells per polyp lack in the study [242]. I could resemble the size changes observed in a study by Bisbee and can show that reduced population growth is probably caused by a prolonged cell cycle in animals reared at lower temperatures [263]. These results indicate that size changes occur independently of advantages in population growth rates and that distinct evolutionary mechanisms have to determine these size adjustments. Sebens [71] suggested a prey size dependent body size adaptation for clonal and indeterminate growing organism. However, it is unlikely that prey directly caused the body size changes observed in my and previous experiments, since all polyps were fed with *Artemia* nauplii in a standardized protocol [242, 263]. More likely appears the possibility that larger body size is a form of nutrient storage in *Hydra*. Lower temperatures indicate forthcoming winter and the associated lack of prey. This could cause an increase in body size along with a reduction in population growth to raise the probability of survival during long courses of starvation. Inversely, high temperatures are usually accompanied by expansion of prey populations, allowing for a reduction of tissue maintenance costs, due to fewer cells. This comes to the cost of reduced starvation resistance, but with the advantage of being able to allocate more resources into reproduction. Similarly, in times of good nutrient availability at stable temperatures, budding might be increased to a maximum and the surplus of energy is used to expand food storage.

4.2 Neuronal control of plastic adaptation of body size to environment

There have been various evidences that neurones and nerve cell factors can regulate body size in several species. In *C. elegans* sensory nerve cells can mediate changes in cell size and thus body size [360]. Furthermore, the most important size regulating factors ILP and TGF-β show neuronal expression in the nematode [209, 356, 378]. Moreover, it has been shown that *C. elegans* senses temperature via thermo-sensitive neurons and adjusts size to temperature cues [379–381]. *Drosophila* nerve cells can mediate the size difference of the sexual dimorphism similarly as glia and cholinergic neurons can alter body size in a nutrient dependent way [382, 383]. In humans, there are congenital brain deformations, which cause a deficiency of growth hormones without structural defects of the pituitary gland, causing reduced height in these patients (e. g. septo-optic dysplasia) [384]. All these neuronal signals eventually lead to changes in IIS and/or TGF-β signaling, which directly affect growth rates and developmental timing in the different organisms. These alterations of the IIS and TGF-β are often mediated by direct neuronal interaction [360, 382] or caused by secondary hormones like the GH in humans [183, 384]. This renders the two pathways highly variable to different environmental and efferent intrinsic signals, which eventually mediate phenotypic plasticity. Unraveling the inputs in these regulations will be key to understand how organisms adjust their own developmental programs to the given environmental conditions, which have ecological and eventually evolutionary relevance.

There is good evidence, that a similar mechanism of IIS and TGF-β signaling exists in *Hydra*, as colleagues have described neuron specific expression of ILPs in *Hydra*, resembling a similar expression pattern as in *C. elegans* or *Drosophila* [385, 386]. I could show that INSR-KD controls developmental timing for bud initiation and thus body size. Additionally it has been a reported, that pharmacological interference with neuronal activity in *Hydra* leads to dwarfish animals [387]. Differently sized mutants grow to similar sizes if nerve cells are depleted in *Hydra* and nerve cell transplantations from these animals can alter the size of the recipient animal [388]. It would be interesting to see if the effect of temperature on body size in *Hydra* is also mediated via nerve cells. Although, basic patterning and growth behavior is mediated by the epithelial cell line in *Hydra*, nerve cells seem to coordinate these processes and adjust them to the environmental conditions [389, 390]. These features render *Hydra* a suitable model to investigate the signal transduction via the rather simple nerve cell system to developmental processes, like body size regulation. Since there exists this general pattern of neuronal derived environment sensing across diverse species for body size regulation, the results obtained in this model are very likely to be transferable to other organisms and even humans.

4.3 Bud formation resembles limb bud formation of higher organisms

Noteworthy is the parallel regulation of limb bud formation in vertebrates and bud initiation/elongation in *Hydra*. Although the exact mechanism of bud formation regulation in *Hydra* is missing, there are at least similar factors involved. In vertebrates initial expression of T-box transcription factor (Tbx) and pituitary homeobox (Pitx) at the site of the later limb induces the expression of Wnt members and FGF10, which in turn drives the expression of Wnt3 [391–395]. Together with a BMP, Wnt induces the expression of FGF8. FGF8 forms a regulative network with BMPs, Gremlin and Hh family members, which forms the apical ectodermal ridge (AER) and causes limb bud elongation [85, 392, 396] (Figure 20).

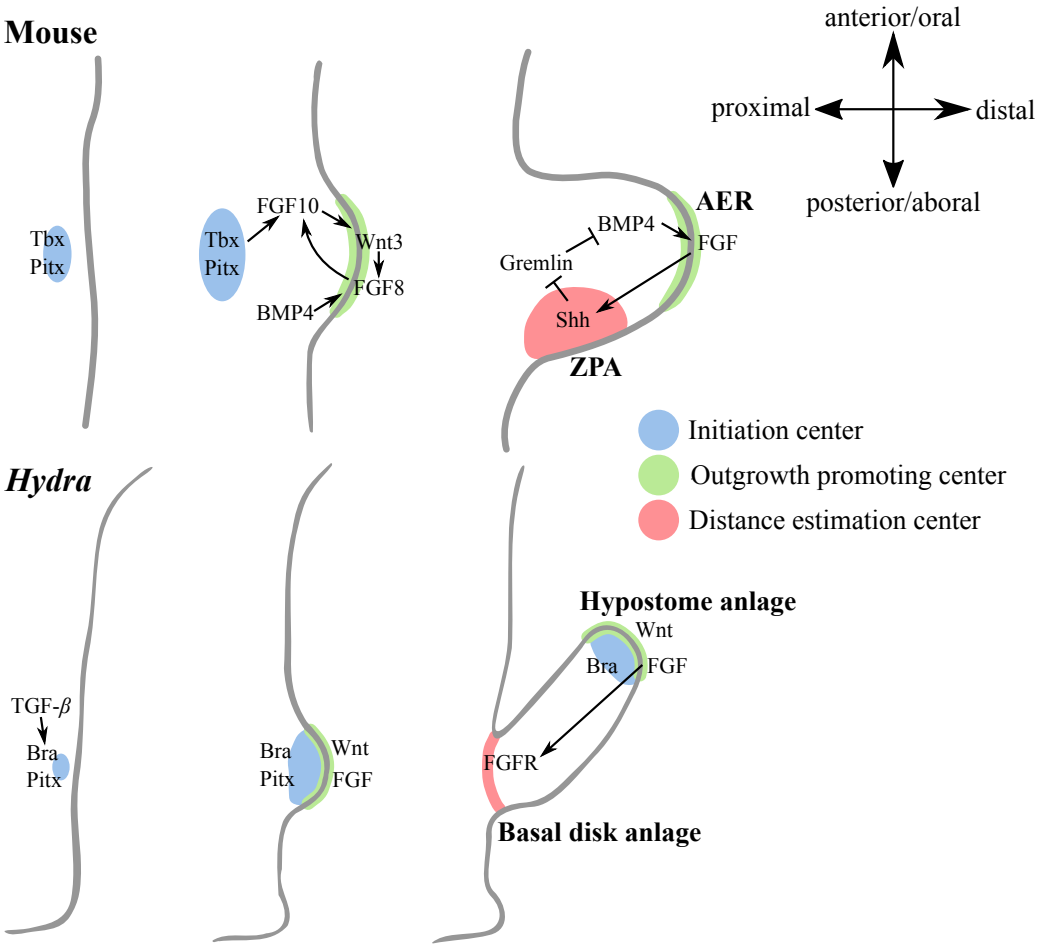

Figure 20: *The bud formation of* Hydra *resembles bud formation in vertebrates. Tbx/Bra and Pitx initiate the formation of a limb/bud protrusion. The tip starts to express Wnt and FGF and forms the AER in vertebrates and the hypostome anlage in* Hydra*. FGF mediates the signal back to the base of the protrusion and drives limb/bud outgrowth. The distance is measured by the ZPA in mouse and the basal disk anlage in* Hydra*. The outgrowth might be terminated, if the FGF signal becomes too faint due to the long distance of the distance estimation center and the tip of the outgrowing limb/bud.*

In *Hydra* there is a similar sequence of events seen during bud formation. Wnt induces the expression of a Nodal-like protein (another TGF-β member), which induces Pitx [253]. This is accompanied by the expression of Bra (a Tbx homolog) in the tip of the early bud, even before a bud protrusion can be seen [397]. Another signaling center of Wnt is generated in the protrusion, which later forms the hypostomal Wnt-center of the bud [398]. Afterwards FGF expression is observed and is necessary for bud elongation and detachment [254, 399–401]. Whether the sequence of events reflects also the action of regulation is not clear for *Hydra*, but the similarity is striking and suggests that the mechanism of limb formation is evolutionarily conserved in the prebilaterian *Hydra* (Figure 20). I could show in this work, that IIS and temperature cues are upstream regulators for the bud initiation, directly affecting the TGF-β pathway. Parallel obtained results in the lab additionally indicate an interaction of IIS and temperature with the Wnt signaling, suggesting IIS as a master regulator for bud formation in *Hydra* [288]. Thus, the initial function of IIS and TGF-β signaling can be considered to link environmental factors to coordinate developmental programs and adjust them to the needs of the given environment.

4.4 A putative, conserved signaling pathway regulates developmental timing and size in all metazoans

The size regulatory effect of IIS is usually thought to be mediated by its growth factor function and activation of the PI3K pathway which leads to the cell proliferation. Thus, defects in the insulin pathway lead to reduced proliferation rates and less tissue growth in a cell autonomous way, though ILP secretion is regulated on organismal level [350, 402]. However, these effects seem to apply only, if the organism is still in the growing phase of its development. *Hydra* showed neither a reduction of proliferation rates nor in cell sizes, but increased body size with the knockdown of the INSR, which excludes this route of size regulation. Interestingly, there is also a tight interaction of IIS, TGF-β signaling and switches in developmental phases (usually sexual maturation). This interaction has been linked to the end of the animal's growth phase and the beginning of the reproductive phase (Figure 21). These switches are usually mediated by some kind of steroid hormone, which in turn changes gene expression on a global scale to mediate the transition from growth to reproduction [73, 356, 403] and are induced after reaching a certain 'critical size' [59, 296, 297]. However, *Hydra* does not leave the growth phase throughout life, although a clear switch between a budding (reproduction) and a growing phase can be observed after a strain specific critical size has been reached [242].

In *C. elegans*, IIS and TGF-β are the main inputs for steroid hormone (dafachronic acid) production and are activated upon favorable environmental conditions, like high nutrient levels, low population density or moderate temperatures [209, 378]. TGF-β has growth promoting function in *C. elegans* where it is the major factor for body size control [317]. Interestingly, IIS signaling is only mildly associated with body size changes [222], but is rather associated with longevity in *C. elegans* [209]. Both signals can change the developmental decisions of the nematode and promote fast progression through the larval stages to reach sexual maturity. These effects are mediated by the production and secretion of dafachronic acid [356, 404, 405]. *C. elegans*, however does not possess a variable growing phase, as the fate of every single cell is clearly defined and the organism consists of defined number of cells (959 for hermaphrodites, 1031 for males) [406, 407]. This reduces body size regulation to the level of cell size regulation, which is affected predominantly by TGF-β signaling and to a much lesser degree by IIS [222, 317]. Body size regulation is thus less dependent on the developmental phase and growth factor signals in *C. elegans*. However, *C. elegans* serves as an instructive model for the understanding

of signaling events leading to developmental decisions, which are very important for size regulation in other animals. The derived cascade serves as a prototype for regulation of steroid hormone production/secretion which determine developmental phase transitions, e. g. in *Drosophila* and humans [73, 80] (Figure 21). Another interesting feature of the dafachronic acid production is the responsiveness to Wnt signaling, which interacts with IIS in *C. elegans* and relates back to the signaling cascade observed in *Hydra* [288, 408].

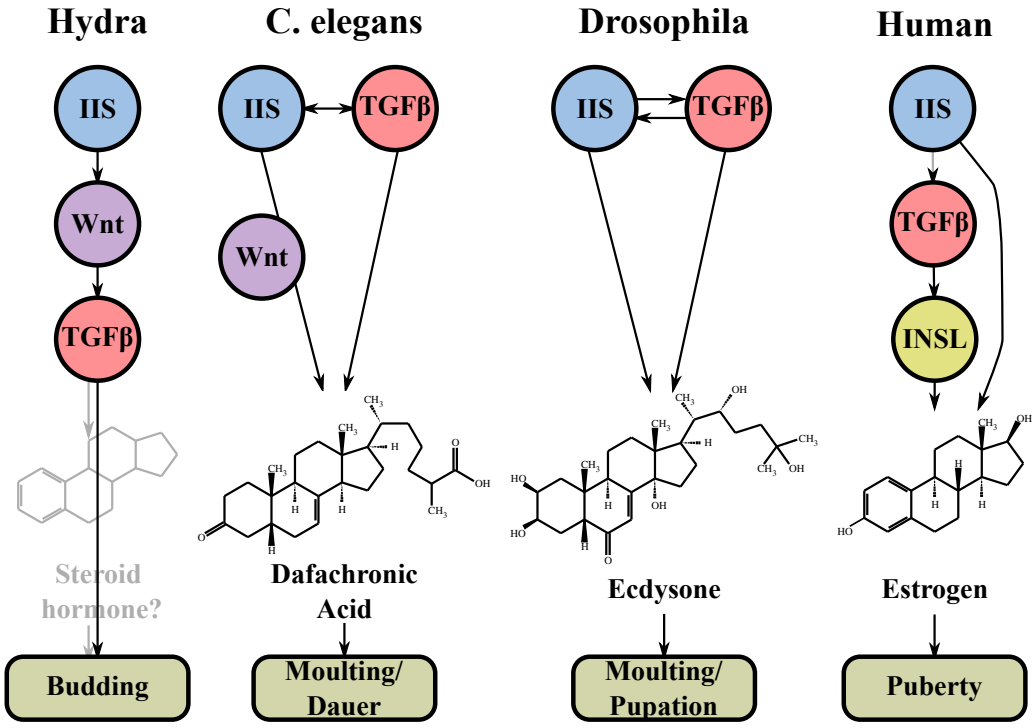

Figure 21: *A common regulation of steroid hormone production, which regulates developmental progression is conserved from nematodes to human. Steroid hormones determines the length of growth phase, point of sexual maturation and thus body size in bilaterians.* Hydra *employs similar molecular mechanisms for body size regulation using a signaling cascade including IIS and TGF-β signaling. Steroid hormone production might be a possible mechanism for bud induction (grey) in* Hydra *as well.*

In *Drosophila*, different developmental steps, as the larval moulting and pupation are controlled by the production and secretion of ecdysone, the fly steroid hormone [80, 409]. Interestingly, the production of ecdysone is regulated by IIS and by the TGF-β signals in the prothoracic gland [357,410]. Specific interference with the IIS in the prothoracic gland leads to abrogation of ecdysone production, which causes either developmental arrest or increased body size, since the ecdysone peaks much later and the growth period in the larval stage is prolonged [80, 410]. This couples the nutritional state of the fly to its developmental staging. There might be a similar mechanism in *Hydra*, which would explain the inversed effect of INSR-KD and FoxO-KD compared to other model organisms. On the TGF-β side, activin has been described as important factor for ecdysone production and priming factor for insulin/IGF sensitivity of the prothoracic gland [357]. Reversely, it has been shown that IIS is controlling activin expression via FoxO, which forms a feed forward loop between the two signaling molecules [411]. This generates the same regulative

axis as it has been observed in *C. elegans* or I described for *Hydra*, except for the steroid hormone.

IIS and estrogen signals are the major determinants of body size in mammals as well, since IIS determines growth rates during childhood, while estrogen terminates the growth phase with the induction of puberty. There are several evidences that IIS, TGF-β and estrogen signaling are closely interacting in mammals, though the exact mechanism of action is still unclear. Estrogen has been recognized as a metabolism regulating agent, which is correlated with hyperinsulinemia and decreased insulin sensitivity [412], while high insulin blood levels are associated with polycystic ovary syndrome (PCOS) [413]. PCOS is caused by increased levels of androgens (estrogen progenitors), which are produced in the adrenal glands and the ovaries. IIS has been shown to increase androgen production in the adrenal glands *in vitro* [358]. In the ovaries, the androgen production is dependent on TGF-β signaling and an insulin like peptide (INSL3) [359]. Furthermore, IGF1 and BMP form a negative regulation network to regulate estrogen production in the granulosa cells of the follicle [414] (Figure 21). How the different factors interact in different tissues, how these eventually feed onset of puberty, and thus determine end of the growth phase or if they do at all, is still unclear, but there is evidence which indicates that the steroid hormone production is dependent on both, IIS and TGF-β signaling in mammals.

A similar regulation mechanism exists in the epiphyseal growth plate. Closure of the epiphyseal growth plate is fixing body size in mammals and is induced by an estrogen pulse during puberty. The epiphyseal growth plate consists of different zones of chondrocytes, which differentiate by Wnt signaling from mesenchymal stem cells, proliferate due to TGF-β and BMP signaling, start to enlarge by hypertrophy and eventually die. They leave behind an extracellular matrix scaffold, which is used by invading osteoblasts to ossificate the bone [351]. It was hypothesized that the chondrocytes have only a limited proliferation capacity and that estrogen induces proliferation, which leads to exhaustion of this capacity and eventually closes the epiphyseal plate [415]. Local and systemic IGF1 signals can promote proliferation of the chondrocytes which increases body size [351] and can drive osteoblast and chondrocyte differentiation to mature the bone [416]. The interactions between, IGF, BMP, TGF-β, and estrogen are less clear, though it is very likely that these interactions exist. IGF1, for instance, is locally expressed upon estrogen reception in chrondrocytes of the bone, and many bone specific signals are dependent on active IIS in the chondrocytes [417].

Taken together, there is a close relationship between IIS and TGF-β signaling and steroid hormone production across all metazoans. I showed that *Hydra* uses the same developmental pathways (IIS and TGF-β signaling) to regulate its body size as they are described in other model organism and that it might not be unlikely to find a *Hydra* specific steroid hormone involved in this regulation. A steroid hormone would also be a good way to transmit the ILP and Wnt signals located in the head [245, 271] to the site of budding in the body column. I also should note, that the proposed hierarchy of ILP-Wnt-TGF-β signals for bud induction is the simplest explanation, which my experiments and those of others [253,288] support, but that I cannot exclude more complicated interactions between those pathways or single members of the pathways. At least three ILPs [271,385], 11 Wnt [418] and 13 TGF-β [253] ligands have been described, which opens up the possibility of various interactions of any kind. However, the given results indicate a rather hierarchically signaling structure in *Hydra*.

Interestingly, body size regulation is a certainly underestimated factor in the research of the described pathways and their interaction. Especially in mammals, the attention on body size and the interaction between estrogen, IIS, TGF-β signaling and the termination of the growth period has been lacking. For *Hydra* the question remains whether budding

and size regulation are mediated by steroid hormones, though there are indications for such a model, as there have been reports for head activating functions for calcitriol, which is structurally related to steroid hormones [387].

How sexual maturation is induced and which environmental and intrinsic sensors take part in its regulation could answer the question of body size determination across all species in the future. It will be interesting to see, how body size is encoded within the genetics of the individual species and how environmental conditions adjust the genetic interactions to preserve a maximum fitness.

4.5 Conclusion

The aim of this thesis was to understand environmental dependent and intrinsic size regulation in *Hydra*. To achieve this, I developed a theoretical model to understand cell dynamics in the polyps and how different parameters contribute to size regulation, development and fitness. Furthermore, I used the model to derive the contribution of apoptosis to our understanding of the cell dynamics in *Hydra* (see chapter I).

I further used animals reared at different temperatures and an INSR-KD strain, which show altered body sizes, to unravel the underlying molecular pathways for size regulation in *Hydra* (see chapter II). I could show that both, temperature cues and IIS regulate TGF-β signaling and by that control bud initiation in *Hydra*. Budding is the main regulative mechanism in *Hydra* to stabilize cell number in the polyp, as predicted by the computational model. Reduction in IIS or temperature, lead to changes of a critical size set point controlling bud initiation and later onset of bud initiation. This in turn leads to an increase of the cell number in the polyp and let me conclude that the effector pathway or budding is the TGF-β signaling cascade [253]. Interference with this pathway induced premature budding and reduced total size of the polyp.

The integration of IIS and temperature cues into the conserved TGF-β pathway renders this signaling cascade a major mediator for developmental phenotypic plasticity and key regulator for size regulation. The interaction of IIS and TGF-β has been linked to switching developmental programs from a growing and developing organism to the sexual mature and fully grown adult across a variety of animal species [73, 350, 356, 357, 410]. Usually this involves a steroid hormone, which has not yet been identified in *Hydra*. I showed now that the integration of temperature signals and IIS into TGF-β signaling is conserved to prebilaterian and suggest a common cascade which mediates environment dependent body size regulation across all animal species.

4.6 Outlook

Here I presented another attempt to answer the ever occurring question in biology of how body size is regulated in animals and how environmental cues influence this regulation. I showed that the early emerging metazoan *Hydra* uses conserved mechanisms, IIS and TGF-β signaling, to regulate its body size and to integrate environmental signals into its development. I concluded that the initial function of IIS was not to regulate the cell proliferation, but rather to induce developmental transition from a growth to a reproductive phase. However, there remain many open questions. How is the temperature signal sensed and how is it transmitted to the TGF-β signaling? What role does the nervous system in coordination of developmental mechanisms in *Hydra* and other species play? How is the threshold (critical size) set for the individual animal, which, if crossed, induces the developmental switch to reproductive phase where size is fixed? Is *Hydra* also using a steroid hormone to facilitate this switch from a growing to a budding polyp? What

are the consequences of altered body sizes for the fitness of *Hydra*? Finding answers to these question will enlarge our understanding of body size regulation and integration of environmental signals in developmental processes, not only in *Hydra* but in all animal species.

5 Abbreviations

4EBP	eukaryotic translation initiation factor 4E binding protein
ACV	activin-like protein
ACVR2a	Activin-Receptor IIa
AER	apical ectodermal ridge
ALP	alsterpaullone
AMPK	AMP-activated protein kinase
AP-1	activator protein 1
APAF1	apoptotic protease activating factor 1
ATF	activating transcription factor
ATP1A	sodium/potassium transporting ATPase subunit alpha
BAD	BCL-2 antagonist of cell death
BAK	BCL-2 antagonist/killer
BAX	BCL-2 associated X protein
BCL	B-cell lymphoma
Bim	BCL-2 interacting mediator of cell death
BMP	bone morphogenetic protein
Bra	Brachyury
BrdU	Bromodeoxyuridine
CAK	CDK activating kinase
CALM	calmodulin
Cer	cerberus
cdc	cell division cycle
CDK	cyclin dependent kinase
CREB	cAMP responsive element binding protein
DAG	diacylglycerol
DAN	domain BMP antagonist
DE	differential expression
DOK	downstream of kinase
EGF	epithelial growth factor
ER	endoplasmatic reticulum
ERK	extracellular receptor kinase
ETFDH	electron transfer flavoprotein dehydrogenase
FASL	first apoptosis signal ligand
FGF	fibroblast growth factor
FGFR	FGF receptor
FoxO	forkhead box protein O
Gab	GRB associated binding protein
GFP	green fluorescent protein
GH	growth hormone
GPCR	G-protein coupled receptor
GRB	growth factor receptor bound protein
GSK3-β	glycogen signaling kinase 3 β
GWAS	genome wide association study
Hh	hedgehog
HIF	hypoxia induced factor 1α
HM	*Hydra* medium
HP	hairpin
i-cell	interstitial cell
IGF	insulin like growth factor
IIS	insulin/IGF signaling
ILP	insulin like peptide
INHB	inhibin
InsP3R	inositol-3-phosphate receptor
INSR	insulin/insulin like peptide receptor
IP3	inositol-3-phosphate
IRS	insulin receptor substrate
JNK	c-Jun N-terminal kinase
KD	knockdown
KO	KEGG ontology
mTOR	mechanistic target of rapamycin
MAPK	mitogen activated protein kinase
MAPKK	mitogen activated protein kinase kinase
MAPKKK	mitogen activated protein kinase kinase kinase
MDM2	mouse double minute homolog 2
miR	micro RNA
MPAO	polyamine oxidase
MXD	Myc associated factor X interacting protein
ORF	open reading frame
OTOF	otoferlin
PCOS	polycystic ovary syndrome
PDGF	platelet derived growth factor
PGR	population growth rate
PI3K	3-phospho-inositol kinase
PIP2	phosphatidyl-inositol-2-phosphate
PIP3	phosphatidyl-inositol-3-phosphate
Pitx	pituitary homeobox
PKB	protein kinase B
PKC	protein kinase C
PKD1L2	polycystic kidney disease protein 1 like 2
PLC	phospho-lipase C
PPP1R3	protein phosphatase 1 regulatory subunit 3
PRAS40	proline rich AKT substrate of 40 kD

PTEN	phosphatase and Tensin homolog
Ras	rat sarcoma
REDD	regulated in development and DNA-damage response 1
RP	large subunit ribosomal protein
RTK	receptor tyrosine kinase
S6K	p70S6 kinase
SGK1	serine/threonin protein kinase 1
Shh	sonic hedgehog
SHIP	SH2 domain containing and inositol-5-phosphatase
Tbx	T-box transcription factor
TCF	ternary complex factor
TGF-β	transforming growth factor β
THBS	thrombospondin
TNF-α	tumor necrosis factor α
TNFR	tumor necrosis factor receptor
TSC2	tuberous sclerosis 2
TSR	temperature size rule
TTC19	tetratricopeptide repeat domain 19
Wnt	wingless and Int-1 protein
ZPA	zone of polarizing activity

6 References

[1] Schmidt-Nielsen K (1984) Scaling: Why is Animal Size so Important? *Trends in Neurosciences* 8:241.

[2] Roff D (1981) On Being the Right Size. *The American Naturalist* 118:405–422.

[3] Kaur H, Singh R (2011) Two new species of Myxobolus (Myxozoa: Myxosporea: Bivalvulida) infecting an Indian major carp and a cat fish in wetlands of Punjab, India. *Journal of Parasitic Diseases* 35:169–176.

[4] Branch TA, Abubaker EMN, Mkango S, Butterworth DS (2007) Separating southern blue whale subspecies based on length frequencies of sexually mature females. *Marine Mammal Science* 23:803–833.

[5] N. E, Thompson DW (1945) On Growth and Form. *The Journal of Philosophy* 42:557.

[6] Calder WA (1984) *Size, Function, and Life History*, Doover books on biology, psychology and medicine (Dover Publications).

[7] Peters RH (1983) *The Ecological Implications of Body Size*, Cambridge Studies in Ecology (Cambridge University Press).

[8] Galilei G (1914) *Dialogues Concerning Two New Sciences [1638]* eds Crew H, de Salvio A (http://oll.libertyfund.org/titles/753, New York), p 300.

[9] McMahon T (1973) Size and shape in biology. *Science* 179:1201–1204.

[10] Hill A (1949) Dimensions of Animals and their Muscular Dynamics. *Nature* 164:820–820.

[11] Damuth J (1981) Population density and body size in mammals. *Nature* 290:699–700.

[12] Garland T (1983) The relation between maximal running speed and body mass in terrestrial mammals. *Journal of Zoology* 199:157–170.

[13] Alexander R (1984) The Gaits of Bipedal and Quadrupedal Animals. *The International Journal of Robotics Research* 3:49–59.

[14] Damuth J (1987) Interspecific allometry of population density in mammals and other animals: the independence of body mass and population energy-use. *Biological Journal of the Linnean Society* 31:193–246.

[15] Chappell R (1989) Fitting bent lines to data, with applications to allometry. *Journal of Theoretical Biology* 138:235–256.

[16] Kleiber M (1932) Body size and metabolism. *Hilgardia* 6:315–353.

[17] Hemmingsen AM (1960) *Energy metabolism as related to body size and respiratory surfaces, and its evolution* (Nordisk Insulinlaboratorium) Vol. 9, pp 1–110.

[18] West GB, Brown JH, Enquist BJ (1997) A general model for the origin of allometric scaling laws in biology. *Science* 276:122–126.

[19] Savage VM, Gillooly JF, Brown JH, West GB, Charnov EL (2004) Effects of Body Size and Temperature on Population Growth. *The American Naturalist* 163:429–441.

[20] Promislow DEL, Harvey PH (1990) Living fast and dying young: A comparative analysis of life-history variation among mammals. *Journal of Zoology* 220:417–437.

[21] Speakman JR (2005) Body size, energy metabolism and lifespan. *Journal of Experimental Biology* 208:1717–1730.

[22] Sibly RM, Brown JH (2007) Effects of body size and lifestyle on evolution of mammal life histories. *Proceedings of the National Academy of Sciences* 104:17707–17712.

[23] Johnson CN (1999) Relationships between Body Size and Population Density of Animals: The Problem of the Scaling of Study Area in Relation to Body Size. *Oikos* 85:565.

[24] Brown JH, Gillooly JF, Allen AP, Savage VM, West GB (2004) Toward a metabolic theory of ecology. *Ecology* 85:1771–1789.

[25] Bonner JT (2006) *Why Size Matters: From Bacteria to Blue Whales* (Princeton University Press).

[26] Kingsolver JG, Pfennig DW (2004) Individual-Level Selection As a Cause of Cope'S Rule of Phyletic Size Increase. *Evolution* 58:1608.

[27] Kingsolver JG, Huey RB (2008) Size, temperature, and fitness: three rules. *Evolutionary Ecology Research* 10:251–268.

[28] Cope ED (1904) *The primary factors of organic evolution* (Open Court).

[29] McLain DK (1993) Cope's Rules, Sexual Selection, and the Loss of Ecological Plasticity. *Oikos* 68:490–500.

[30] Baker J, Meade A, Pagel M, Venditti C (2015) Adaptive evolution toward larger size in mammals. *Proceedings of the National Academy of Sciences* 112:5093–5098.

[31] Bonnet T, Wandeler P, Camenisch G, Postma E (2017) Bigger Is Fitter? Quantitative Genetic Decomposition of Selection Reveals an Adaptive Evolutionary Decline of Body Mass in a Wild Rodent Population. *PLoS Biology* 15:1–21.

[32] Jablonski D (1997) Body-size evolution in cretaceous molluscs and the status of Cope's rule.

[33] Blanckenhorn WU (2000) The Evolution of Body Size: What Keeps Organisms Small? *The Quarterly Review of Biology* 75:385–407.

[34] Newbolt CH, et al. (2017) Factors influencing reproductive success in male white-tailed deer. *The Journal of Wildlife Management* 81:206–217.

[35] García-Navas V, Bonnet T, Bonal R, Postma E (2016) The role of fecundity and sexual selection in the evolution of size and sexual size dimorphism in New World and Old World voles (Rodentia: Arvicolinae). *Oikos* 125:1250–1260.

[36] Kleiman DG (1977) Monogamy in mammals. *The Quarterly review of biology* 52:39–69.

[37] Wootton R, Evans G (1976) Cost of egg production in the three spined stickleback (Gasterosteus aculeatus L.). *Journal Of Fish Biology* 8:385–395.

[38] Cavicchi S, Guerra D, Natali V, Pezzoli C, Giorgi G (1989) Temperature-Related Divergence in Experimental Populations of Drosophila melanogaster II. Correlation Between Fitness and Body Dimensions. *Journal of Evolutionary Biology* 2:235–252.

[39] Honěk A, Honek A (1993) Intraspecific Variation in Body Size and Fecundity in Insects: A General Relationship. *Oikos* 66:483.

[40] Nobili G, Accordi F (1997) Body size, age and fecundity variation in different populations of the smooth newt triturus vulgaris meridionalis in central Italy. *Italian Journal of Zoology* 64:313–318.

[41] Calvo D, Molina JM (2005) Fecundity-body size relationship and other reproductive aspects of Streblote panda (Lepidoptera: Lasiocampidae). *Annals of the Entomological Society of America* 98:191–196.

[42] Berger D, Walters R, Gotthard K (2008) What limits insect fecundity? Body size- and temperature-dependent egg maturation and oviposition in a butterfly. *Functional Ecology* 22:523–529.

[43] Monroe MJ, South SH, Alonzo SH (2015) The evolution of fecundity is associated with female body size but not female-biased sexual size dimorphism among frogs. *Journal of Evolutionary Biology* 28:1793–1803.

[44] Gotthard K, Berger D, Walters R (2007) What Keeps Insects Small? Time Limitation during Oviposition Reduces the Fecundity Benefit of Female Size in a Butterfly. *The American Naturalist* 169:768–779.

[45] Richner H (1992) The Effect of Extra Food on Fitness in Breeding Carrion Crows. *Ecology* 73:330–335.

[46] Fox CW (1997) The Ecology of Body Size in a Seed Beetle, Stator limbatus: Persistence of Environmental Variation Across Generations? *Evolution* 51:1005.

[47] Metcalfe NB, Monaghan P (2001) Compensation for a bad start: Grow now, pay later? *Trends in Ecology and Evolution* 16:254–260.

[48] Gergs A, Jager T (2014) Body size-mediated starvation resistance in an insect predator. *Journal of Animal Ecology* 83:758–768.

[49] Knapp M (2016) Relative importance of sex, pre-starvation body mass and structural body size in the determination of exceptional starvation resistance of Anchomenus dorsalis (Coleoptera: Carabidae). *PLoS ONE* 11.

[50] Heijmans BT, et al. (2008) Persistent epigenetic differences associated with prenatal exposure to famine in humans. *Proceedings of the National Academy of Sciences* 105:17046–17049.

[51] Bergmann C (1847) *Über die Verhältnisse der Wärmeö konomie der Thiere zu ihrer Grösse* Vol. 1, pp 595–708.

[52] RAY C (1960) The application of Bergmann's and Allen's Rules to the poikilotherms. *Journal of morphology* 106:85–108.

[53] Atkinson D (1994) Temperature and Organism Size—A Biological Law for Ectotherms? *Advances in Ecological Research* 25:1–58.

[54] Fusco G, Minelli A (2010) Phenotypic plasticity in development and evolution: facts and concepts. *Philosophical Transactions of the Royal Society B: Biological Sciences* 365:547–556.

[55] Cavicchi S, Guerra D, Giorgi G, Pezzoli C (1985) Temperature-related divergence in experimental populations of Drosophila melanogaster. I. Genetic and developmental basis of wing size and shape variation. *Genetics* 109:665–689.

[56] Huey RB, Patridge L, Fowler K (1991) Thermal Sensitivity of Drosophila melanogaster Responds Rapidly to Laboratory Natural Selection. *Evolution* 45:751.

[57] Partridge L, Barrie B, Fowler K, French V (1994) Evolution and Development of Body Size and Cell Size in Drosophila melanogaster in Response to Temperature. 48:1269–1276.

[58] Gardner JL, Peters A, Kearney MR, Joseph L, Heinsohn R (2011) Declining body size: A third universal response to warming? *Trends in Ecology and Evolution* 26:285–291.

[59] Ferrezuelo F, et al. (2012) The critical size is set at a single-cell level by growth rate to attain homeostasis and adaptation. *Nature Communications* 3:1012.

[60] Sung Y, et al. (2013) Size homeostasis in adherent cells studied by synthetic phase microscopy. *Proceedings of the National Academy of Sciences* 110:16687–16692.

[61] Son S, et al. (2012) Direct observation of mammalian cell growth and size regulation. *Nature Methods* 9:910–912.

[62] Kafri R, et al. (2013) Dynamics extracted from fixed cells reveal feedback linking cell growth to cell cycle. *Nature* 494:480–483.

[63] Tyson JJ, Diekmann O (1986) Sloppy size control of the cell division cycle. *Journal of Theoretical Biology* 118:405–426.

[64] Conlon I, Raff M (1999) Size control in animal development. *Cell* 96:235–244.

[65] Lloyd AC (2013) The Regulation of Cell Size. *Cell* 154:1194–1205.

[66] Amodeo AA, Skotheim JM (2016) Cell-Size Control. *Cold Spring Harbor Perspectives in Biology* 8:a019083.

[67] Miettinen TP, Björklund M (2016) Cellular Allometry of Mitochondrial Functionality Establishes the Optimal Cell Size. *Developmental Cell* 39:370–382.

[68] Zetterberg A, Engström W, Dafgård E (1984) The relative effects of different types of growth factors on DNA replication, mitosis, and cellular enlargement. *Cytometry* 5:368–375.

[69] Zetterberg A, Larsson O (1991) Coordination between cell growth and cell cycle transit in animal cells. *Cold Spring Harbor Symposia on Quantitative Biology* 56:137–147.

[70] Ginzberg MB, Kafri R, Kirschner M (2015) Cell biology. On being the right (cell) size. *Science (New York, N.Y.)* 348:1245075.

[71] Sebens KP (1987) The Ecology of Indeterminate Growth in Animals. *Annual Review of Ecology and Systematics* 18:371–407.

[72] Mumby HS, et al. (2015) Distinguishing between determinate and indeterminate growth in a long-lived mammal. *BMC Evolutionary Biology* 15:214.

[73] Smith EP, et al. (1994) Estrogen Resistance Caused by a Mutation in the Estrogen-Receptor Gene in a Man. *New England Journal of Medicine* 331:1056–1061.

[74] Price DA (1991) Puberty in children with idiopathic growth hormone deficiency on growth hormone treatment: preliminary analysis of the data from the Kabi Pharmacia International Growth Study. *Acta paediatrica Scandinavica. Supplement* 379:117–24; discussion 125.

[75] Clayton PE, Trueman JA (2000) Leptin and puberty. *Archives of disease in childhood* 83:1–4.

[76] Topaloglu AK, et al. (2009) TAC3 and TACR3 mutations in familial hypogonadotropic hypogonadism reveal a key role for Neurokinin B in the central control of reproduction. *Nature Genetics* 41:354–358.

[77] Perry JRB, et al. (2009) Meta-analysis of genome-wide association data identifies two loci influencing age at menarche. *Nature Genetics* 41:648–650.

[78] Polesskaya A, et al. (2007) Lin-28 binds IGF-2 mRNA and participates in skeletal myogenesis by increasing translation efficiency. *Genes and Development* 21:1125–1138.

[79] Zhu H, et al. (2010) Lin28a transgenic mice manifest size and puberty phenotypes identified in human genetic association studies. *Nature Genetics* 42:626–630.

[80] Gokhale RH, Shingleton AW (2015) Size control: The developmental physiology of body and organ size regulation. *Wiley Interdisciplinary Reviews: Developmental Biology* 4:335–356.

[81] Ghosh SM, Testa ND, Shingleton AW (2013) Temperature-size rule is mediated by thermal plasticity of critical size in Drosophila melanogaster. *Proceedings of The Royal Society B: Biological Sciences* 280:20130174.

[82] Callier V, Nijhout HF (2011) Control of body size by oxygen supply reveals size-dependent and size-independent mechanisms of molting and metamorphosis. *Proceedings of the National Academy of Sciences* 108:14664–14669.

[83] Atkinson D, Morley SA, Hughes RN (2006) From cells to colonies: At what levels of body organization does the 'temperature-size rule' apply? *Evolution and Development* 8:202–214.

[84] Forster J, Hirst AG (2012) The temperature-size rule emerges from ontogenetic differences between growth and development rates. *Functional Ecology* 26:483–492.

[85] Verheyden JM, Sun X (2008) An Fgf/Gremlin inhibitory feedback loop triggers termination of limb bud outgrowth. *Nature* 454:638–641.

[86] Ribatti D (2017) A revisited concept: Contact inhibition of growth. From cell biology to malignancy. *Experimental Cell Research* 359:17–19.

[87] Dong J, et al. (2007) Elucidation of a Universal Size-Control Mechanism in Drosophila and Mammals. *Cell* 130:1120–1133.

[88] Tao W, et al. (1999) Human homologue of the Drosophila melanogaster lats tumour suppressor modulates CDC2 activity. *Nature Genetics* 21:177–181.

[89] West-Eberhard MJ (1998) Evolution in the light of developmental and cell biology, and vice versa. *Proceedings of the National Academy of Sciences of the United States of America* 95:8417–9.

[90] West-Eberhard MJ (2003) *Developmental plasticity and evolution* (Oxford University Press) Vol. 424, p 794.

[91] West-Eberhard MJ (2005) Developmental plasticity and the origin of species differences. *Proceedings of the National Academy of Sciences* 102:6543–6549.

[92] Bruce Alberts; Alexander Johnson; Julian Lewis; David Morgan; Martin Raff; Keith Roberts; Peter Walter; John Wilson; Tim Hunt (2015) *Molecular Biology of the Cell*, 500 Tips (Garland Science).

[93] Shaltiel IA, Krenning L, Bruinsma W, Medema RH (2015) The same, only different - DNA damage checkpoints and their reversal throughout the cell cycle. *Journal of cell science* 128:607–20.

[94] Nie Z, et al. (2012) c-Myc Is a Universal Amplifier of Expressed Genes in Lymphocytes and Embryonic Stem Cells. *Cell* 151:68–79.

[95] van Riggelen J, Yetil A, Felsher DW (2010) MYC as a regulator of ribosome biogenesis and protein synthesis. *Nature reviews. Cancer* 10:301–9.

[96] Bretones G, Delgado MD, León J (2015) Myc and cell cycle control. *Biochimica et biophysica acta* 1849:506–516.

[97] Meloche S, Pouysségur J (2007) The ERK1/2 mitogen-activated protein kinase pathway as a master regulator of the G1- to S-phase transition. *Oncogene* 26:3227–3239.

[98] Prendergast GC (1999) Mechanisms of apoptosis by c-Myc. *Oncogene* 18:2967–2987.

[99] Steiger D, Furrer M, Schwinkendorf D, Gallant P (2008) Max-independent functions of Myc in Drosophila melanogaster. *Nature Genetics* 40:1084–1091.

[100] Poortinga G, et al. (2011) c-MYC coordinately regulates ribosomal gene chromatin remodeling and Pol I availability during granulocyte differentiation. *Nucleic Acids Research* 39:3267–3281.

[101] Terzi MY, Izmirli M, Gogebakan B (2016) The cell fate: senescence or quiescence. *Molecular Biology Reports* 43:1213–1220.

[102] Hayflick L, Moorhead P (1961) The serial cultivation of human diploid cell strains. *Experimental Cell Research* 25:585–621.

[103] Bodnar AG, et al. (1998) Extension of life-span by introduction of telomerase into normal human cells. *Science* 279:349–352.

[104] d'Adda di Fagagna F, et al. (2003) A DNA damage checkpoint response in telomere-associated senescence. *Nature* 426:194–198.

[105] Fausto N (2004) Liver regeneration and repair: Hepatocytes, progenitor cells, and stem cells. *Hepatology* 39:1477–1487.

[106] Álvarez-Errico D, Vento-Tormo R, Sieweke M, Ballestar E (2015) Epigenetic control of myeloid cell differentiation, identity and function. *Nature Reviews Immunology* 15:7–17.

[107] Nakayama K, et al. (1996) Mice Lacking p27Kip1Display Increased Body Size, Multiple Organ Hyperplasia, Retinal Dysplasia, and Pituitary Tumors. *Cell* 85:707–720.

[108] Kiyokawa H, et al. (1996) Enhanced growth of mice lacking the cyclin-dependent kinase inhibitor function of P27Kip1. *Cell* 85:721–732.

[109] Fero ML, et al. (1996) A syndrome of multiorgan hyperplasia with features of gigantism, tumorigenesis, and female sterility in p27(Kip1)-deficient mice. *Cell* 85:733–44.

[110] Nakayama K, et al. (2000) Targeted disruption of Skp2 results in accumulation of cyclin E and p27(Kip1), polyploidy and centrosome overduplication. *The EMBO journal* 19:2069–81.

[111] Fantl V, Stamp G, Andrews A, Rosewell I, Dickson C (1995) Mice lacking cyclin D1 are small and show defects in eye and mammary gland development. *Genes & Development* 9:2364–2372.

[112] Rane SG, et al. (1999) Loss of Cdk4 expression causes insulin-deficient diabetes and Cdk4 activation results in β-islet cell hyperplasia. *Nature Genetics* 22:44–52.

[113] Datar SA, Jacobs HW, de la Cruz AF, Lehner CF, Edgar BA (2000) The Drosophila cyclin D-Cdk4 complex promotes cellular growth. *The EMBO journal* 19:4543–54.

[114] Meyer CA, et al. (2000) Drosophila Cdk4 is required for normal growth and is dispensable for cell cycle progression. *The EMBO journal* 19:4533–42.

[115] Gallant P, Shiio Y, Cheng PF, Parkhurst SM, Eisenman RN (1996) Myc and Myx Homologs in Drosophila. *Science (New York, N.Y.)* 274:1523–1527.

[116] Trumpp A, et al. (2001) c-Myc regulates mammalian body size by controlling cell number but not cell size. *Nature* 414:768–773.

[117] Elmore S (2007) Apoptosis: A Review of Programmed Cell Death. *Toxicologic Pathology* 35:495–516.

[118] Shalini S, Dorstyn L, Dawar S, Kumar S (2015) Old, new and emerging functions of caspases. *Cell Death & Differentiation* 22:526–539.

[119] Czabotar PE, Lessene G, Strasser A, Adams JM (2014) Control of apoptosis by the BCL-2 protein family: implications for physiology and therapy. *Nature Reviews Molecular Cell Biology* 15:49–63.

[120] Fridman JS, Lowe SW (2003) Control of apoptosis by p53. *Oncogene* 22:9030–9040.

[121] Redza-Dutordoir M, Averill-Bates DA (2016) Activation of apoptosis signalling pathways by reactive oxygen species. *Biochimica et Biophysica Acta - Molecular Cell Research* 1863:2977–2992.

[122] Sendoel A, Hengartner MO (2014) Apoptotic Cell Death Under Hypoxia. *Physiology* 29:168–176.

[123] Bakker WJ, Harris IS, Mak TW (2007) FOXO3a Is Activated in Response to Hypoxic Stress and Inhibits HIF1-Induced Apoptosis via Regulation of CITED2. *Molecular Cell* 28:941–953.

[124] Meier P, Finch A, Evan G (2000) Apoptosis in development. *Nature* 407:796–801.

[125] Shima H, et al. (1998) Disruption of the p70(s6k)/p85(s6k) gene reveals a small mouse phenotype and a new functional S6 kinase. *The EMBO journal* 17:6649–59.

[126] Montagne J, et al. (1999) Drosophila S6 kinase: A regulator of cell size. *Science* 285:2126–2129.

[127] Saxton RA, Sabatini DM (2017) mTOR Signaling in Growth, Metabolism, and Disease. *Cell* 168:960–976.

[128] Ma XM, Blenis J (2009) Molecular mechanisms of mTOR-mediated translational control. *Nature Reviews Molecular Cell Biology* 10:307–318.

[129] Laplante M, Sabatini DM (2012) mTOR Signaling in Growth Control and Disease. *Cell* 149:274–293.

[130] Magnuson B, Ekim B, Fingar DC (2012) Regulation and function of ribosomal protein S6 kinase (S6K) within mTOR signalling networks. *Biochemical Journal* 441:1–21.

[131] Zhang H, Stallock JP, Ng JC, Reinhard C, Neufeld TP (2000) Regulation of cellular growth by the Drosophila target of rapamycin dTOR. *Genes & development* 14:2712–24.

[132] Oldham S, Montagne J, Radimerski T, Thomas G, Hafen E (2000) Genetic and biochemical characterization of dTOR, the Drosophila homolog of the target of rapamycin. *Genes and Development* 14:2689–2694.

[133] Brogiolo W, et al. (2001) An evolutionarily conserved function of the drosophila insulin receptor and insulin-like peptides in growth control. *Current Biology* 11:213–221.

[134] Pearson G, et al. (2001) Mitogen-activated protein (MAP) kinase pathways: regulation and physiological functions. *Endocrine reviews* 22:153–83.

[135] Hoshi M, Nishida E, Sakai H (1988) Activation of a Ca2+-inhibitable protein kinase that phosphorylates microtubule-associated protein 2 in vitro by growth factors, phorbol esters, and serum in quiescent cultured human fibroblasts. *Journal of Biological Chemistry* 263:5396–5401.

[136] Heldin CH, Westermark B (1999) Mechanism of action and in vivo role of platelet-derived growth factor. *Physiological reviews* 79:1283–316.

[137] Cunnick JM, Mei L, Doupnik CA, Wu J (2001) Phosphotyrosines 627 and 659 of Gab1 Constitute a Bisphosphoryl Tyrosine-based Activation Motif (BTAM) Conferring Binding and Activation of SHP2. *Journal of Biological Chemistry* 276:24380–24387.

[138] Yu Y, Feig LA (2002) Involvement of R-Ras and Ral GTPases in estrogen-independent proliferation of breast cancer cells. *Oncogene* 21:7557–7568.

[139] McKay MM, Morrison DK (2007) Integrating signals from RTKs to ERK/MAPK. *Oncogene* 26:3113–3121.

[140] Rozengurt E (2007) Mitogenic signaling pathways induced by G protein-coupled receptors. *Journal of cellular physiology* 213:589–602.

[141] Mendoza MC, Er EE, Blenis J (2011) The Ras-ERK and PI3K-mTOR pathways: Cross-talk and compensation. *Trends in Biochemical Sciences* 36:320–328.

[142] Roux PP, Ballif BA, Anjum R, Gygi SP, Blenis J (2004) Tumor-promoting phorbol esters and activated Ras inactivate the tuberous sclerosis tumor suppressor complex via p90 ribosomal S6 kinase. *Proceedings of the National Academy of Sciences* 101:13489–13494.

[143] Ma L, Chen Z, Erdjument-Bromage H, Tempst P, Pandolfi PP (2005) Phosphorylation and functional inactivation of TSC2 by Erk: Implications for tuberous sclerosis and cancer pathogenesis. *Cell* 121:179–193.

[144] Sordella R, et al. (2002) Modulation of CREB activity by the Rho GTPase regulates cell and organism size during mouse embryonic development. *Developmental Cell* 2:553–565.

[145] Liu J, Lin A (2005) Role of JNK activation in apoptosis: A double-edged sword. *Cell Research* 15:36–42.

[146] Bode AM, Dong Z (2007) The functional contrariety of JNK. *Molecular Carcinogenesis* 46:591–598.

[147] Johnson GL, Nakamura K (2007) The c-jun kinase/stress-activated pathway: Regulation, function and role in human disease. *Biochimica et Biophysica Acta - Molecular Cell Research* 1773:1341–1348.

[148] Davis RJ (2000) Signal transduction by the JNK group of MAP kinases. *Cell* 103:239–52.

[149] Lin A (2003) Activation of the JNK signaling pathway: Breaking the brake on apoptosis. *BioEssays* 25:17–24.

[150] Verma G, Datta M (2012) The critical role of JNK in the ER-mitochondrial crosstalk during apoptotic cell death. *Journal of Cellular Physiology* 227:1791–1795.

[151] Zhao HF, Wang J, Tony To SS (2015) The phosphatidylinositol 3-kinase/Akt and c-Jun N-terminal kinase signaling in cancer: Alliance or contradiction? (Review). *International Journal of Oncology* pp 429–436.

[152] Bogoyevitch MA, Kobe B (2006) Uses for JNK: the Many and Varied Substrates of the c-Jun N-Terminal Kinases. *Microbiology and Molecular Biology Reviews* 70:1061–1095.

[153] Zhang S, et al. (2016) The c-Jun N-terminal kinase (JNK) is involved in H5N1 influenza A virus RNA and protein synthesis. *Archives of Virology* 161:345–351.

[154] Meng Q, Xia Y (2011) c-Jun, at the crossroad of the signaling network. *Protein and Cell* 2:889–898.

[155] Ono K, Han J (2000) The p38 signal transduction pathway Activation and function. *Cellular Signalling* 12:1–13.

[156] Bonney EA (2017) Mapping out p38MAPK. *American Journal of Reproductive Immunology* 77:e12652.

[157] Sherr CJ (2006) Divorcing ARF and p53: An unsettled case. *Nature Reviews Cancer* 6:663–673.

[158] Balla T (2013) Phosphoinositides: tiny lipids with giant impact on cell regulation. *Physiological reviews* 93:1019–137.

[159] Krugmann S, et al. (2002) Identification of ARAP3, a novel PI3K effector regulating both Arf and Rho GTPases, by selective capture on phosphoinositide affinity matrices. *Molecular Cell* 9:95–108.

[160] Falasca M, Maffucci T (2012) Regulation and cellular functions of class II phosphoinositide 3-kinases. *Biochemical Journal* 443:587–601.

[161] Kim D, et al. (2013) TopHat2: Accurate alignment of transcriptomes in the presence of insertions, deletions and gene fusions. *Genome Biology* 14:R36.

[162] Manning BD, Cantley LC (2007) AKT/PKB signaling: navigating downstream. *Cell* 129:1261–74.

[163] van der Heide LP, Hoekman MFM, Smidt MP (2004) The ins and outs of FoxO shuttling: mechanisms of FoxO translocation and transcriptional regulation. *Biochemical Journal* 380:297–309.

[164] Berridge MJ (2009) Inositol trisphosphate and calcium signalling mechanisms. *Biochimica et Biophysica Acta - Molecular Cell Research* 1793:933–940.

[165] Yang CF, Kazanietz MG (2003) Divergence and complexities in DAG signaling: Looking beyond PKC. *Trends in Pharmacological Sciences* 24:602–608.

[166] Hamilton MJ, et al. (2011) Role of SHIP in cancer. *Experimental Hematology* 39:2–13.

[167] Tu Z, et al. (2001) Embryonic and hematopoietic stem cells express a novel SH2-containing inositol 5'-phosphatase isoform that partners with the Grb2 adapter protein. *Blood* 98:2028–38.

[168] Hopkins BD, Hodakoski C, Barrows D, Mense SM, Parsons RE (2014) PTEN function: The long and the short of it. *Trends in Biochemical Sciences* 39:183–190.

[169] Oldham S, et al. (2002) The Drosophila insulin/IGF receptor controls growth and size by modulating PtdInsP(3) levels. *Development (Cambridge, England)* 129:4103–9.

[170] Chen WS, et al. (2001) Growth retardation and increased apoptosis in mice with homozygous disruption of the Akt1 gene. *Genes & development* 15:2203–8.

[171] Rintelen F, Stocker H, Thomas G, Hafen E (2001) PDK1 regulates growth through Akt and S6K in Drosophila. *Proceedings of the National Academy of Sciences of the United States of America* 98:15020–5.

[172] Tuttle RL, et al. (2001) Regulation of pancreatic beta-cell growth and survival by the serine/threonine protein kinase Akt1/PKBalpha. *Nature medicine* 7:1133–1137.

[173] Lawlor MA, et al. (2002) Essential role of PDK1 in regulating cell size and development in mice. *Embo J* 21:3728–3738.

[174] Robitzki A, et al. (1989) Demonstration of an endocrine signaling circuit for insulin in the sponge Geodia cydonium. *The EMBO journal* 8:2905–9.

[175] Skorokhod A, et al. (1999) Origin of Insulin Receptor-Like Tyrosine Kinases in Marine Sponges. *The Biological Bulletin* 197:198–206.

[176] De Meyts P (2004) Insulin and its receptor: Structure, function and evolution. *BioEssays* 26:1351–1362.

[177] Barbieri M, Bonafè M, Franceschi C, Paolisso G (2003) Insulin/IGF-I-signaling pathway: an evolutionarily conserved mechanism of longevity from yeast to humans. *American journal of physiology. Endocrinology and metabolism* 285:E1064–71.

[178] Jones JI, Clemmons DR (1995) Insulin-like growth factors and their binding proteins: Biological actions. *Endocrine Reviews* 16:3–34.

[179] Okamoto N, et al. (2009) A Fat Body-Derived IGF-like Peptide Regulates Postfeeding Growth in Drosophila. *Developmental Cell* 17:885–891.

[180] Husson SJ, Mertens I, Janssen T, Lindemans M, Schoofs L (2007) Neuropeptidergic signaling in the nematode Caenorhabditis elegans. *Progress in Neurobiology* 82:33–55.

[181] Nässel DR, Kubrak OI, Liu Y, Luo J, Lushchak OV (2013) Factors that regulate insulin producing cells and their output in drosophila. *Frontiers in Physiology* 4 SEP:1–12.

[182] Fernandes de Abreu DA, et al. (2014) An Insulin-to-Insulin Regulatory Network Orchestrates Phenotypic Specificity in Development and Physiology. *PLoS Genetics* 10:e1004225.

[183] Bier DM (1991) Growth hormone and insulin-like growth factor I: Nutritional pathophysiology and therapeutic potential. *Acta Paediatrica Scandinavica* 80 Suppl.:119–128.

[184] Sun XJ, et al. (1991) Structure of the insulin receptor substrate IRS-1 defines a unique signal transduction protein. *Nature* 352:73–7.

[185] Yonezawa K, et al. (1992) Insulin-dependent formation of a complex containing an 85-kDa subunit of phosphatidylinositol 3-kinase and tyrosine-phosphorylated insulin receptor substrate 1. *Journal of Biological Chemistry* 267:25958–25966.

[186] Backer JM, et al. (1992) Phosphatidylinositol 3'-kinase is activated by association with IRS-1 during insulin stimulation. *The EMBO journal* 11:3469–79.

[187] Skolnik EY, et al. (1993) The function of GRB2 in linking the insulin receptor to Ras signaling pathways. *Science (New York, N.Y.)* 260:1953–5.

[188] Tamemoto H, et al. (1994) Insulin resistance and growth retardation in mice lacking insulin receptor substrate-1. *Nature* 372:182–6.

[189] Araki E, et al. (1994) Alternative pathway of insulin signalling in mice with targeted disruption of the IRS-1 gene. *Nature* 372:186–190.

[190] Withers DJ, et al. (1998) Disruption of IRS-2 causes type 2 diabetes in mice. *Nature* 391:900–904.

[191] Burks DJ, et al. (2000) IRS-2 pathways integrate female reproduction and energy homeostasis. *Nature* 407:377–382.

[192] Fantin VR, Wang Q, Lienhard GE, Keller SR (2000) Mice lacking insulin receptor substrate 4 exhibit mild defects in growth, reproduction, and glucose homeostasis. *American journal of physiology. Endocrinology and metabolism* 278:E127–33.

[193] Bouzakri K, et al. (2006) siRNA-based gene silencing reveals specialized roles of IRS-1/Akt2 and IRS-2/Akt1 in glucose and lipid metabolism in human skeletal muscle. *Cell Metabolism* 4:89–96.

[194] Wu A, Chen J, Baserga R (2008) Nuclear insulin receptor substrate-1 activates promoters of cell cycle progression genes. *Oncogene* 27:397–403.

[195] Lee CH, et al. (1993) Nck associates with the SH2 domain-docking protein IRS-1 in insulin-stimulated cells. *Proceedings of the National Academy of Sciences* 90:11713–11717.

[196] Noguchi T, Matozaki T, Horita K, Fujioka Y, Kasuga M (1994) Role of SH-PTP2, a protein-tyrosine phosphatase with Src homology 2 domains, in insulin-stimulated Ras activation. *Molecular and cellular biology* 14:6674–82.

[197] Sun XJ, et al. (1996) The Fyn Tyrosine Kinase Binds Irs-1 and Forms a Distinct Signaling Complex during Insulin Stimulation. *Journal of Biological Chemistry* 271:10583–10587.

[198] Arrandale JM, et al. (1996) Insulin signaling in mice expressing reduced levels of syp. *Journal of Biological Chemistry* 271:21353–21358.

[199] Sasaoka T, Kobayashi M (2000) The Functional Significance of Shc in Insulin Signaling as a Substrate of the Insulin Receptor. *Endocrine Journal* 47:373–381.

[200] Lehr S, et al. (2000) Identification of major tyrosine phosphorylation sites in the human insulin receptor substrate Gab-1 by insulin receptor kinase in vitro. *Biochemistry* 39:10898–10907.

[201] Cai D, Dhe-Paganon S, Melendez PA, Lee J, Shoelson SE (2003) Two New Substrates in Insulin Signaling, IRS5/DOK4 and IRS6/DOK5. *Journal of Biological Chemistry* 278:25323–25330.

[202] Holt LJ, Siddle K (2005) Grb10 and Grb14: enigmatic regulators of insulin action–and more? *The Biochemical journal* 388:393–406.

[203] Holt LJ, et al. (2009) Dual Ablation of Grb10 and Grb14 in Mice Reveals Their Combined Role in Regulation of Insulin Signaling and Glucose Homeostasis. *Molecular Endocrinology* 23:1406–1414.

[204] Yu Y, et al. (2011) Phosphoproteomic Analysis Identifies Grb10 as an mTORC1 Substrate That Negatively Regulates Insulin Signaling. *Science* 332:1322–1326.

[205] Morris D, Cho KW, Zhou Y, Rui L (2008) SH2B1 directly enhances insulin action by both stimulating the insulin receptor and inhibiting tyrosine dephosphorylation of IRS proteins. *Diabetes* 57:A383–A383.

[206] Wolkow CA, Muñoz MJ, Riddle DL, Ruvkun G (2002) Insulin Receptor Substrate and p55 Orthologous Adaptor Proteins Function in the Caenorhabditis elegans daf-2 /Insulin-like Signaling Pathway. *Journal of Biological Chemistry* 277:49591–49597.

[207] Ruan Y, Chen C, Cao Y, Garofalo RS (1995) The Drosophila Insulin Receptor Contains a Novel Carboxyl-terminal Extension Likely to Play an Important Role in Signal Transduction. *Journal of Biological Chemistry* 270:4236–4243.

[208] Yenush L, et al. (1996) The Drosophila insulin receptor activates multiple signaling pathways but requires insulin receptor substrate proteins for DNA synthesis. *Molecular and Cellular Biology* 16:2509–2517.

[209] Kimura KD, Tissenbaum HA, Liu Y, Ruvkun G (1997) Daf-2, an insulin receptor-like gene that regulates longevity and diapause in Caenorhabditis elegans. *Science* 277:942–946.

[210] Salih DAM, Brunet A (2008) FoxO transcription factors in the maintenance of cellular homeostasis during aging. *Current opinion in cell biology* 20:126–36.

[211] Demontis F, Perrimon N (2009) Integration of Insulin receptor/Foxo signaling and dMyc activity during muscle growth regulates body size in Drosophila. *Development* 136:983–993.

[212] Peck B, Ferber EC, Schulze A (2013) Antagonism between FOXO and MYC Regulates Cellular Powerhouse. *Frontiers in Oncology* 3:1–6.

[213] He Q, et al. (2014) Shorter men live longer: Association of height with longevity and FOXO3 genotype in American men of Japanese ancestry. *PLoS ONE* 9:1–8.

[214] Hosaka T, et al. (2004) Disruption of forkhead transcription factor (FOXO) family members in mice reveals their functional diversification. *Proceedings of the National Academy of Sciences* 101:2975–2980.

[215] Teleman AA, Hietakangas V, Sayadian AC, Cohen SM (2008) Nutritional Control of Protein Biosynthetic Capacity by Insulin via Myc in Drosophila. *Cell Metabolism* 7:21–32.

[216] Dabour N, et al. (2011) Cricket body size is altered by systemic RNAi against insulin signaling components and epidermal growth factor receptor. *Development Growth and Differentiation* 53:857–869.

[217] Koyama T, Rodrigues MA, Athanasiadis A, Shingleton AW, Mirth CK (2014) Nutritional control of body size through FoxO-Ultraspiracle mediated ecdysone biosynthesis. *eLife* 3:1–20.

[218] Eijkelenboom A, Burgering BMT (2013) FOXOs: signalling integrators for homeostasis maintenance. *Nature Reviews Molecular Cell Biology* 14:83–97.

[219] Liu JP, Baker J, Perkins AS, Robertson EJ, Efstratiadis A (1993) Mice carrying null mutations of the genes encoding insulin-like growth factor I (Igf-1) and type 1 IGF receptor (Igf1r). *Cell* 75:59–72.

[220] Böhni R, et al. (1999) Autonomous control of cell and organ size by CHICO, a Drosophila homolog of vertebrate IRS1-4. *Cell* 97:865–875.

[221] Shingleton AW, Das J, Vinicius L, Stern DL (2005) The temporal requirements for insulin signaling during development in Drosophila. *PLoS Biology* 3:1607–1617.

[222] So S, Miyahara K, Ohshima Y (2011) Control of body size in C. elegans dependent on food and insulin/IGF-1 signal. *Genes to Cells* 16:639–651.

[223] Trembley A (1744) *Memoires, pour servir à l'historie d'un genre de polypes d'eau douce, à bras en forme de cornes* p 406.

[224] Browne EN (1909) The production of new hydranths in Hydra by the insertion of small grafts. *Journal of Experimental Zoology* 7:1–23.

[225] Spemann H, Mangold H (1924) Über Induktion von Embryonalanlagen durch Implantation artfremder Organisatoren. *Archiv für Mikroskopische Anatomie und Entwicklungsmechanik* 100:599–638.

[226] Chapman JA, et al. (2010) The dynamic genome of Hydra. *Nature* 464:592–596.

[227] Wittlieb J, Khalturin K, Lohmann JU, Anton-Erxleben F, Bosch TCG (2006) Transgenic Hydra allow in vivo tracking of individual stem cells during morphogenesis. *Proceedings of the National Academy of Sciences of the United States of America* 103:6208–6211.

[228] Schwentner M, Bosch TC (2015) Revisiting the age, evolutionary history and species level diversity of the genus Hydra (Cnidaria: Hydrozoa). *Molecular Phylogenetics and Evolution* 91:41–55.

[229] Cleave HJV, Hyman LH (1940) The Invertebrates: Protozoa Through Ctenophora. *American Midland Naturalist* 24:499.

[230] Schierwater B, et al. (2009) Concatenated analysis sheds light on early metazoan evolution and fuels a modern "urmetazoon" hypothesis. *PLoS Biology* 7.

[231] Field KG, et al. (1988) Molecular Phylogeny of the Animal Kingdom. *Science* 239:748–753.

[232] Wainright P, Hinkle G, Sogin M, Stickel S (1993) Monophyletic origins of the metazoa: an evolutionary link with fungi. *Science* 260:340–342.

[233] Nielsen C (2008) Six major steps in animal evolution: Are we derived sponge larvae? *Evolution and Development* 10:241–257.

[234] Holstein T (1981) The morphogenesis of nematocytes in Hydra and Forskålia: an ultrastructural study. *Journal of ultrastructure research* 75:276–90.

[235] Tardent P, Holstein T (1982) Morphology and morphodynamics of the stenotele nematocyst of Hydra attenuata Pall. (Hydrozoa, Cnidaria). *Cell and tissue research* 224:269–90.

[236] Littlefield CL (1985) Germ cells in Hydra oligactis males. I. Isolation of a subpopulation of interstitial cells that is developmentally restricted to sperm production. *Developmental biology* 112:185–93.

[237] Littlefield CL (1991) Cell lineages in Hydra: Isolation and characterization of an interstitial stem cell restricted to egg production in Hydra oligactis. *Developmental Biology* 143:378–388.

[238] Nishimiya-Fujisawa C, Kobayashi S (2012) Germline stem cells and sex determination in Hydra. *International Journal of Developmental Biology* 56:499–508.

[239] Martin VJ, Littlefield CL, Archer WE, Bode HR (1997) Embryogenesis in hydra. *Biological Bulletin* 192:345–363.

[240] Clarkson SG, Wolpert L (1967) Bud morphogenesis in hydra. *Nature*.

[241] Otto JJ, Campbell RD (1977) Budding in Hydra attenuata: Bud stages and fate map. *Journal of Experimental Zoology* 200:417–428.

[242] Otto JJ, Campbell RD (1977) Tissue economics of hydra: regulation of cell cycle, animal size and development by controlled feeding rates. *Journal of cell science* 28:117–32.

[243] Holstein TW, Hobmayer E, David CN (1991) Pattern of epithelial cell cycling in hydra. *Developmental biology* 148:602–611.

[244] Liu TT, Chang JT (1946) Number of Tentacles in Hydra vulgaris as a Genetic Character. *Nature* 157:728–728.

[245] Hobmayer B, et al. (2000) WNT signalling molecules act in axis formation in the diploblastic metazoan Hydra. *Nature* 407:186–189.

[246] Minobe S, Fei K, Yan L, Sarras MP, Werle MJ (2000) Identification and characterization of the epithelial polarity receptor 'Frizzled' in Hydra vulgaris. *Development Genes and Evolution* 210:258–262.

[247] Lengfeld T, et al. (2009) Multiple Wnts are involved in Hydra organizer formation and regeneration. *Developmental biology* 330:186–99.

[248] MacWilliams HK (1983) Hydra transplantation phenomena and the mechanism of Hydra head regeneration. II. Properties of the head activation. *Developmental biology* 96:239–57.

[249] MacWilliams HK (1983) Hydra transplantation phenomena and the mechanism of Hydra head regeneration. I. Properties of the head inhibition. *Developmental Biology* 96:217–238.

[250] Turing AM (1952) The Chemical Basis of Morphogenesis. *Philosophical Transactions of the Royal Society B: Biological Sciences* 237:37–72.

[251] Gierer A, Meinhardt H (1972) A theory of biological pattern formation. *Kybernetik* 12:30–39.

[252] Technau U, et al. (2000) Parameters of self-organization in Hydra aggregates. *Proceedings of the National Academy of Sciences* 97:12127–12131.

[253] Watanabe H, et al. (2014) Nodal signalling determines biradial asymmetry in Hydra. *Nature* 515:112–115.

[254] Lange E, Bertrand S, Holz O, Rebscher N, Hassel M (2014) Dynamic expression of a Hydra FGF at boundaries and termini. *Development Genes and Evolution* 224:235–244.

[255] Bosch TC (2007) Why polyps regenerate and we don't: Towards a cellular and molecular framework for Hydra regeneration. *Developmental Biology* 303:421–433.

[256] Hemmrich G, et al. (2012) Molecular signatures of the three stem cell lineages in hydra and the emergence of stem cell function at the base of multicellularity. *Molecular biology and evolution* 29:3267–80.

[257] Bosch TCG (2009) Hydra and the evolution of stem cells. *BioEssays* 31:478–486.

[258] David CN, Campbell RD (1972) Cell cycle kinetics and development of Hydra attenuata. I. Epithelial cells. *Journal of cell science* 11:557–68.

[259] Campbell RD, David CN (1974) Cell cycle kinetics and development of Hydra attenuata. II. Interstitial cells. *Journal of cell science* 16:349–58.

[260] Bode H, et al. (1973) Quantitative analysis of cell types during growth and morphogenesis in Hydra. *Wilhelm Roux Archiv für Entwicklungsmechanik der Organismen* 171:269–285.

[261] Wanek N, Campbell RD (1983) Roles of ectodermal and endodermal epithelial cells in hydra morphogenesis: Construction of chimeric strains. *Journal of Experimental Zoology* 225:89–97.

[262] Takano J, Sugiyama T (1984) Genetic analysis of developmental mechanisms in hydra. XII. Analysis of chimaeric hydra produced from a normal and a slow-budding strain (L4). *Journal of embryology and experimental morphology* 80:155–173.

[263] Bisbee BJW, Bisbee JW (1973) Size determination in Hydra: the roles of growth and budding. *Journal of embryology and experimental morphology* 30:1–19.

[264] Campbell RD (1967) Tissue dynamics of steady state growth in Hydra littoralis. I. Patterns of cell division. *Developmental biology* 15:487–502.

[265] Campbell RD (1967) Tissue dynamics of steady state growth in Hydra littoralis. II. Patterns of tissue movement. *Journal of Morphology* 121:19–28.

[266] Bosch TC, David CN (1984) Growth regulation in Hydra: relationship between epithelial cell cycle length and growth rate. *Developmental biology* 104:161–171.

[267] Cikala M, Wilm B, Hobmayer E, Böttger A, David CN (1999) Identification of caspases and apoptosis in the simple metazoan Hydra. *Current Biology* 9:959–962.

[268] Lasi M, et al. (2010) The molecular cell death machinery in the simple cnidarian Hydra includes an expanded caspase family and pro- and anti-apoptotic Bcl-2 proteins. *Cell Research* 20:812–825.

[269] Böttger A, Alexandrova O (2007) Programmed cell death in Hydra. *Seminars in Cancer Biology* 17:134–146.

[270] Lasi M, David CN, Böttger A (2010) Apoptosis in pre-Bilaterians: Hydra as a model. *Apoptosis* 15:269–278.

[271] Steele RE, et al. (1996) Response to insulin and the expression pattern of a gene encoding an insulin receptor homologue suggest a role for an insulin-like molecule in regulating growth and patterning in Hydra. *Development Genes and Evolution* 206:247–259.

[272] Fujisawa T (2008) Hydra Peptide Project 1993-2007. *Development, Growth & Differentiation* 50:S257–S268.

[273] Koyanagi M, Ono K, Suga H, Iwabe N, Miyata T (1998) Phospholipase C cDNAs from sponge and hydra: antiquity of genes involved in the inositol phospholipid signaling pathway. *FEBS letters* 439:66–70.

[274] Herold M, Cikala M, MacWilliams H, David CN, Böttger A (2002) Cloning and characterisation of PKB and PRK homologs from Hydra and the evolution of the protein kinase family. *Development genes and evolution* 212:513–9.

[275] Bridge D, et al. (2010) FoxO and Stress Responses in the Cnidarian Hydra vulgaris. *PLoS ONE* 5:e11686.

[276] Boehm AMAM, et al. (2013) FoxO is a critical regulator of stem cell maintenance in immortal Hydra. *Proceedings of the National Academy of Sciences* 109:17.

[277] Arvizu F, Aguilera A, Salgado LM (2006) Activities of the protein kinases STK, PI3K, MEK, and ERK are required for the development of the head organizer in Hydra magnipapillata. *Differentiation* 74:305–312.

[278] Buzgariu W, Chera S, Galliot B (2008) *Methods to investigate autophagy during starvation and regeneration in hydra.* (Elsevier Inc.) Vol. 451, 1 edition, pp 409–437.

[279] Sebestyén F, et al. (2017) Insulin/IGF Signaling and Life History Traits in Response to Food Availability and Perceived Density in the Cnidarian Hydra vulgaris. *Zoological Science* 34:318–325.

[280] Manuel GC, Reynoso R, Gee L, Salgado LM, Bode HR (2006) PI3K and ERK 1-2 regulate early stages during head regeneration in hydra. *Development, growth & differentiation* 48:129–38.

[281] Chera S, Ghila L, Wenger Y, Galliot B (2011) Injury-induced activation of the MAPK/CREB pathway triggers apoptosis-induced compensatory proliferation in hydra head regeneration. *Development Growth and Differentiation* 53:186–201.

[282] Shimizu H (2012) Transplantation analysis of developmental mechanisms in Hydra. *International Journal of Developmental Biology* 56:463–472.

[283] McFall-Ngai M, et al. (2013) Animals in a bacterial world, a new imperative for the life sciences. *Proceedings of the National Academy of Sciences* 110:3229–3236.

[284] Bosch TC (2013) Cnidarian-Microbe Interactions and the Origin of Innate Immunity in Metazoans. *Annual Review of Microbiology* 67:499–518.

[285] Bosch TC, Grasis JA, Lachnit T (2015) Microbial ecology in Hydra: Why viruses matter. *Journal of Microbiology* 53:193–200.

[286] Gilbert SF, Bosch TC, Ledón-Rettig C (2015) Eco-Evo-Devo: Developmental symbiosis and developmental plasticity as evolutionary agents. *Nature Reviews Genetics* 16:611–622.

[287] Deines P, Bosch TC (2016) Transitioning from microbiome composition to microbial community interactions: The potential of the metaorganism hydra as an experimental model. *Frontiers in Microbiology* 7:1–7.

[288] Mortzfeld BM (2018) Longevity factor FoxO controls development, size and microbiome resilience in Hydra. *PhD Thesis*.

[289] Proskuryakov SY, Konoplyannikov AG, Gabai VL (2003) Necrosis: A specific form of programmed cell death? *Experimental Cell Research* 283:1–16.

[290] Buzgariu W, Crescenzi M, Galliot B (2014) Robust G2 pausing of adult stem cells in Hydra. *Differentiation* 87:83–99.

[291] Boehm AM, et al. (2013) FoxO is a critical regulator of stem cell maintenance in immortal Hydra. *Annals of Neurosciences* 20:17.

[292] Mortzfeld BM, Bosch TC (2017) Eco-Aging: stem cells and microbes are controlled by aging antagonist FoxO. *Current Opinion in Microbiology* 38:181–187.

[293] Dańko MJ, Kozłowski J, Schaible R (2015) Unraveling the non-senescence phenomenon in Hydra. *Journal of Theoretical Biology* 382:137–149.

[294] SUGIYAMA T, FUJISAWA T (1979) Genetic Analysis of Developmental Mechanisms in Hydra Vii. Statistical Analyses of Developmental -Morphological Characters and Cellular Compositions. *Development, Growth & Differentiation* 21:361–375.

[295] Hackney JF, Zolali-Meybodi O, Cherbas P (2012) Tissue Damage Disrupts Developmental Progression and Ecdysteroid Biosynthesis in Drosophila. *PLoS ONE* 7:481–491.

[296] Davidowitz G, D'Amico LJ, Nijhout HF (2003) Critical weight in the development of insect body size. *Evolution and Development* 5:188–197.

[297] Uppaluri S, Brangwynne CP (2015) A size threshold governs Caenorhabditis elegans developmental progression. *Proceedings of the Royal Society B: Biological Sciences* 282:20151283.

[298] Meinhardt H, Gierer A (1974) Applications of a theory of biological pattern formation based on lateral inhibition. *Journal of cell science* 15:321–46.

[299] Nijhout HF, Davidowitz G, Roff DA (2006) A quantitative analysis of the mechanism that controls body size in Manduca sexta. *Journal of Biology* 5:1–15.

[300] Roth S (2011) Mathematics and biology: A Kantian view on the history of pattern formation theory. *Development Genes and Evolution* 221:255–279.

[301] van Rossum G (1991) Python.

[302] Lenhoff HM, Brown RD (1970) Mass culture of hydra: an improved method and its application to other aquatic invertebrates. *Laboratory Animals* 4:139–154.

[303] Greber MJ, David CN, Holstein TW (1992) A quantitative method for separation of living Hydra cells. *Roux's Archives of Developmental Biology* 201:296–300.

[304] Graf L, Gierer A (1980) Size, shape and orientation of cells in budding hydra and regulation of regeneration in cell aggregates. *Wilhelm Roux's Archives of Developmental Biology* 188:141–151.

[305] Benjamini Y, Hochberg Y (1995) Controlling the false discovery rate: a practical and powerful approach to multiple testing. *Journal of the Royal Statistical Society* 57:289–300.

[306] Ashton KG (2002) Patterns of within-species body size variation of birds: Strong evidence for Bergmann's rule. *Global Ecology and Biogeography* 11:505–523.

[307] Gouws EJ, Gaston KJ, Chown SL (2011) Intraspecific body size frequency distributions of insects. *PLoS ONE* 6:1–8.

[308] Callier V, Nijhout HF (2013) Body size determination in insects: A review and synthesis of size- and brain-dependent and independent mechanisms. *Biological Reviews* 88:944–954.

[309] Edgar BA (2006) How flies get their size: Genetics meets physiology. *Nature Reviews Genetics* 7:907–916.

[310] Zuo W, Moses ME, West GB, Hou C, Brown JH (2012) A general model for effects of temperature on ectotherm ontogenetic growth and development. *Proceedings of the Royal Society B: Biological Sciences* 279:1840–1846.

[311] Gibert P, De Jong G (2001) Temperature dependence of development rate and adult size in drosophila species: Biophysical parameters. *Journal of Evolutionary Biology* 14:267–276.

[312] Crickmore MA, Mann RS (2008) The control of size in animals: Insights from selector genes. *BioEssays* 30:843–853.

[313] Colombani J, et al. (2005) Antagonistic actions of ecdysone and insulins determine final size in Drosophila. *Science (New York, N.Y.)* 310:667–670.

[314] Mattila J, Bremer A, Ahonen L, Kostiainen R, Puig O (2009) Drosophila FoxO Regulates Organism Size and Stress Resistance through an Adenylate Cyclase. *Molecular and Cellular Biology* 29:5357–5365.

[315] Wells JM, et al. (2007) Wnt/β-catenin signaling is required for development of the exocrine pancreas. *BMC Developmental Biology* 7:4.

[316] Swarup S, Verheyen EM (2012) Wnt/wingless signaling in drosophila. *Cold Spring Harbor Perspectives in Biology* 4:1–15.

[317] Suzuki Y, et al. (1999) A BMP homolog acts as a dose-dependent regulator of body size and male tail patterning in Caenorhabditis elegans. *Development (Cambridge, England)* 126:241–250.

[318] Pennetier D, et al. (2012) Size control of the Drosophila hematopoietic niche by bone morphogenetic protein signaling reveals parallels with mammals. *Proceedings of the National Academy of Sciences* 109:3389–3394.

[319] Dineen A, Gaudet J (2014) TGF-β signaling can act from multiple tissues to regulate C. elegans body size. *BMC Developmental Biology* 14:43.

[320] Marouli E, et al. (2017) Rare and low-frequency coding variants alter human adult height. *Nature* 542:186–190.

[321] Hizli S, et al. (2007) Nutritional stunting. *Pediatric Endocrinology Reviews* 4:186–195.

[322] Stini WA (1972) Malnutrition, body size and proportion. *Ecology of Food and Nutrition* 1:121–126.

[323] Kolss M, Vijendravarma RK, Schwaller G, Kawecki TJ (2009) Life-history consequences of adaptation to larval nutritional stress in drosophila. *Evolution* 63:2389–2401.

[324] Vijendravarma RK, Narasimha S, Kawecki TJ (2012) Chronic malnutrition favours smaller critical size for metamorphosis initiation in Drosophila melanogaster. *Journal of Evolutionary Biology* 25:288–292.

[325] Renault D, Salin C, Vannier G, Vernon P (1999) Survival and chill-coma in the adult lesser mealworm, Alphitobius diaperinus (Coleoptera: Tenebrionidae), exposed to low temperatures. *Journal of Thermal Biology* 24:229–236.

[326] Willott SJ, Hassall M (1998) Life-history responses of British grasshoppers (Orthoptera: Acrididae) to temperature change. *Functional Ecology* 12:232–241.

[327] Pigliucci M, Murren CJ, Schlichting CD (2006) Phenotypic plasticity and evolution by genetic assimilation. *The Journal of experimental biology* 209:2362–2367.

[328] Greene E (1999) in *The Origin and Evolution of Larval Forms* (Elsevier), pp 379—-VIII.

[329] Price TD, Qvarnstrom A, Irwin DE (2003) The role of phenotypic plasticity in driving genetic evolution. *Proceedings of the Royal Society B: Biological Sciences* 270:1433–1440.

[330] Schlichting CD (2004) The role of phenotypic plasticity in diversification. *Phenotypic plasticity: functional and conceptual approaches* pp 191–200.

[331] Pfennig DW, et al. (2010) Phenotypic plasticity's impacts on diversification and speciation. *Trends in Ecology and Evolution* 25:459–467.

[332] Jones OR, et al. (2014) Diversity of ageing across the tree of life. *Nature* 505:169–173.

[333] Broun M, Gee L, Reinhardt B, Bode HR (2005) Formation of the head organizer in hydra involves the canonical Wnt pathway. *Development (Cambridge, England)* 132:2907–2916.

[334] Schroeder LA, Callaghan WM (1981) Thermal tolerance and acclimation of two species of Hydra. *Limnology and Oceanography* 26:690–696.

[335] Haas BJ, et al. (2013) De novo transcript sequence reconstruction from RNA-seq using the Trinity platform for reference generation and analysis. *Nature Protocols* 8:1494–1512.

[336] Simão FA, Waterhouse RM, Ioannidis P, Kriventseva EV, Zdobnov EM (2015) BUSCO: Assessing genome assembly and annotation completeness with single-copy orthologs. *Bioinformatics* 31:3210–3212.

[337] Fischer D, Eisenberg D (1999) Finding families for genomic ORFans. *Bioinformatics* 15:759–762.

[338] Khalturin K, Hemmrich G, Fraune S, Augustin R, Bosch TC (2009) More than just orphans: are taxonomically-restricted genes important in evolution? *Trends in Genetics* 25:404–413.

[339] Porter AG, Jänicke RU (1999) Emerging roles of caspase-3 in apoptosis. *Cell Death and Differentiation* 6:99–104.

[340] Su N, Jin M, Chen L (2014) Role of FGF/FGFR signaling in skeletal development and homeostasis: Learning from mouse models. *Bone Research* 2:14003.

[341] Kakugawa S, et al. (2015) Notum deacylates Wnt proteins to suppress signalling activity. *Nature* 519:187–192.

[342] Artavanis-Tsakonas S, Rand MD, Lake RJ (1999) Notch signaling: Cell fate control and signal integration in development. *Science* 284:770–776.

[343] Scherer A, Graff JM (2000) Calmodulin differentially modulates Smad1 and Smad2 signaling. *Journal of Biological Chemistry* 275:41430–41438.

[344] Daniel C, et al. (2004) Thrombospondin-1 is a major activator of TGF-beta in fibrotic renal disease in the rat in vivo. *Kidney international* 65:459–468.

[345] Gillooly JF, Brown JH, West GB, Savage VM, Charnov EL (2001) Effects of size and temperature on metabolic rate. *Science (New York, N.Y.)* 293:2248–51.

[346] Porte D, Baskin DG, Schwartz MW (2005) Insulin signaling in the central nervous system: A critical role in metabolic homeostasis and disease from C. elegans to humans. *Diabetes* 54:1264–1276.

[347] Shirakawa J, et al. (2017) Insulin Signaling Regulates the FoxM1/PLK1/CENP-A Pathway to Promote Adaptive Pancreatic β Cell Proliferation. *Cell Metabolism* 25:868–882.e5.

[348] Michaelson D, Korta DZ, Capua Y, Hubbard EJA (2010) Insulin signaling promotes germline proliferation in C. elegans. *Development* 137:671–680.

[349] Mazerbourg S, et al. (2005) Identification of receptors and signaling pathways for orphan bone morphogenetic protein/growth differentiation factor ligands based on genomic analyses. *Journal of Biological Chemistry* 280:32122–32132.

[350] Hyun S (2013) Body size regulation and insulin-like growth factor signaling. *Cellular and Molecular Life Sciences* 70:2351–2365.

[351] Emons J, Chagin AS, Sävendahl L, Karperien M, Wit JM (2011) Mechanisms of growth plate maturation and epiphyseal fusion. *Hormone Research in Paediatrics* 75:383–391.

[352] Kramer JM, Davidge JT, Lockyer JM, Staveley BE (2003) Expression of Drosophila FOXO regulates growth and can phenocopy starvation. *BMC Developmental Biology* 3:1–14.

[353] Wang J, Tokarz R, Savage-Dunn C (2002) Body size regulation in C. elegans. 4998:4989–4998.

[354] von Bertalanffy L (1938) A Quantitative Theory Of Organic Growth (Inquiries On Growth Laws . II). *Human Biology* 10:181–213.

[355] Mailleret L, Lemesle V (2009) A note on semi-discrete modelling in the life sciences. *Philosophical Transactions of the Royal Society A: Mathematical, Physical and Engineering Sciences* 367:4779–4799.

[356] Fielenbach N, Antebi A (2008) C. elegans dauer formation and the molecular basis of plasticity. *Genes & Development* 22:2149–2165.

[357] Gibbens YY, Warren JT, Gilbert LI, O'Connor MB (2011) Neuroendocrine regulation of Drosophila metamorphosis requires TGF /Activin signaling. *Development* 138:2693–2703.

[358] L'Allemand D, et al. (1996) Insulin-like growth factors enhance steroidogenic enzyme and corticotropin receptor messenger ribonucleic acid levels and corticotropin steroidogenic responsiveness in cultured human adrenocortical cells. *The Journal of Clinical Endocrinology & Metabolism* 81:3892–3897.

[359] Glister C, et al. (2013) Functional link between bone morphogenetic proteins and insulin-like peptide 3 signaling in modulating ovarian androgen production. *Proceedings of the National Academy of Sciences* 110:E1426–E1435.

[360] Fujiwara M, Sengupta P, McIntire SL (2002) Regulation of body size and behavioral state of C. elegans by sensory perception and the egl-4 cGMP-dependent protein kinase. *Neuron* 36:1091–1102.

[361] Franzenburg S, et al. (2013) Distinct antimicrobial peptide expression determines host species-speci fi c bacterial associations. *Proceedings of the National Academy of Sciences of the United States of America* 110:E3730–E3738.

[362] Song L, Florea L (2015) Rcorrector: efficient and accurate error correction for Illumina RNA-seq reads. *GigaScience* 4:48.

[363] Martin M (2011) Cutadapt removes adapter sequences from high-throughput sequencing reads. *EMBnet.journal* 17:10.

[364] Quast C, et al. (2013) The SILVA ribosomal RNA gene database project: Improved data processing and web-based tools. *Nucleic Acids Research* 41:590–596.

[365] Langmead B, Salzberg SL (2012) Fast gapped-read alignment with Bowtie 2. *Nature methods* 9:357–359.

[366] Fu L, Niu B, Zhu Z, Wu S, Li W (2012) Sequence analysis CD-HIT : accelerated for clustering the next-generation sequencing data. *Bioinformatics (Oxford, England)* 28:3150–3152.

[367] Patro R, Mount SM, Kingsford C (2014) Sailfish enables alignment-free isoform quantification from RNA-seq reads using lightweight algorithms. *Nature biotechnology* 32:462–4.

[368] Srivastava A, Sarkar H, Gupta N, Patro R (2016) RapMap: A rapid, sensitive and accurate tool for mapping RNA-seq reads to transcriptomes. *Bioinformatics* 32:i192–i200.

[369] Kanehisa M, Sato Y, Morishima K (2016) BlastKOALA and GhostKOALA: KEGG Tools for Functional Characterization of Genome and Metagenome Sequences. *Journal of Molecular Biology* 428:726–731.

[370] Jones P, et al. (2014) InterProScan 5: Genome-scale protein function classification. *Bioinformatics* 30:1236–1240.

[371] Krebs S, Fischaleck M, Blum H (2009) A simple and loss-free method to remove TRIzol contaminations from minute RNA samples. *Analytical Biochemistry* 387:136–138.

[372] Schmieder R, Edwards R (2011) Quality control and preprocessing of metagenomic datasets. *Bioinformatics* 27:863–864.

[373] R Development Core Team (2016) R: A Language and Environment for Statistical Computing. *R Foundation for Statistical Computing Vienna Austria* 0:{ISBN} 3–900051–07–0.

[374] Love MI, Anders S, Huber W (2014) *Differential analysis of count data - the DESeq2 package* Vol. 15, p 550.

[375] Leek JT, Johnson WE, Parker HS, Jaffe AE, Storey JD (2012) The SVA package for removing batch effects and other unwanted variation in high-throughput experiments. *Bioinformatics* 28:882–883.

[376] Charnov EL (1993) *Life History Invariants: Some Explorations of Symmetry in Evolutionary Ecology*, Life History Invariants: Some Explorations of Symmetry in Evolutionary Ecology (Oxford University Press).

[377] West GB, Brown JH, Enquist BJ (2001) A general model for ontogenetic growth\r. *Nature* 413:628–631.

[378] Patterson GI, Padgett RW (2000) TGFβ-related pathways: Roles in Caenorhabditis elegans development. *Trends in Genetics* 16:27–33.

[379] Hedgecock EM, Russell RL (1975) Normal and mutant thermotaxis in the nematode Caenorhabditis elegans. *Proceedings of the National Academy of Sciences* 72:4061–4065.

[380] Byerly L, Cassada R, Russell R (1976) The life cycle of the nematode Caenorhabditis elegans. *Developmental Biology* 51:23–33.

[381] Kammenga JE, et al. (2007) A Caenorhabditis elegans wild type defies the temperature-size rule owing to a single nucleotide polymorphism in tra-3. *PLoS Genetics* 3:0358–0366.

[382] Okamoto N, Nishimura T (2015) Signaling from Glia and Cholinergic Neurons Controls Nutrient-Dependent Production of an Insulin-like Peptide for Drosophila Body Growth. *Developmental Cell* 35:295–310.

[383] Sawala A, Gould AP (2017) The sex of specific neurons controls female body growth in Drosophila. *PLoS biology* 15:e2002252.

[384] Kelberman D, Dattani MT (2007) Genetics of septo-optic dysplasia. *Pituitary* 10:393–407.

[385] Xiang X (2016) Towards understanding the ancestral role of insulin-like-peptides (ILPs) in Hydra. *PhD Thesis* p 131.

[386] Krause T (2017) Functional characterization of Insulin-like peptides in Hydra. *Bachelor Thesis* p 49.

[387] Müller WA, Bartsch C, Bartsch H, Maidonis I, Bayer E (1998) Low-molecular-weight hormonal factors that affect head formation in Hydra. *International Journal of Developmental Biology* 42:825–828.

[388] Marcum Ba, Campbell RD (1978) Developmental roles of epithelial and interstitial cell lineages in hydra: analysis of chimeras. *Journal of cell science* 32:233–247.

[389] Marcum BA, Campbell RD, Romero J (1977) Polarity reversal in nerve-free hydra. *Science (New York, N.Y.)* 197:771–773.

[390] Marcum BA, Campbell RD (1978) Development of Hydra lacking nerve and interstitial cells. *Journal of cell science* 29:17–33.

[391] Ohuchi H, et al. (1997) The mesenchymal factor, FGF10, initiates and maintains the outgrowth of the chick limb bud through interaction with FGF8, an apical ectodermal factor. *Development (Cambridge, England)* 124:2235–44.

[392] Rodriguez-Esteban C, et al. (1999) The T-box genes Tbx4 and Tbx5 regulate limb outgrowth and identity. *Nature* 398:814–818.

[393] Kawakami Y, et al. (2001) WNT signals control FGF-dependent limb initiation and AER induction in the chick embryo. *Cell* 104:891–900.

[394] Ng JK, et al. (2002) The limb identity gene Tbx5 promotes limb initiation by interacting with Wnt2b and Fgf10. *Development (Cambridge, England)* 129:5161–70.

[395] Tickle C (2015) How the embryo makes a limb: determination, polarity and identity. *Journal of anatomy* 227:418–30.

[396] Sanz-Ezquerro JJ, Tickle C (2003) Fgf Signaling Controls the Number of Phalanges and Tip Formation in Developing Digits. *Current Biology* 13:1830–1836.

[397] Bielen H, et al. (2007) Divergent functions of two ancient Hydra Brachyury paralogues suggest specific roles for their C-terminal domains in tissue fate induction. *Development* 134:4187–4197.

[398] Philipp I, et al. (2009) Wnt/beta-catenin and noncanonical Wnt signaling interact in tissue evagination in the simple eumetazoan Hydra. *Proceedings of the National Academy of Sciences of the United States of America* 106:4290–5.

[399] Sudhop S (2004) Signalling by the FGFR-like tyrosine kinase, Kringelchen, is essential for bud detachment in Hydra vulgaris. *Development* 131:4001–4011.

[400] Krishnapati LS, Ghaskadbi S (2013) Identification and characterization of VEGF and FGF from Hydra. *International Journal of Developmental Biology* 57:877–886.

[401] Hasse C, et al. (2014) FGFR-ERK signaling is an essential component of tissue separation. *Developmental Biology* 395:154–166.

[402] Koyama T, Mirth CK (2018) Unravelling the diversity of mechanisms through which nutrition regulates body size in insects. *Current Opinion in Insect Science* 25:1–8.

[403] Tennessen JM, Thummel CS (2011) Coordinating growth and maturation - Insights from drosophila. *Current Biology* 21:R750–R757.

[404] Gerisch B, Weitzel C, Kober-Eisermann C, Rottiers V, Antebi A (2001) A Hormonal Signaling Pathway Influencing C. elegans Metabolism, Reproductive Development, and Life Span. *Developmental Cell* 1:841–851.

[405] Jia K, Albert PS, Riddle DL (2002) DAF-9, a cytochrome P450 regulating C. elegans larval development and adult longevity. *Development (Cambridge, England)* 129:221–31.

[406] Sulston J, Horvitz H (1977) Post-embryonic cell lineages of the nematode, Caenorhabditis elegans. *Developmental Biology* 56:110–156.

[407] Kimble J, Hirsh D (1979) The postembryonic cell lineages of the hermaphrodite and male gonads in Caenorhabditis elegans. *Developmental Biology* 70:396–417.

[408] Essers MAG (2005) Functional Interaction Between -Catenin and FOXO in Oxidative Stress Signaling. *Science* 308:1181–1184.

[409] Warren JT, et al. (2006) Discrete pulses of molting hormone, 20-hydroxyecdysone, during late larval development ofDrosophila melanogaster: Correlations with changes in gene activity. *Developmental Dynamics* 235:315–326.

[410] Mirth C, Truman JW, Riddiford LM (2005) The role of the prothoracic gland in determining critical weight for metamorphosis in Drosophila melanogaster. *Current Biology* 15:1796–1807.

[411] Bai H, Kang P, Hernandez AM, Tatar M (2013) Activin Signaling Targeted by Insulin/dFOXO Regulates Aging and Muscle Proteostasis in Drosophila. *PLoS Genetics* 9.

[412] Gupte AA, Pownall HJ, Hamilton DJ (2015) Estrogen: An emerging regulator of insulin action and mitochondrial function. *Journal of Diabetes Research* 2015.

[413] Diamanti-Kandarakis E, Dunaif A (2012) Insulin resistance and the polycystic ovary syndrome revisited: An update on mechanisms and implications. *Endocrine Reviews* 33:981–1030.

[414] Nakamura E, et al. (2012) Mutual regulation of growth hormone and bone morphogenetic protein system in steroidogenesis by rat granulosa cells. *Endocrinology* 153:469–480.

[415] Weise M, et al. (2001) Effects of estrogen on growth plate senescence and epiphyseal fusion. *Proceedings of the National Academy of Sciences* 98:6871–6876.

[416] Fujita T, et al. (2004) Runx2 induces osteoblast and chondrocyte differentiation and enhances their migration by coupling with PI3K-Akt signaling. *Journal of Cell Biology* 166:85–95.

[417] Shahi M, Peymani A, Sahmani M (2017) Regulation of Bone Metabolism. *Reports of biochemistry & molecular biology* 5:73–82.

[418] Guder C, et al. (2006) The Wnt code: cnidarians signal the way. *Oncogene* 25:7450–60.

7 List of publications

7.1 Publications

1. Fiedler T, Salomon A, Adam S, Herzmann N, Taubenheim J, Kirsten P (2013) Impact of bacteria and bacterial components on osteogenic and adipogenic differentiation of adipose-derived mesenchymal stem cells. *Experimental Cell Research* 319:2883–2892.

2. Murillo-Rincon AP, Klimovich AV, Pemöller E, Taubenheim J, Mortzfeld BM, Augustin R, Bosch TCG (2017) Spontaneous body contractions are modulated by the microbiome of Hydra. *Scientific Reports* 7:1–9

3. Mortzfeld BM, Taubenheim J, Fraune S, Klimovich AV, Bosch TCG (2018) Stem cell transcription factor FoxO controls microbiome resilience in hydra. *Frontiers in Microbiology* 9:1–10.

7.2 Manuscripts

1. Mortzfeld BM*, Taubenheim J*, Klimovich AV, Fraune S, Bosch TCG. Environment-dependent body size in *Hydra* is controlled by Wnt and TGF-β signaling. (Ready for submission)

   (*These authors contributed equally to this work)

2. Taubenheim J, Bosch TCG. The virtual *Hydra*: *in silico* prediction match experimental size, cell, and population growth in *Hydra*. (Ready for submission)

8 Acknowledgements

Ich bedanke mich herzlich bei Professor Thomas Bosch für die wissenschaftliche Betreuung und Förderung, das Kennenlernen seiner wissenschaftlichen Welt, für die zahlreichen anregenden Diskussionen und die Möglichkeit Teil seiner erstklassigen Arbeitsgruppe gewesen sein zu dürfen.

Vielen Dank an Dr. Alexander Klimovich für die inspirierenden Diskussionen über Ergebnisse, die Hinweise zum experimentellen Design und für das Troubleshooting. Seine Hilfe bei Manuskripten, seine Liebe zum Detail und seine geduldige Art haben zu wesentlich Teilen dieser Arbeit beigetragen.

Ich bedanke mich weiterhin bei Dr. Sebastian Fraune für fruchtvolle Diskussionen über fast alle Aspekte dieser Arbeit. Sein Blick für das Wesentliche, seine intelligente Art und Weise Experimente zu entwickeln, sein Humor und seine Motivation haben diese Arbeit mitgeprägt. Außerdem Danke ich ihm als Ratgeber in persönlichen Fragen und zu Entscheidungen im Leben, die die wissenschaftliche Arbeit mit sich bringt. Beide, Sebastian und Alex, haben sich immer Zeit für aufkommende Fragen und Probleme genommen, auch wenn ihr eigener Zeitplan es gerade eigentlich nicht zuließ, auch dafür ein Dankeschön.

Besonderer Dank gilt Dr. Benedikt Mortzfeld, der enger Kooperationspartner, Kollege und guter Freund in dieser Zeit geworden ist. Er half bei der gemeinsamen Entwicklung des Projektes Größenregulation und der Etablierung notwendiger Methoden. Ich danke Kai Rathje für die wissenschaftlichen Anmerkungen zu Abbildungen und Vorträgen und besonders als angenehmen Büropartner, Kollegen und Freund. Beide haben den Labor- und Büroalltag sehr bereichert und erheitert.

Weiterhin bedanke ich mich bei der gesamten Arbeitsgruppe für viele wissenschaftliche und nicht- wissenschaftliche Diskussionen und Gespräche, für die sehr angenehme Arbeitsatmosphäre, die allgemeine Hilfsbereitschaft und den freundschaftlichen Umgang miteinander.

Ich möchte mich bei Professor Philip Rosenstiel und Dr. Maren Falk-Paulsen für die Bereitstellung des Zytometers und die Hilfestellung zur Druchflusszytomtrie bedanken, ohne die dieses Projekt nicht umsetzbar gewesen wäre.

Ich bedanke mich herzlich bei meinen Eltern für die Unterstützung in jeder Lebenslage schon während des Studiums und auch während der Doktorarbeit. Ihr Rückhalt machte viele Dinger leichter und ließ mich viele Dinge weniger verbissen sehen.

Besonderer Dank gilt meiner Frau Claudia Taubenheim. Ohne ihre Unterstützung in allen Bereichen hätte ich diese Arbeit nicht vollenden können. Sie hat mir den Rücken zu Hause frei gehalten, wissenschaftlich mit mir diskutiert, Fehler korrigiert und war einfach immer da. Sie hat unsere gemeinsamen Kinder gehütet, damit ich diese Arbeit in Ruhe schreiben konnte. Deine Liebe und dein Rückhalt haben diese Arbeit erst ermöglicht.

9 Erklärung

Hiermit erkläre ich, dass ich die vorliegende Dissertation nach den Regeln guter wissenschaftlicher Praxis eigenständig verfasst und keine anderen als die angegebenen Hilfsmittel und Quellen benutzt habe. Dabei habe ich keine Hilfe, außer der wissenschaftlichen Beratung durch meinen Doktorvater Prof. Dr. Dr. h.c. Thomas C. G. Bosch in Anspruch genommen. Des Weiteren erkläre ich, dass ich noch keinen Promotionsversuch unternommen habe.

Teile dieser Arbeit wurden bereits zur Publikation eingereicht.

Kiel, den 27.07.2018:

_____

Jan Taubenheim